

Optical and Electrical Biosensors: A Chemist's View

Proefschrift

ter verkrijging van de graad van doctor
aan de Technische Universiteit Delft,
op gezag van de Rector Magnificus prof. ir. K. C. A. M. Luyben,
voorzitter van het College voor Promoties,
in het openbaar te verdedigen op maandag 9 november 2015 om 10:00 uur

door

Daniela ULLIEN

Master of Science
The Hebrew University of Jerusalem, Israel
geboren te Vladimir, USSR

This dissertation has been approved by the
promotor: Prof. dr. E. J. R. Sudhölter
copromotor: Dr. ir. L. C. P. M. de Smet

Composition of the doctoral committee:
Rector Magnificus, chairperson
Prof. dr. E. J. R. Sudhölter, promotor
Dr. ir. L. C. P. M. de Smet, copromotor
Dr. W. F. Jager, Applied Sciences, TU Delft

Independent members:

Prof. dr. ir. A. van den Berg, Electrical Engineering, Mathematics
and Computer Science, University of Twente
Prof. dr. I. W. C. E. Arends, Applied Sciences, TU Delft
Prof. dr. J. H. van Esch, Applied Sciences, TU Delft
Prof. dr. U. Stauffer, Mechanical, Maritime and Materials
Engineering, TU Delft

Dr. W. F. Jager TU Delft has, as supervisor, contributed significantly to the
preparation of this dissertation.



This research was financially supported by the Dutch Technology
Foundation STW, which is part of the Netherlands Organisation for
Scientific Research (NWO) and partly funded by the Ministry of Economic
Affairs (project number 10255) and it was in collaboration with the Delft
Institute of Microsystems and Nanoelectronics (DIMES), Philips Research,
the Netherlands Organization for Applied Scientific Research (TNO) and
Erasmus Medical Center, Rotterdam, the Netherlands.

Printed by: Ipskamp Drukkers B. V.

Front: Anna Tchigrinski

Copyright © 2015 by D. Ullien

ISBN: 978-94-6186-555-7

An electronic version of this dissertation is available at
<http://repository.tudelft.nl/>.

Contents

Contents	iii
Samenvatting	vii
Summary.....	xi
Preface	xv
1. General Introduction	1
1.1 Introduction	2
1.2 Silicon Nanowire Field-Effect Transistor	4
1.3 Microring Resonator	6
2. Organic Surface Modification of Silicon Nanowire-Based Sensor Devices	11
2.1 Introduction	12
2.1.1 Scope and Organization of this Review Chapter	12
2.2 SiO _x -covered SiNW-based Sensor Devices	15
2.2.1 Covalent Functionalization	15
2.2.2 Non-Covalent Functionalization	25
2.3 Oxide-Free SiNW-based Sensor Devices.....	28
2.3.1 Hydrosilylation.....	28
2.3.2 Organic Monolayers: Si-C versus SiO _x -C	29
2.3.3 Hydrosilylation on SiNW-based Sensor Devices	30
2.3.4 Electrografting of Diazonium Salts	36
2.3.5 Organic Monolayers on oxide-free SiNW devices: towards sensing	38
2.4 Concluding Remarks and Outlook	39

3. Controlled Amino-functionalization by Electrochemical Reduction of Bromo and Nitro Azo Benzene Layers Bound to Si(111) Surfaces	47
3.1 Introduction	49
3.2 Experimental Section	54
3.2.1 Materials and Reagents	54
3.2.2 Electrochemical Equipment	54
3.2.3 Sample Treatment	54
3.2.4 XPS	56
3.2.5 Atomic Force Microscopy (AFM)	56
3.2.6 Ellipsometry	56
3.3 Results and Discussion	57
3.3.1 Electrografting onto H-terminated Si(111)	57
3.3.2 Electroreduction of Grafted Layers	61
3.3.3 Functionalization of the Reduced Layers	66
3.4 Conclusions	68
 4. Silicon Nanowire Field-Effect Transistors: Electrical Sensors for Biosensing Applications.....	71
4.1 Introduction	72
4.2 DIMES/TU Delft SiNW FETs	73
4.2.1 Design and Fabrication	73
4.2.2 Experimental Set-up	75
4.2.3 Results and Discussion: Electrical Characterizations	76
4.2.4 Conclusions	80
4.3 Philips SiNW FETs	81
4.3.1 Design and Fabrication	81
4.3.2 Measurement Set-up	82
4.3.3 Results and Discussion: Electrical Characterizations	84
4.3.4 Conclusions	90

5. Protein Detection on Biotin-derivatized Polyallylamine by Optical Microring Resonators.....	93
5.1 Introduction	94
5.2 Material and Methods	95
5.2.1 Materials	95
5.2.2 Microring Resonator	95
5.2.3 Optical Set-up	98
5.2.4 Synthesis of Biotinylated PAH.....	100
5.2.5 Polyelectrolyte Deposition and Streptavidin Immobilization..	101
5.3 Results	101
5.3.1 MRR Sensitivity	101
5.3.2 MRR Response to PEs Deposition	102
5.3.3 Biotinylated PAH/ Streptavidin	105
5.4 Discussion	107
5.5 Conclusions	108
 6. Influenza A Detection by Free-space Coupled Optical Microring Resonators	111
6.1 Introduction	112
6.2 Materials and Methods	114
6.2.1 Materials	114
6.2.2 MRR layout	115
6.2.3 Free-space coupling	115
6.2.4 Chemical-biological layer deposition	116
6.2.5 Ellipsometry measurements	117
6.3 Results and Discussion	118
6.3.1 Layer-by-layer deposition	118
6.3.2 Antigen detection	119
6.3.3 Pre- and post-treatment of the MRR devices	125
6.4 Conclusions	129

7. Conclusions and Outlook	133
7.1 Conclusions	134
7.2 Outlook	136
Appendix A.....	139
Appendix B.....	143
Appendix C.....	147
List of PhD Publications	151
Acknowledgements.....	153
Curriculum Vitae.....	155

Samenvatting

Sensoren zijn onontbeerlijk geworden in de moderne maatschappij. Ze verbeteren de kwaliteit van leven, vooral in vakgebieden als persoonlijke medische diagnostisering en behandeling. Toch blijft er een behoefte bestaan voor snellere, meer gevoelige en selectieve detectiemethoden om betrouwbaar en snel diagnoses te kunnen stellen. Er zijn enorme inspanningen geleverd in de ontwikkeling van *point-of-care* (POC)-apparaten om snelle en betrouwbare diagnoses mogelijk te maken. Dit omvat ook onderzoek naar een grote verscheidenheid aan elektrische en optische (bio)sensorplatformen.

Dit proefschrift behandelt twee verschillende types van zulke biosensoren, die goedkoop en op grote schaal kunnen worden gemaakt en die gebaseerd zijn op bewezen halfgeleidertechnologieën. Er is speciale aandacht besteed aan Influenza A-detectie. Zowel silicium nanodraad veldeffect-transistoren (SiNW FET's) als optische microring-resonatoren (MRR's) zijn in detail onderzocht. Het werkingsprincipe van deze apparaten is kort beschreven in de introductie van dit proefschrift. Het actieve transductie-oppervlak van deze platformen is gemaakt van silica (SiO_2) en kan worden geëetst tot oxidevrij silicium (Si-H) voor een verbetering van de sensorgevoeligheid. Er wordt een uitgebreid overzicht van de literatuur gepresenteerd over de diversiteit van de modificatiestrategieën van silica en silicium.

De functionalisering van het oppervlak is van cruciaal belang voor het bereiken van de gewenste selectiviteit en de prestaties van de POC-apparaten. De covalente aanhechting van organosilanen wordt veel gebruikt. In dit proefschrift hebben we gekozen voor verschillende manieren voor de selectieve oppervlaktebehandeling, te weten, het *electrograften* met zogenaamde aryldiazoniumzouten en de laag-voor-laag-afzetting met polyelektrolieten (PE's). *Electrograften* en

aryldiazoniumzouten laten een precieze controle van het functionaliseren van specifieke gebieden van het sensoroppervlak toe. Dit is dus van het allergrootste belang voor het selectief modifieren van een SiNW die onderdeel uitmaakt van een collectie aan SiNW's. De laag-voor-laag-afzetting met PE's is een simpele en snelle functionaliseringsmethode. Door (bio)gefunctionaliseerde polyelektrolieten te gebruiken, kunnen (bio)receptoren eenvoudig gedeponneerd worden.

Het eerste experimentele gedeelte van dit proefschrift richt zich op het werk dat gerelateerd is aan elektrische biosensoren. Er zijn broom- en nitro-aryldiazoniumzouten op vlakke Si-H modeloppervlakken elektrochemisch vastgezet, gevolgd door een gecontroleerde elektroreductie van de verkregen multilagen. Via deze elektrochemische tweestaps-methode zijn amino-getermineerde dunne films verkregen die verdere functionalisering met carboxylzuur-getermineerde stoffen mogelijk maken, zoals die aanwezig zijn in eiwitten. Gecontroleerde amino-terminatie – verkregen tijdens de elektroreductie-stappen – toont de mogelijkheden in toepassingen van deze methode op SiNW's, en dan vooral in de richting van het verkrijgen van multi-gefunctionaliseerde SiNW op één platform.

SiNW FET-apparaten zijn via twee verschillende bronnen verkregen: uit de *clean rooms* van DIMES/TU Delft en die van Philips Research. Er zijn initiële, elektrische karakterisaties uitgevoerd waarbij de SiNW FETs zowel in contact met lucht als in contact met vloeistoffen waren. Dit om de sensormogelijkheden van deze apparaten te verifiëren, nog vóór de meer complexe experimenten. Het is aangetoond dat de laag-voor-laag-afzetting van PE's met tegengestelde ladingen leidt tot een alternerende verschuiving van het drempelvoltage van de SiNW FET-apparaten, wat te verwachten is volgens gerapporteerde studies. Terwijl vooronderzoek naar Influenza A-detectie beperkt was door een beperking in het aantal beschikbare SiNW FET-apparaten, is het werk PE's bemoedigend om verder onderzoek in dit veld uit te voeren.

Het tweede gedeelte van dit proefschrift beschrijft het werk dat gedaan is naar optische microring-resonatoren (MMR's). Allereerst was het concept om eiwitbinding (hier: Streptavidine) via een laag-voor-laag-benadering met behulp van een nieuw gesynthetiseerde biogetinyleerde polyallylamine hydrochloride (PAH) succesvol bestudeerd.

Tot slot is de methode om biofunctionalisering van een MMR met Streptavidine uitgebreid om antilichamen complementair aan Influenza A antigenen te koppelen. Dit deel is uitgevoerd met een nieuw ontwikkeld MRR-systeem waarbij het laserlicht kan worden ingekoppeld zonder het gebruik van glasvezelkabels. Deze opstelling is genereus beschikbaar gesteld door onze nauwe samenwerking met TNO-Delft. Voorlopige resultaten tonen dat het mogelijk is om Influenza A antigenen tot zo laag als 10 ng/mL waar te nemen! Toch is verdere ontwikkeling van het huidige systeem een vereiste, bijvoorbeeld door de concentratie-afhankelijkheid te bestuderen. Het systeem is goed geoptimaliseerd door een succesvolle vermindering in vervuiling door het gebruik van een Bovine Serum Albumin (BSA)-voorbehandeling. Daarbovenop is de gevoeligheid van het apparaat verhoogd door een voorbehandeling met bleek. Er is ook ontdekt dat het apparaat geregenereerd kan worden door het wassen met bleek.

Concluderend geven de gepresenteerde experimenten een beter inzicht in de oppervlaktefunctionalisatie van biosensoren, maar nog belangrijker, in hun invloed op hun prestatie als biosensor. Het uitgevoerde onderzoek vergemakkelijkt toekomstige ontwikkelingen van POC-apparaten, voornamelijk het gebruik van MRR-systemen.

Summary

Sensors have become indispensable in modern society. They improve the quality of life, especially in the field of personal medical diagnosis and treatment. However, there is an ongoing need for faster, more sensitive and selective diagnosis, allowing reliable and fast diagnoses. Enormous effort has been put in the development of point-of-care (POC) devices to facilitate rapid and reliable diagnosis. This includes research on a large variety of electrical and optical platforms.

This thesis covers work related to two different types of such biosensors that are compatible with low-cost and large-scale production based on known semiconductor technologies. Special attention was given to influenza A detection. In more detail, both silicon nanowire field-effect transistors (SiNW FETs) and optical microring resonators (MRRs) were under investigation. The working principal of these devices were described briefly in the introduction of the thesis. The active transducer surface of these platforms is made of silica (SiO_2) and can be etched to oxide-free silicon (Si-H) for achieving better performance with respect to its sensitivity. An extensive review on the diversity of modification strategies reported in literature on silica and silicon for such devices is presented.

Surface functionalization is critical for achieving the desired selectivity in the performance of POC devices. The covalent attachment of organosilanes is widely used. In this thesis we have chosen to explore different approaches for selective surface modification, *i.e.* the electrografting with aryldiazonium salts and the layer-by-layer deposition with polyelectrolytes (PEs). Electrografting of aryldiazonium salts allows a precise control of functionalising specific areas of the sensor surface. Hence, it is of paramount interest for selective SiNWs modification in an array arrangement. The layer-by-layer deposition with PEs is a simple and

quick functionalization method. Using (bio)functionalised polyelectrolytes, (bio) receptors can be easily deposited.

The first experimental part of the thesis focuses on the work related to electrical biosensors. Electrografting of bromo and nitro aryl diazonium salts onto planar Si-H model surfaces was performed, followed by the controlled electroreduction of the obtained multilayers. *Via* this two-step electrochemical method amino-terminated thin films were obtained, allowing further functionalization with carboxylic acid-terminated compounds like those present in proteins. Controlled amino termination obtained during the electroreduction step shows the possibility of application of this method to SiNWs and especially points toward the prospect of obtaining multi-functionalized SiNW arrays.

SiNW FET devices were obtained from two different sources, from the cleanrooms at DIMES/TU Delft and Philips Research. Initial electrical characterizations in contact with air and in contact with liquid were performed to verify the sensing capabilities of the devices prior to the more complex experiments. It has been shown that the layer-by-layer deposition of PEs of opposite charge led to alternating shifts of the threshold voltage of the SiNW FET devices, which is in line with reported studies. While preliminary research on influenza A detection was limited due to a limited number of available SiNW FET devices, the work performed on PEs is encouraging to continue investigation in this field.

The second part of this thesis describes the work done on optical microring resonators (MRRs). Initially, the concept of protein (here streptavidin) binding *via* a layer-by-layer approach making use of a newly synthesized biotinylated polyallylamine hydrochloride (PAH) was successfully studied.

Finally, the method of biofunctionalization of an MRR with streptavidin was extended to couple antibodies complementary to influenza A antigens. This part was performed with a newly developed free-space coupled MRR system, generously provided by our close

collaborators within TNO-Delft. Preliminary results show sensing of influenza A antigen down to a 10 ng/ml concentration! Still, further improvements to the current system are required, for instance to observe concentration-dependency. The system was well optimized by a successful reduction of fouling using Bovine Serum Albumin (BSA) pre-treatments. In addition, the sensitivity of the device was increased by a bleach pre-treatment. Also was found that the device can be regenerated by washing with bleach.

In conclusion, the presented experiments give better insight into the surface functionalization of biosensors and most importantly into their influence on the biosensor performance. The research performed during this thesis facilitates further development of POC devices, in particular the use of free-space coupled MRR devices.

Preface

Sensors play an important role in our modern life. They make life more comfortable, supportable and sometimes even possible. For instance, simple sensors monitor the temperature in every household refrigerator for food control. In addition, sensors for quick diagnosis of patients with cardiovascular diseases improve patients' prognosis. Furthermore, modern blood glucose meters make everyday blood testing easy, fast and convenient. These matured examples are a model for all sensors under development, but not all modern devices have already reached the objectives in terms of ease of use, portability, cheapness and improved sensitivity.

Rapid scientific progress in the fields of nanotechnology and microfluidics have improved the performance of many sensor devices. Thousands of new diagnostic tests are introduced each year. The success of these tests depends mainly on their low cost, high sensitivity and high selectivity. Such devices come in many forms as they are designed to be applied in different principles of work and for different purposes. This thesis is dedicated to two different types of sensor platforms: silicon nanowire field-effect transistors (SiNW FETs) and silicon microring resonators (MRRs) within the scope of the detection of influenza A virus. In both cases the emphasis is on the sensor sensitivity and selectivity by tailoring the surface of the sensors platforms with the appropriate (bio)chemical functionalities. These two types of sensors have the same surface, namely silicon oxide, allowing the same chemical treatment. The general goal of the thesis is to explore different novel surface modification strategies for SiNW FET and Si MRR devices, and to apply most promising methods for influenza A sensing.

To build a biosensor, which has a biological detection element, one needs an intermediate layer, i.e. a chemical recognition element, for

combining a 'lively' biological part of the sensor to the 'cold' inorganic transducer element. The focus of the thesis is to fabricate such a chemical recognition element and to verify its working capabilities. Two main strategies were explored: 1) a non-covalent approach by means of polyelectrolyte multilayers, and 2) a covalent approach by means of electrografting.

A description of the different components of a sensor, in general, and the working principle of the SiNW FETs and MRRs, in particular, is presented in **Chapter 1**.

Chapter 2 reviews reported methods of silicon modification. It gives an overview on surface modification techniques reported in literature based on the case of SiNW FET devices. However, the part on surface modification of silicon oxide is relevant for MRRs too. A concise overview of surface modification techniques that have been applied on MRRs is presented in the introduction of Chapter 5. Chapter 2 was published in a book, entitled **Nanowires-Implementations and Applications** as *Organic Surface Modification of Silicon Nanowire-based Sensor Devices*, InTech, 2011. This review was updated by highlighting the most recent developments in the field of silicon surface modifications.

Chapter 3 covers our electrografting work performed on a reference substrate, i.e. planar silicon samples. It was published in **Phys. Chem. Chem. Phys.** as *Controlled Amino-functionalization by Electrochemical Reduction of Bromo and Nitro Azo Benzene Layers Bound to Si(111) Surfaces*, 2014. This work shows a deeper understanding of the formation of electrografted diazonium layers on hydrogenated silicon. Tuning of the subsequent electroreduction step showed the possibility of multi-functionalized SiNW arrays, demonstrating the potential of this approach to be applied on SiNW devices.

Chapter 4 depicts preliminary results on detecting influenza A with SiNW FETs in collaboration with the Delft Institute of Microsystems and Nanoelectronics (DIMES) and Philips Research, the Netherlands. A brief

description of the device fabrication processes is introduced, followed by the reports on electrical characterizations in air, in liquid, pH sensing, layer-by-layer addition of polyelectrolytes, and finally an effort in influenza A detection.

Chapter 5 describes the design and use of silicon-on-insulator MRR chips for (bio)sensing purposes and was performed in close collaboration with TNO, the Netherlands Organisation for Applied Scientific Research. It shows the results on protein (here streptavidin) detection on optical MRRs using the layer-by-layer approach. The novel application of polyelectrolytes that were covalently functionalized (here with biotin) for analyte capturing on the MRR chips was published in *Optics Express* as *Protein Detection on Biotin-derivatized Polyallylamine by Optical Microring Resonator*, 2014. This work was done using out-of-plane grating couplers to couple light in and out of the MRR.

Chapter 6 continues the work on biotinylated polyallylamine utilization for influenza A detection in collaboration with TNO and Erasmus Medical Center Rotterdam, the Netherlands. It shows preliminary results on virus detection with different concentrations using the MRR technique. The design and characteristics of the unique MRR system are described in the proceedings of the 19th annual symposium of the *IEEE Photonics Society* as *'Click & Measure' Optical Interfacing to Silicon-On-Insulator Chips*, 2014. Here, the coupling of light was done by a unique free-space coupling method designed by TNO. In addition, the chapter reports on methods for improving sensitivity of the MRR device and its regeneration.

Chapter 7 concludes the thesis with a general discussion and the main conclusions from the preceding chapters and presents an outlook for future work.

Chapter 1

General Introduction

Abstract

This chapter introduces the basic concepts of (bio)sensors and describes the working principles of the two sensing devices that were investigated during the research described in this thesis, i.e. silicon nanowire field-effect transistors (SiNW FETs) and optical microring resonators (MRRs).

1.1 Introduction

Sensors are an integral part of our everyday modern life. Touchscreens in tablets and smartphones, oxygen sensors for monitoring the oxygen amount in exhaust gases, breath analyzers for estimating blood alcohol content, and pregnancy tests are just a small variety of examples of available sensors. Important sensors are those developed for medical purposes, because they may improve patient's well-being and save lives. For instance, patients with diabetes type 1 use glucose meters 4 to 10 times per day to monitor glucose levels in blood to be able to adjust insulin levels.

Sensors can be divided into three main groups: physical, chemical and biosensors. Physical sensors measure physical phenomena like distance, mass or temperature. Chemical sensors evaluate chemical substances, while biosensors detect biological species. All of these devices have to be connected to a measuring unit, called a transducer, to record observable response of the system. A generalized scheme with the different elements of a biosensor as an example is presented in Fig. 1.

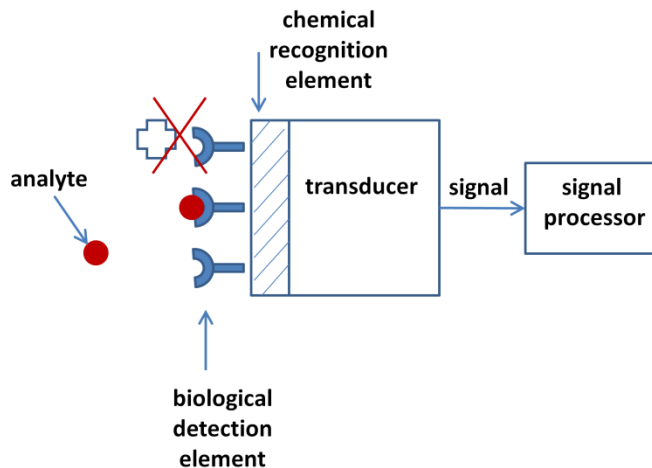


Figure 1: A scheme of different elements of a biosensor, including a biological detection element, a chemical recognition element and a transducer.

As can be seen from Fig. 1 a biosensor responds selectively to a particular analyte. A proper detection element is the key component for high selectivity of any sensor. Since in biosensors the detection element has a biological character, it is a challenge to make a proper connection with the transducer, which is often inorganic in nature. For this reason an intermediate chemical modification (Fig. 1, chemical recognition element) is necessary to construct a working device. There are different methods for the immobilization of a biological detection element, including adsorption, microencapsulation, entrapment, covalent attachment and cross-linking.

The usual transducer for a biosensor produces an electrical or optical signal that is, ideally, proportional to the concentration of the analyte. This can be realized by a specific interaction between the analyte (i.e. the target species) and its host (i.e. the receptor), which generates a physical change that can be detected by a transducer. Transducers based on electrical signals are popular because of their low cost and simplicity of production, making use of well-established complementary metal-oxide-semiconductor (CMOS) technologies. At the same time, rapid progress and recognition of photon-driven devices was enabled through the use of optical fibers.

The working principal of the two types of devices used in this thesis, i.e. silicon nanowire field-effect transistor (SiNW FET) and microring resonator (MRR), is described and illustrated in the following sections. A principal advantage of these techniques, compared to other popular label-free technologies such as surface plasmon resonance (SPR) or electrochemical impedance spectroscopy (EIS), is their compatibility with semiconductor technologies for mass-production of low-cost devices. Compared to the relatively large dimensions of other techniques, the nano size of SiNW FET might bring sensing of biomolecules to the single molecule level. However, SiNW FET measurements should be carried out in low ionic concentrations to reduce Debye screening effects¹, this prevents the direct use of unprocessed blood or urine. In contrast to SiNW FETs,

MRR devices do not have such limitation. The sensing with MRR is possible in any concentration of a sensing solution. In addition, the sensing profile extends to tens of nanometers above the MRR surface². Both of these techniques are of great interest for developing point-of-care (POC) diagnostics and have been under investigation in literature for multiple target analysis³.

1.2 Silicon Nanowire Field-Effect Transistor

An example of a sensor with an electrical transducer is the silicon nanowire field-effect transistor (SiNW FET). The first SiNW FET sensor was introduced in 2001 by the Lieber group⁴ and since then this type of platform has gained a lot of attention as a viable candidate for a medical biosensor, e.g. in cancer research⁵.

Figure 2a shows a schematic representation of SiNW FET. The electrical characteristics of such a FET device are achieved through the electrical current modulations of a conductive channel of a small nanometer-sized wire made of silicon, placed between two electrical contacts, called a source and a drain (Fig. 2a). The conductivity of a FET device depends on the third contact, i.e. a gate. By applying different potentials on a gate, the electrical current in the NW either stops or passes. The gate potential can be applied through a back gate or a front gate contact in the case of the measurements in the liquid phase (Fig. 2, BG and FG, respectively). The point where the NW is open, or starts to conduct, is called a threshold voltage (V_t). As one option, it can be defined as a voltage at which a current of 1 nA is reached (Fig. 2b).

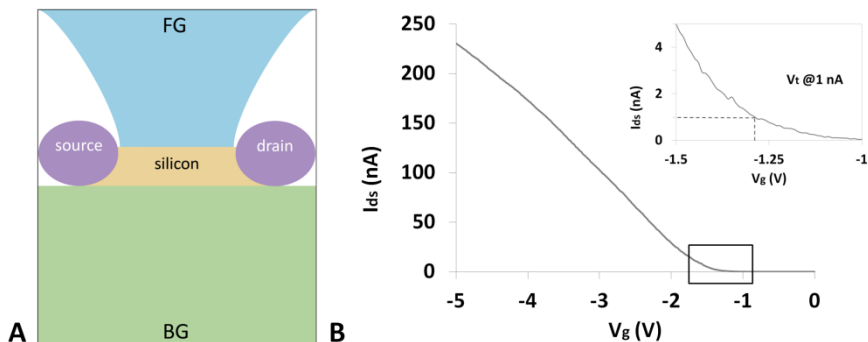


Figure 2: (a) A simplified scheme of SiNW FET, (b) typical electrical characteristics of a p-type SiNW FET, with a definition of a threshold voltage, V_t , at 1 nA current (inset) and a current through a NW, I_{ds} .

NW FET devices can sense events happening on or near its surface, even to an extent of single molecule binding, owing to its increased surface-to-volume ratio. Changes on the surface of the NW due to binding of charged^{4, 6, 7} as well as uncharged^{8, 9} species can be monitored. As an example, a simple case of a pH sensing with a p-type doped SiNW FET will be discussed. In a p-type SiNW holes are the majority charge carriers. As a consequence, the SiNW FET device will be open by applying negative potentials on a gate (Fig. 2b; expelling the electrons from the nanowire). The threshold voltage can vary depending on the doping density (the higher the doping density, the smaller potentials one need to apply to open the device). The SiNW surface is typically covered with an oxide layer (native or thermally grown) and allows pH sensing due to the dissociation of the silanol groups (SiOH) with protons in a sensing liquid (Fig. 3).

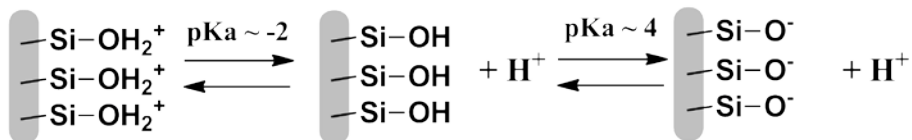


Figure 3: A scheme of surface charge of the silicon oxide depending on solution acidity.

In more detail, at very low pH, the SiNW surface is positively charged, due to protonation of the surface silanol groups. The positive charges deplete the p-type channel and threshold voltage moves to more negative potentials. At higher pH values the positive surface charge reduces and becomes neutral. At even higher pH values, the surface silanol groups deprotonate and the surface becomes negatively charged. The presence of negative charges on the silicon surface will shift the threshold voltage to more positive potentials. Thus, we expect to observe a trend of an increase of V_t with decreasing pH values. Upon binding of molecules that have charges, e.g. biomolecules or polyelectrolytes, comparable changes in the device characteristics take place.

1.3 Microring Resonator

An example of a sensor with an optical transducer is the microring resonator (MRR). As is the silicon NW FET, this is also a label-free technology for sensing biomolecules, such as cancer markers^{10, 11}, viruses¹² or DNA.^{13, 14}

An MRR consists of a set of waveguides: input, output and a closed loop (Fig. 4a). Light passes through the input waveguide into the device, couples through the external losses to the closed loop, i.e. the microring resonator, and exits eventually through the output waveguide to the external detector (Fig. 4a). Light coupling between the waveguides is allowed only at wavelengths, λ , that match a resonance condition:

$$\lambda = \frac{2\pi r n_{\text{eff}}}{m}$$

where m is an integer value, r is the MRR radius, n_{eff} is the effective refractive index of the medium. Figure 4b (unbroken line) shows typical MRR transmission spectra of the mounted device.

The sensing of an analyte with an MRR is elicited by the interaction between the evanescent field extended from the MRR and the analyte present in the sensing solution. Biological molecules ($n=1.4-1.6$) have

higher refractive index than water ($n=1.33$). Consequently, their presence near/or at the surface of the MRR increases the effective refractive index of the medium. Changes in the refractive index, happening upon specific binding of an analyte, cause a shift in the MRR resonance wavelengths according to $\Delta\lambda \propto \Delta n_{\text{eff}}$ (Fig. 4b, broken line). Photons that travel multiple times through a closed loop frequently interact with the analyte and increase sensor sensitivity. Binding events can be traced by following the change in the wavelength with time (Fig. 4c).

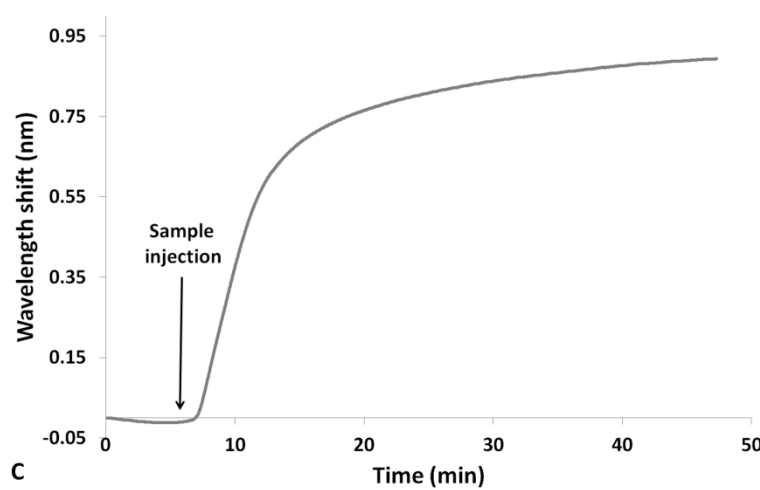
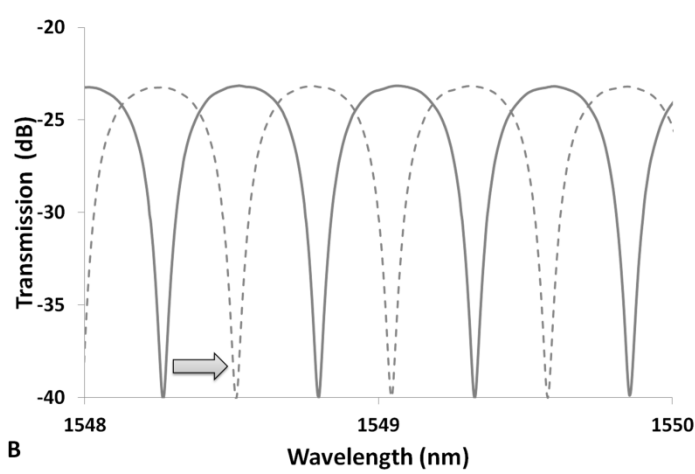
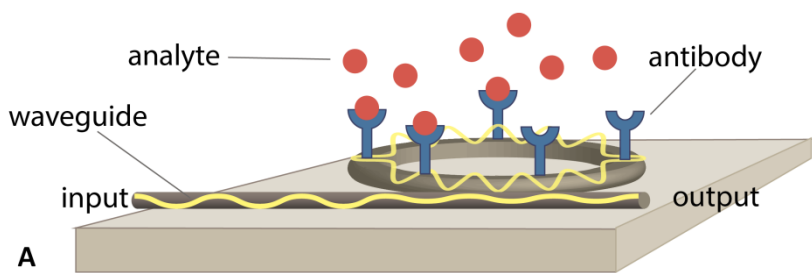


Figure 4: (a) An illustration of a microring resonator sensing an analyte, (b) a resonance wavelength shift due to change in the refractive index, (c) wavelength shift vs. time graph.

References

1. E. Stern, R. Wagner, F. J. Sigworth, R. Breaker, T. M. Fahmy and M. A. Reed, *Nano Lett*, **2007**, *7*, 3405-3409.
2. M. S. Luchansky, A. L. Washburn, T. A. Martin, M. Iqbal, L. C. Gunn and R. C. Bailey, *Biosens Bioelectron*, **2010**, *26*, 1283-1291.
3. A. J. Qavi, A. L. Washburn, J. Y. Byeon and R. C. Bailey, *Anal Bioanal Chem*, **2009**, *394*, 121-135.
4. Y. Cui, Q. Wei, H. Park and C. M. Lieber, *Science*, **2001**, *293*, 1289-1292.
5. G. J. Zhang and Y. Ning, *Anal Chim Acta*, **2012**, *749*, 1-15.
6. Y. L. Bunimovich, Y. S. Shin, W. S. Yeo, M. Amori, G. Kwong and J. R. Heath, *J Am Chem Soc*, **2006**, *128*, 16323-16331.
7. X. T. Vu, R. Stockmann, B. Wolfrum, A. Offenhäusser and S. Ingebrandt, *Phys Status Solidi A*, **2010**, *207*, 850-857.
8. Y. Engel, R. Elnathan, A. Pevzner, G. Davidi, E. Flaxer and F. Patolsky, *Angew Chem*, **2010**, *49*, 6830-6835.
9. Y. Paska, T. Stelzner, O. Assad, U. Tisch, S. Christiansen and H. Haick, *ACS Nano*, **2012**, *6*, 335-345.
10. A. L. Washburn, L. C. Gunn and R. C. Bailey, *Anal Chem*, **2009**, *81*, 9499-9506.
11. A. L. Washburn, M. S. Luchansky, A. L. Bowman and R. C. Bailey, *Anal Chem*, **2010**, *82*, 69-72.
12. M. S. McClellan, L. L. Domier and R. C. Bailey, *Biosens Bioelectron*, **2012**, *31*, 388-392.
13. A. Ramachandran, S. Wang, J. Clarke, S. J. Ja, D. Goad, L. Wald, E. M. Flood, E. Knobbe, J. V. Hryniewicz, S. T. Chu, D. Gill, W. Chen, O. King and B. E. Little, *Biosens Bioelectron*, **2008**, *23*, 939-944.
14. M. S. Luchansky and R. C. Bailey, *Anal Chem*, **2012**, *84*, 793-821.

Chapter 2

Organic Surface Modification of Silicon Nanowire-Based Sensor Devices

Abstract

This chapter reviews the diversity of surface modification strategies on silicon nanowire-based sensors that have been introduced in literature.

Previous versions of this chapter appeared as:

- *Louis C.P.M. de Smet, Daniela Ullien, Marleen Mescher, Ernst J.R. Sudhölter "Organic Surface Modification of Silicon Nanowire-Based Sensor Devices" in Nanowires - Implementations and Applications, Abbass Hashim (Ed), InTech, Rijeka, Croatia, 2011.*
- *Section 2.2 of the PhD Thesis of Marleen Mescher (TU Delft, 2014).*

2.1 Introduction

About 15 years ago silicon nanowire (SiNW)-based electronic devices appeared on the scenery of (bio)sensing tools. Since their introduction¹ SiNW-based sensor devices have gained considerable interest as a general platform for ultra-sensitive, electrical detection of biological and chemical species (Figure 1). Although SiO_x can be used for the detection of protons², and gases³, the specific detection of other analytes, including ions and biomolecules requires the presence of an affinity layer that interacts with the analyte of interest. Such a layer can be added on top of the nanowire by the modification of the nanowire surface. In this chapter we review the surface modification strategies that have been explored on SiNW-based devices over the past decade.

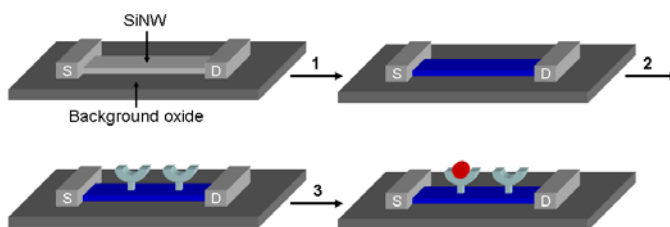


Figure 1. Schematic representation of a SiNW-based device (top left), of which the nanowire has been chemically modified (step 1), followed by the immobilization of receptors (step 2) and the binding of an analyte (step 3). S and D stand for source and drain, respectively.

2.1.1 Scope and Organization of this Review Chapter

This chapter focuses on surface modification strategies of SiNW-based devices. Our review concentrates on electrical devices that consist of in plane orientated SiNWs, which are positioned between two ohmic contacts, often referred to as source and drain. This chapter was initially published in 2011 as a book review⁴, and was updated in 2014 by co-author Marleen Mescher in Section 2.2 of her PhD thesis.⁵ We specify the updated parts in the last paragraph of this section.

For an extensive overview of different materials that have been explored to prepare NW-based sensors, including silicon, we refer to the review of Ramgir et al.⁶ Several reviews on SiNW-based devices have been written with a clear focus on the chemical-vapour-deposition fabricated NWs by the Lieber and Zhou groups⁷⁻⁹ or top-down fabricated SiNW-based sensors from the Reed group¹⁰. In this chapter we will discuss issues related to the modification of SiNW-based devices with organic compounds. The topics of SiO_x ¹¹ and Si-H ¹¹⁻¹³ surface modification with covalently linked organic monolayers have been reviewed extensively. However, the main focus of these reviews is on the modification of large planar substrates, while the focus of this chapter is on SiNW-based devices. A review by Wanekaya et al. contains a paragraph on the covalent functionalization of SiNWs with biomolecules¹⁴. Very recent reviews also include sections with brief schemes for SiNWs functionalization.^{15, 16} Very recently, our group published a review paper on gas-phase sensing with SiNW-based FETs reviewing different modification strategies.¹⁷

In this chapter we aim to give an overview of all the different surface modification strategies that have been explored to modify SiNW-based devices, including non-covalent immobilization strategies. The methods can be divided into different categories (Table 1). The first one is based on silanization chemistry i.e., the reaction between hydroxyl-terminated surfaces and organosilanes. Also other compounds like activated ester or organophosphonates have been covalently attached to SiO_x surfaces. In addition, polyelectrolytes and bilayers have been physically adsorbed onto SiO_x surfaces. Polymer membranes and nanoparticles were also deposited on SiNW FETs. The next approach follows the route of oxide removal, followed by the reaction with (ω -functionalized)-1-alkenes or alkynes. The most recent development in SiNW functionalization uses electrochemistry to covalently attach aryldiazonium salts to H-terminated silicon. This type

of chemistry was also explored on planar silicon samples and it is comprehensively reviewed in Chapter 3 of this thesis.

Since the first publication of the review in 2011 the following parts of the chapter were updated by Marleen Mescher: non-covalent functionalization (including electrodeposition of nanoparticles and drop casting of ion sensitive membranes) and oxide-free covalent functionalization (including electrografting of diazonium salts). Compared to the 2011 version, the current chapter contains updates on the following topics, all relevant to the scope of this thesis:

- Section 2.2.2 with an additional example of layer-by-layer polymer adsorption,
- Section 2.3.1 with an example of alkyne hydrosilylation,
- Section 2.3.4 with diazonium electrografting.

Table 1. Overview of the different strategies used in the modification of SiNW-based devices.

Surface	Modification Method	Type of Binding	Nature Film	# Papers (year of first report)	§
SiO _x	Silanization	Covalent	Monolayer	>100 (2001)	2.2.1
SiO _x	Esterification	Covalent	Monolayer	1 (2004)	2.2.1
SiO _x	Phosphorization	Covalent	Monolayer	1 (2008)	2.2.1
SiO _x	Layer-by-Layer	Electrostatic	Multilayers	3 (2010)	2.2.2
SiO _x	Supported lipid membranes	Electrostatic	Bilayer	2 (2009)	2.2.2
SiO _x	Drop casting of ion sensitive membranes	Physisorption	Membrane	3 (2012)	*
SiO _x	Electrodeposition of nanoparticles	Covalent	Monolayer	2 (2007)	*
Si-H	Hydrosilylation	Covalent	Monolayer	9 (2006)	2.3.1
Si-H	Electrografting of diazonium salts	Covalent	Multilayers	1 (2014)	2.3.4

* This method was reviewed in the PhD thesis of Marleen Mescher ⁵

2.2 SiO_x-covered SiNW-based Sensor Devices

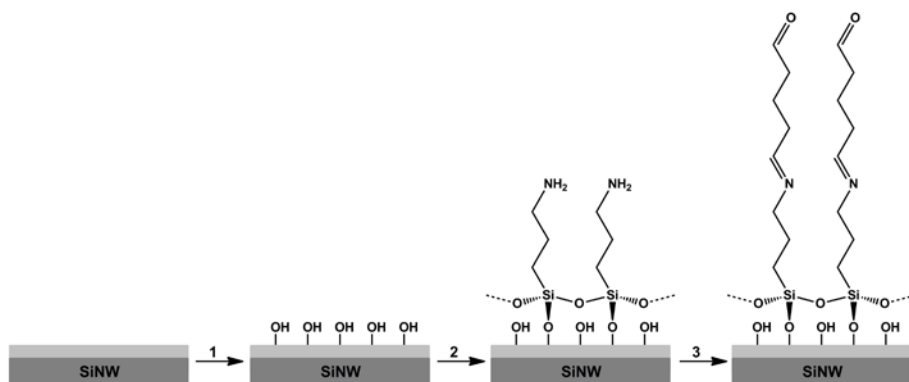
Cleaned silicon surfaces exposed in an ambient environment such as air or solutions will oxidize spontaneously¹⁸. The silicon oxide layer, in this chapter referred to as SiO_x -either native oxide or oxide grown under controlled conditions-, passivates the silicon surface. This allows the silicon to be used as an electronic material in processing and application environments. After fabrication, or at least after exposure to ambient environment, also SiNWs contain a SiO_x layer. Typically the thickness of this SiO_x layer on the NW is 1.5-10 nm, whereas the background oxide is usually >10 nm. It is important to note that -in terms of surface modification- one cannot discriminate between the oxide of the nanowire and background oxide; both are modified. The surface modifications described in §2.2 deal with SiO_x-coated SiNW devices.

2.2.1 Covalent Functionalization

Silanization

The most applied method to functionalize silica surfaces is through the self-assembly of organofunctional alkoxy silane and chlorosilane molecules. While early silane-based monolayer work is based on Langmuir-Blodgett techniques, the first silane-based self-assembled monolayer was reported by Sagiv in 1980¹⁹. In general, a hydroxylated surface is introduced into a solution of a silane derivative in an organic solvent, but gas-phase methods have also been used¹¹. In all cases, thorough cleaning of the substrate is a must for obtaining a clean oxide layer with high density of silanol groups on the surface ($\sim 10^{15}$ per cm²)¹¹. Scheme 1 gives a schematic representation of the formation of a silane monolayer onto SiO_x surfaces. It should be noted that this chemistry is not limited to SiO_x surfaces; other hydroxylated oxides surfaces can be modified as well (e.g., Al₂O₃²⁰).

Also in the case of the surface functionalization of the SiO_x surfaces of SiNW-based devices the most applied method is silanization. Figure 2 gives an overview of the different silane derivatives that have been used, while Table 2 gives a number of examples of surface silanization, together with the target analytes. It should be noted that on planar SiO_x substrates more compounds have been used; here we aim to give an overview for SiNW-based devices only. Table 2 summarizes the first papers on SiNW-based sensor devices and selected papers that use other silanization methods. We have categorized the references in terms of pH sensors, biosensors, cation sensors and gas sensors. This way, the cited work does not only represent the diversity of silane compounds that have been used, it also shows the variation in further (bio)functionalization of SiNW-based devices.



Scheme 1. Schematic representation of the 1) cleaning/hydroxylation of the SiO_x surface, 2) silanization (here: silane **1a**, Figure 2), and 3) further functionalization with glutaraldehyde. It should be noted that the exact structure of the bonded silanes is arbitrary as also two or three silanol groups per attached molecule may have reacted with the surface hydroxyl groups. Here we adapted the scheme from Aswal et al.¹¹.

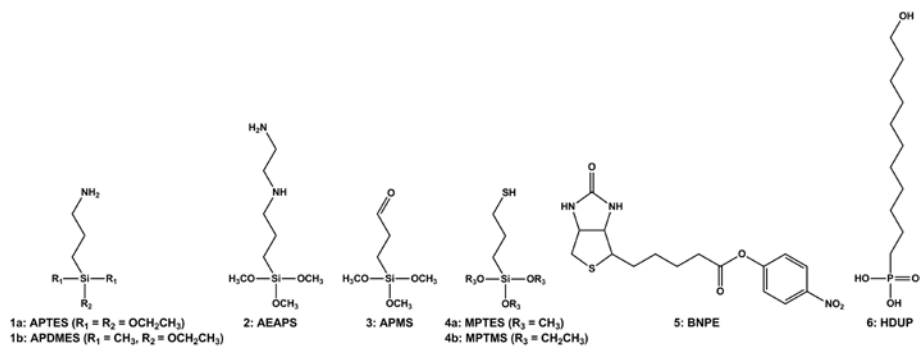


Figure 2. Compounds that have been used in the modification on SiO_x -coated NWs in NW-based devices: 3-aminopropyltriethoxysilane (APTES, 1a), (3-aminopropyl)-dimethylethoxysilane (APDMES, 1b), *N*-(2-aminoethyl)-3-aminopropyltrimethoxysilane (AEAPS, 2), 3-aldehydepropyltrimethoxysilane (APTMS, 3), mercaptopropyltriethoxysilane (MPTES, 4a), biotin 4-nitrophenyl ester (BNPE, 5) and 11-hydroxyundecyl-phosphonate (HDUP, 6).

Table 2. Examples of surface modifications on SiO_x-covered SiNW devices and target analytes. GA = Glutaraldehyde; EDC = 1-Ethyl-3-[3-dimethylaminopropyl]carbodiimide hydrochloride; PSA = Prostate specific antigen; ATP = Adenosine triphosphate; TNT = Trinitrotoluene; CRP = C-reactive protein; *The chemical structures of the silanes are given in Figure 2; **The silicon nanowires are covered with a layer of 10 nm Al₂O₃, grown by atomic layer deposition.

Sensor Type	Surface Modification*		Receptor	Analyte	Ref.
pH	SiO ₂			H ⁺	2
	APTES (1a)			H ⁺	2, 21, 22
	APTES (1a)		DNA-templated polymerization of aniline	H ⁺	23
Bio			Biotin	Streptavidin	2
	APTES (1a)		15-mer ss-DNA	Hybridization-induced charges in poly-T/poly-A 15-mer DNA	24
	APDMES (1b)		16-mer ss-DNA	Complementary DNA	22
	MPTMS (4b)		12-mer ss-DNA	Single mismatch	25
	APMS (3)		Monoclonal antibodies	PSA	26
	APMS (3)		Antibody	influenza	27
	APMS (3)		Tyrosine kinase	ATP	28
	APTES (1a)	GA	Estrogen receptors protein	Estrogen response elements	29
	APTES (1a)	GA	Anti-PSA	PSA	30
	APTES** (1a)	GA	Glucose oxidase	Glucose	20
	APTES (1a)	GA	Anti-CRP	CRP	31, 32
	APTES (1a)		EDC-supported carboxy-phenylboronic acid (CPBA)	Dopamine	33
	AEAPS (2)		Gold nanoparticles	Thiol-terminated enzyme	34
Cations	SiO ₂		Calmodulin	Ca ²⁺	2
	MPTES (4)			Hg ⁺ , Cd ⁺	35
	AEAPS (2)	GA	(phosphor)tyrosine	Ca ²⁺	36
	APMS (3)		Gly-Gly-His	Cu ²⁺	37
Gas	APTES (1a)			TNT	38

3-Aminopropyltriethoxysilane

The first paper of the Lieber group on SiNW-based devices shows the utilization of silane-based functionalization of SiO_x -coated nanowires². The devices were chemically modified with 3-aminopropyltriethoxysilane (APTES, Figure 2, silane 1a). The resulting devices showed a linear source-drain conductance versus pH-response for pH values from 2 to 9. The authors explained these results by the presence of both NH_3^+ and SiOH groups, which have different acid dissociation constants. At low pH, the amino group is protonated, and acts as a positive gate, which depletes hole carriers in the p-type SiNW and decreases the conductance. At high pH, the SiOH group is deprotonated, causing an increase in conductance. Ma et al. realized pH sensitivity via the enzymatic polymerization of aniline, which was templated by DNA on APTES²³ (Figure 3). The direct use of the stretched, immobilized DNA molecules as templates prevents the agglomeration of the polyaniline/DNA complexes formed in solution.

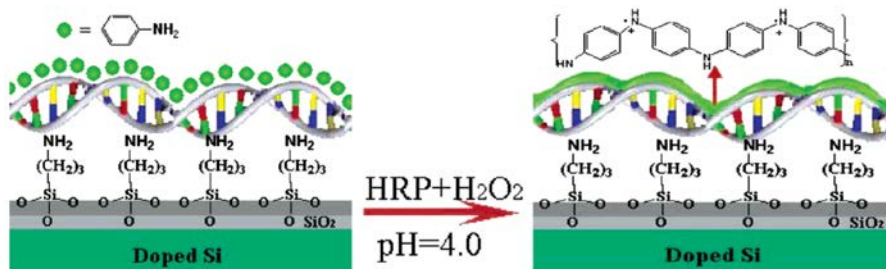


Figure 3. Fabrication of a polyaniline nanowire immobilized on a Si surface with stretched double-stranded DNA as a guiding template, resulting in pH sensitivity. HRP stands for horseradish peroxidase. Figure from reference 23.

Besides its use as sensitive layer in the detection of protons, recently APTES has also been used as sensing layer for the vapor-phase detection of 2,4,6-trinitrotoluene (TNT)³⁸. The sensing mechanism is based on the acid-base interaction between the amino-terminated nanowire surface and the

polarized TNT nitro groups, which have a weak basicity. The binding of electron-deficient TNT to the amino groups on the SiNW sensor surface is believed to result in the formation of charge-transfer complexes, which act as effective molecular gating elements. The conductance response of the resulting devices has a clear relation with the concentration of the explosive analytes and the device was found to be able to distinguish the target analyte from structurally related compounds. This example nicely shows that SiNW-based sensors are not only sensitive to changes in charges, but also to changes in charge density.

Given its reactivity towards aldehyde, carboxylic acid and epoxy functionalities, APTES has become the most frequently used linker compound for further (bio)functionalization of SiNWs. The activation procedure of the SiO_x nanowire surface using an oxygen plasma, followed by the immersion in a solution of APTES in ethanol and subsequent heating of the chip as reported by the Lieber group² is commonly used^{20, 32}. Alternative approaches have been reported as well, e.g., the use of UV/ozone for the surface activation, followed by the use of neat APTES³³. Also toluene³¹ and acetone²⁴ have been used as a solvent in the silanization step.

Because of the possibility of hydrogen bond formation between the amine of APTES and the SiO_x surface, both head and tail groups can be oriented towards the surface, which can result in a large disorder in APTES layers³⁹. Additionally, cross-linking between the alkoxy silane units may yield oligomerized silane structures on the surface, resulting in rough layers that are thicker than a monolayer. The optimal conditions for solvent-based silanization using APTES were investigated on planar surfaces⁴⁰. The morphology and growth kinetics of APTES films deposited from solutions were found to be affected by reaction time, solution concentration, and temperature. Experiments with an APTES concentration

of 1% only produced good films when the reaction was time-limited (1 h). Increasing the reaction time increased the APTES film thickness.

To overcome the problem of the disordered monolayers, Lin et al. performed a post-treatment of APTES-functionalized devices²⁴. After the APTES modification, they aligned the internal dipoles of the APTES molecules using high electric fields, thus decreasing the disorder in the monolayer. In addition, it is shown that the source-drain conductance of the APTES-functionalized devices changes upon UV illumination. The authors explained this by a strengthening effect of the internal APTES dipoles by UV illumination. Additionally, UV illumination excites extra charge carriers in the nanowire. Depending on the size of both effects, the resistance of the nanowire can be increased or decreased, which is measurable with the produced devices.

A modification that often follows the attachment of APTES to the SiO_x nanowire surface is the reaction with glutaraldehyde (Scheme 1, right). This linker molecule is used to form an aldehyde-terminated surface, which increases the possibilities for further reactions, including the reaction with amine groups of, e.g., anti-bodies³⁰, proteins and enzymes^{20, 29, 41}. Also amino-terminated, single-stranded DNA (ss-DNA) has been attached to APTES/GA-modified surfaces to measure hybridization induced mismatches in 15-mer ss-DNA chains²⁴. The addition of glutaraldehyde is, like that of APTES, both observed from solution^{29, 36} and from the gas phase²⁰.

Li et al. reported the functionalization of an APTES-coated thin oxide gate with a dopamine receptor³³. Although the devices do not belong to the class of SiNW-based sensors, the CMOS open-gate Field-Effect Transistor (FET) devices have (sub)micrometer gate dimensions. They have immobilized carboxyphenylboronic acid onto the APTES layer. The boronic acid group specifically reacts with the catechol functionality of, e.g., dopamine, which was detected in the femtomolar range.

Other Silane Derivatives

Apart from APTES, also other amino-terminated silane derivatives have been used. For example, (3-aminopropyl)-dimethyl-ethoxysilane (APDMES, Figure 2, silane 1b) has been used in the modification of SiNW-based devices to bind a 16-mer ss-DNA²². In contrast to APTES (1a), APDMES (1b) is a mono-alkoxydimethylsilane, which is a crucial difference when it comes to the monolayer quality. Although silanes with only alkoxy group can react with each other, oligomerization cannot take place. Consequently, the use of mono-alkoxydimethylsilanes results in the formation of a true monolayer. Very recently this issue was addressed in a detailed study by Dorvel et al. who synthesized an amino- and an epoxy-terminated mono-alkoxydimethylsilane, which were immobilized onto planer silicon oxide surfaces (Dorvel, 2010).

In addition, *N*-(2-aminoethyl)-3-aminopropyltrimethoxysilane (AEAPS, Figure 2, silane 2) has been applied to immobilize an amino acid³⁶. The nanowires devices were exposed to a solution of AEAPS in water, subsequently washed and finally dried to stimulate cross-linking of the molecules. This was followed by the reaction with glutaraldehyde to produce an aldehyde-terminated surface. Finally, tyrosine and phosphotyrosine were cross-linked with the aldehyde group through the formation of a Schiff base, which was further reduced to a stable secondary amine using sodium cyanoborohydride (NaBH_3CN). The studies, however, do not contain information on potential benefits of the alternative silanization agents used.

Some other functionalities rather than amino groups have been employed in silane chemistry (Figure 2, silanes 3 and 4). Apart from APTES, the Lieber group used 3-aldehydepropyltrimethoxysilane (APMS, Figure 2, silane 3)²⁶ to directly obtain an aldehyde-terminated surface.

Subsequently monoclonal antibodies were attached to detect prostate specific antigens (PSA). The use of APMS enabled them to make a thinner organic layer as compared to combining APTES with glutaraldehyde. As oxygen in air will slowly oxidize aldehydes to acids or peracids, it is advisable to work with freshly prepared APMS surfaces or to make use of the reaction of glutaraldehyde with an APTES surface, directly prior to further functionalization.

As a last example we mention the use of 3-mercaptopropyltriethoxysilane (MPTES, Figure 2, silane 4)³⁵, which was applied to detect Cd^{2+} and Hg^{2+} ions. The thiol-terminated devices showed a linear relation between the logarithm of the Cd^{2+} and Hg^{2+} concentration and the source-drain conductance. The response towards K^+ , Na^+ , Ca^{2+} , Ba^{2+} , and Mg^{2+} (hard Lewis acids) was considerably smaller as compared to Cd^{2+} and Hg^{2+} (soft Lewis acids). This can be explained by the chemical softness of thiol groups, which hardly coordinate with hard Lewis acids.

Alternative Approaches

In this paragraph we address two different types of non silane-based compounds that have been used in the chemical modification of SiO_x surfaces of SiNW-based devices. Hahm and Lieber report on the 4-(dimethylamino)pyridine (DMAP)-catalyzed transesterification of biotin 4-nitrophenyl ester with the hydroxyl groups of SiO_x nanowire surface⁴² (Figure 4, left). Afterwards, the devices were exposed to phosphate buffered saline (PBS) solution of avidin, which was followed by the addition of biotinylated peptide nucleic acid (PNA) capture probes. A generally benefit of the use of PNA over DNA is that it enables sensing in an ultra-low background due to the lack of charges on the peptide backbone. In the work of Hahm and Lieber the surfaces were not analyzed after each modification step. However, based on the electrical characteristics of the modified devices it can be concluded that the PNA

immobilization was successful. It has to be noted though that siloxane ester bonds (Si-O-(CO)) have a limited hydrolytic stability, at least lower than siloxane bonds (Si-O-Si). As a result, this immobilization technique is not often used.

Cattani-Scholz et al. investigated hydroxyalkylphosphonate monolayers as a platform for the biofunctionalization of silicon-based field effect sensor devices⁴³ (Figure 4, right). They employed a stepwise functionalization protocol using 11-hydroxyundecylphosphonate and a maleimide heterobifunctional linker system. The surface chemistry was also performed on planar surfaces, which made it possible to extensively analyze the surfaces after each step. It was found that the hydroxyalkylphosphonate monolayer effectively passivates the Si surface against electrochemical leakage current into the electrolyte solution through the interface, with maximum currents of the order of 10 pA measured at an applied voltage of 200 mV. In a comparative study it has been shown that phosphonate monolayers on the native oxide of Ti-6Al-4V are hydrolytically more stable than the corresponding siloxane monolayers⁴⁴. It is also reported that the monolayer growth is not limited by surface OH content,⁴⁵ making this type of surface modification an interesting alternative for silane-based chemistry.

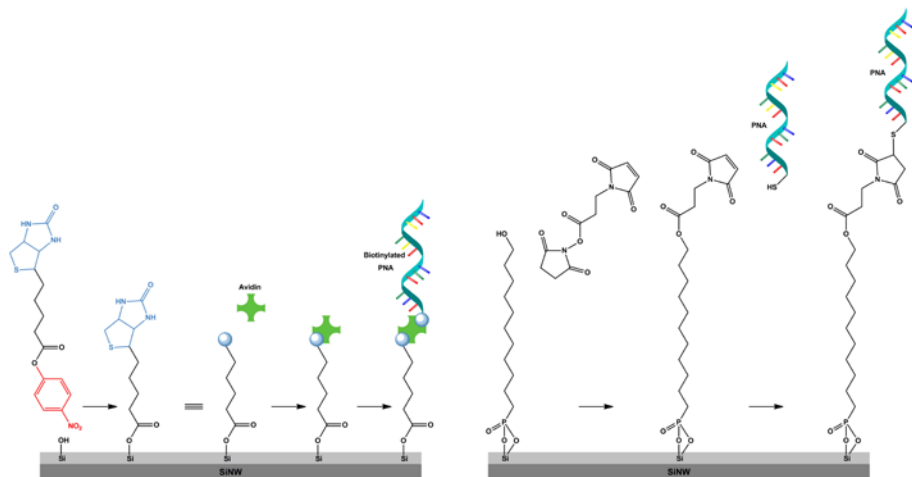


Figure 4. A schematic representation of two different surface chemistries that have been used to attach PNA onto SiO_x : (left) the use of biotin 4-nitrophenyl ester (the blue part of the structure indicates biotin molecule, whereas the red part of the structure indicates the 4-nitrophenyl group, which is used to activate the ester), the following steps involve the use of avidin and biotinylated PNA, and (right) the formation of organophosphonate monolayer, followed by the reactions with a maleimide heterobifunctional linker and subsequently with a thiolated PNA derivative.

2.2.2 Non-Covalent Functionalization

Adsorption of Polyelectrolytes

The negative nature of SiO_x at $\text{pH} > 3.5$ allows one to electrostatically immobilize positively charged polymers (polycations), also called generally polyelectrolytes (PEs). Subsequently a negatively charged polymer (polyanion) can be adsorbed on top. This is possible, since in layer-by-layer depositions after each deposition charge reversal occurs⁴⁶. This method is known as layer-by-layer (LbL) deposition⁴⁷. A variety of deposition methods can be used, including dip-coating, spin-coating, spray-coating and flow-based techniques.

Recently Ingebrandt and coworkers applied the LbL deposition technology onto SiNW-based devices⁴⁸. They immobilized polyallylamine

hydrochloride (PAH: MW 15,000) onto 6 nm thick, thermally grown SiO_x via dip coating. Subsequently polystyrenesulphonate (PSS: MW 60,000-80,000) was immobilized and this sequence was repeated several times to make a stack of 6 bilayers (Figure 5). The thickness of the resulting multilayer has not been reported. Assuming a monolayer thickness of $\sim 2 \text{ nm}$ ^{47, 49} the multistack thickness would be $\sim 24 \text{ nm}$. It has to be noted, however, that the salt concentration has an effect on the layer thickness⁵⁰, which makes it difficult to predict the thickness accurately. Although the noise level of PE-coated devices was slightly higher than that of their standard FET devices, the sensitivity for PE adsorption measurements was 3 to 4 times higher as compared to previous reports.

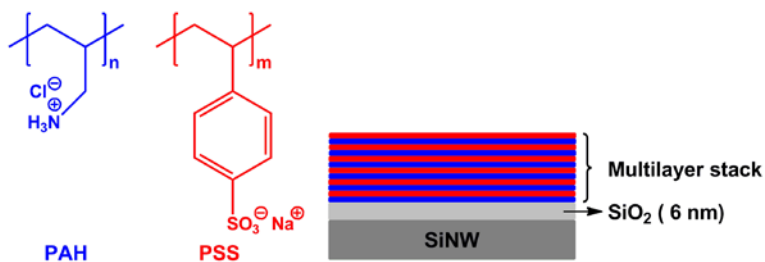


Figure 5. Structures of the polycation polyallylamine hydrochloride (PAH) and polyanion polystyrenesulphonate (PSS) used by Ingebrandt and coworkers to prepare layer-by-layer multilayers onto SiO_x -covered SiNW-based devices.

Dorvel et al. reported electrostatic-driven adsorption of poly-L-lysine (PLL) on hafnium oxide (HfOx)-covered SiNW FETs. HfOx was deposited to increase the electrical insulation of the SiNW surface to prevent current leakage of FET device. Its surface is also negatively charged as for SiOx at certain pH values, allowing electrostatic adsorption of PEs, like the positively charged PLL. The sensing of negatively charged single-stranded DNA (ssDNA) and its complementary strand was realized via adsorption to the already PLL modified SiNW FET. It was found that the use

of lower molecular weight PLL results in a higher density the adsorbed ssDNA layers and hence increasing the sensing sensitivity.

Supported Lipid Membranes

Silica surfaces have also been used as a platform to immobilize model membrane systems like supported lipid bilayers, which have been extensively used in understanding the fundamental properties of biological membranes. However, there have been only a few attempts to apply lipid membranes on nanoelectronic devices. Misra et al. incorporated lipid bilayer membranes into SiNW transistors (Figure 6). In more detail, they covered the NWs and the background oxide with a continuous lipid bilayer shell, forming a barrier between the SiO_x surface and solution species^{51, 52}. The method is based on the fusion of spherical unilamellar vesicles onto a SiNW surface producing a planar conformal lipid bilayer coating⁵³.

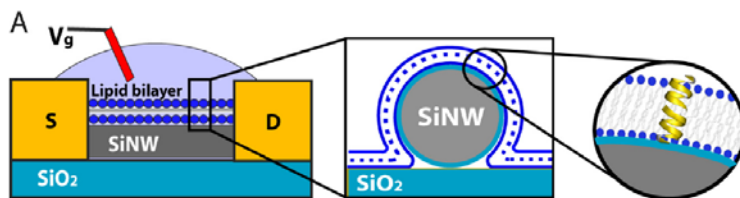


Figure 6. Device schematics showing a SiNW connected to microfabricated source (S) and drain (D) electrodes. Although this is not clear from the figure it should be noted that the source and drain are insulated with Si_3N_4 . The insets show the configuration of the lipid bilayer and a pore channel placed in the bilayer membrane. Figure from reference 51.

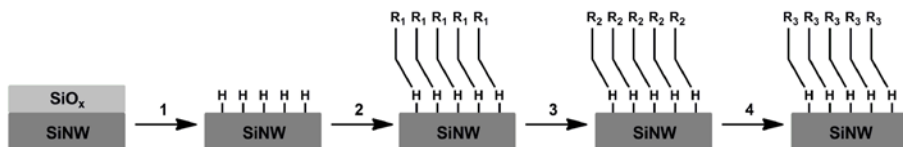
Cyclic voltammetry using potassium ferrocyanide ($\text{K}_4\text{Fe}(\text{CN})_6$) as a redox probe showed that the presence of a lipid bilayer on the NW surface reduced the limiting current by 85-95% relative to the native oxide-covered NW device⁵². Subsequently, two different transmembrane peptides (gramicidin A and alamethicin) were incorporated in the vesicles, resulting in ion channel-containing lipid bilayers after fusion with SiNW-based devices. It was shown that the incorporation of transmembrane peptide

pores ionic-to-electronic-signal-transduction was enabled by using voltage-gated and chemically gated ion transport through the membrane pores.

2.3 Oxide-Free SiNW-based Sensor Devices

2.3.1 Hydrosilylation

As an alternative to silane-based chemistry, silicon substrates can also be modified using so-called hydrosilylation chemistry, e.g., the reaction between a surface Si-H and an organic compound containing a terminal unsaturated carbon-carbon bond (alkenes and alkynes) to form a Si-C linked monolayer (Scheme 2).



Scheme 2. Schematic representation of the 1) etching of the SiO_x surface, yielding a H-terminated surface, 2) formation of Si-C monolayers via hydrosilylation (R₁ represents a functional group that is chemically protected towards the reaction with the H-terminated Si surface, e.g., an ester or amide), 3) deprotection the functional group (represented by R₂, e.g., a carboxylic acid or amine), 4) attachment of a receptor (represented by R₃).

This work has been pioneered by Linford and Chidsey in the early 1990s^{54, 55} and this type of monolayers has continued to attract attention ever since. Hydrosilylation chemistry requires removal of SiO_x, which in most cases is achieved using wet chemistry. On planar silicon surfaces diluted, aqueous HF and NH₄F solutions are used to etch Si(100) and Si(111) substrates, respectively, although a wide variety of etching methods has become available¹⁸. This process results in hydrogen-terminated, oxide-free silicon substrates with Si-H groups. The reaction of H-terminated silicon surfaces with alkenes and alkynes can be performed by making use of high temperatures, UV and visible light irradiation,

electrochemistry, hydrosilylation catalysts (e.g., AlCl_3), and chemomechanical scribing, as summarized in different reviews.^{12, 13, 56, 57}

2.3.2 Organic Monolayers: Si-C versus SiO_x -C

Si-C bonded monolayers have a number of advantages over silane-based monolayers on SiO_x surfaces. First, interface trap densities for Si-C bonded monolayers can be considered remarkably lower than in the case of alkyl chains organic monolayers on naturally oxidized silicon surfaces⁵⁸. Also, as already mentioned in §2.2.1, silane oligomerization can result in rough layers that are thicker than a monolayer. In contrast, the reaction between a H-terminated Si surface and alkenes or alkynes results in a true monolayer. This is related to the involved zipper mechanism, in which each binding of an alkyl chain directly generates a new radical site on the next-nearest Si surface atom⁵⁵. Moreover, the chemical stability of monolayers on SiO_x in aqueous media is poor since the exposure to water pilots the destruction of the monolayer through hydrolysis of Si-O bonds⁵⁹. Organic layers formed by hydrosilylation are stable in a number of environments, including boiling water, organic solvents, acids, and air^{55, 60}.

In the field of SiNW-based devices, the application of Si-C monolayers has a number of other benefits as compared to silane-based surface modifications. First, the removal of SiO_x brings a sensing event (target/analyte interaction) closer to the conducting surface, which increases the sensitivity of the device^{22, 61}. Secondly, the selective functionalization of oxide-free SiNWs is considered to be a supplementary factor that improves the detection sensitivity by avoiding the binding competition between the SiNW and the oxide surface on the rest of the device. Third, several studies show improved electrical properties of Si-C linked monolayers over monolayers on SiO_x , in terms of the flat-band potential and source-drain conductance^{62, 63}.

A crucial difference between the silane-based and alkene-based approach becomes clear from the preparation of amine-terminated monolayers. While in the case of SiO_x unprotected amines can be used, e.g., APTES (§2.2.1), amine-containing alkenes should be chemically protected as amines can react with H-terminated Si surfaces. The tert-butyloxycarbonyl (t-BOC, Figure 7, alkenes **7a** and **7b**) is a commonly used protecting group for primary amines, but other protecting groups have been used as well⁶⁴. Apart from amines, also carboxylic acid and alcohol functionalities should be protected before application in the hydrosilylation chemistry⁵⁶.

Characteristic of the Si-C bonded monolayers is that the molecular cross-section of the attached alkyl chain prevents reaction of all individual Si-H bonds i.e., upon formation of a monolayer on Si(111) about 50-55% of the Si-H sites has reacted⁶⁵, while on Si(100) this is about 30-35%⁶⁶. The remaining, unreacted Si-H sites are a potential source for the formation of interface states, e.g., via oxidation, which is an unfavorable process in terms of device performance.

2.3.3 Hydrosilylation on SiNW-based Sensor Devices

The reported chemistry for functionalizing the oxide-free, H-terminated SiNW sensor devices is mainly done with one method i.e., hydrosilylation catalyzed by UV irradiation. This approach has been applied by different research groups using different etching conditions and probing different types of analytes (Table 3).

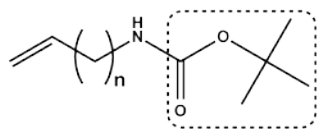
The first report on the modification of oxide-free SiNW-based devices is by Heath and coworkers²². The authors followed an established, multistep protocol^{67, 68} that starts with the hydrosilylation of H-terminated SiNWs with tert-butyl allylcarbamate (Figure 7, alkene **7a**) irradiated at 254 nm (Scheme 4.1). After deprotection, the researchers obtained a

positively charged amine-terminated monolayer on the SiNWs, enabling the adsorption of negatively charged, oligo ss-DNA.

Surface characterization of the nanowires embedded in a device is a challenge, since conventional analytical tools used for surface characterization requires substrate on the micro-scale. For that reason a widely used strategy is to perform the applied chemistry also on planar samples.

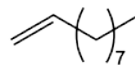
Table 3. Overview of the references that report on the chemical modification of the SiNW-based devices via hydrosilylation chemistry. * The chemical structures of the alkenes are given in Figure 7.

Analyte	Receptor	Alkene*	Oxide	Etching Conditions	Reference
ss-DNA	ss-DNA	7a	native	2% HF _{aq} (3 s)	²²
K ⁺ , Na ⁺	Crown Ether	7b	5-10 nm	1% HF _{aq} (50 s) + NH ₄ F _{aq} (60 s)	⁶⁹
ss-DNA	ss-PNA	7b	~ 5 nm	1% HF _{aq} (50 s) + NH ₄ F _{aq} (60 s)	^{61, 70}
Avidin/ Streptavidin	Biotin	7b	not reported	10:1 v/v 40% NH ₄ F _{aq} / 49% HF _{aq} (5 s)	⁷¹
Antigen	Antibody	7b			
-	-	8, 9			
DPCP		10	not reported	HF	⁷²

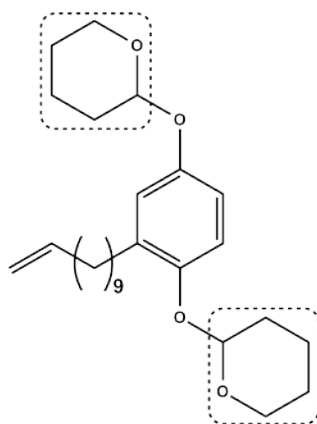


7a: Tert-butyl allylcarbamate (n=1)

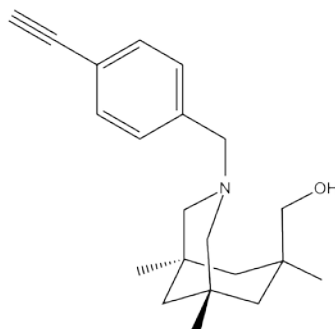
7b: 10-*N*-Boc-amino-dec-1-ene (n=8)



9: 1-Decene



8: Tetrahydropyranyl-terminated alkene



**10: Alkyne derivative
(receptor for
diphenylchlorophosphate)**

Figure 7. Alkene and alkyne derivatives that have been chemically bound on oxide-free SiNW sensor devices. The protecting groups on various alkenes are marked in dashed lines. For alkene **7a** and **7b** the protecting group is *N*-tert-butoxycarbonyl (t-BOC), for alkene **8** it is the tetrahydropyranyl (THP) group. See text for further information.

This strategy was also followed by Bunimovich et al. and the planar Si(100) samples were analyzed by water contact angle and X-ray Photoelectron Spectroscopy measurements. Moreover, this interesting paper compares Si-C and SiO_x-based monolayers. It is shown that the electrical read-out of oxide-free SiNW for sensing of 16-mer complementary oligo-DNA was more profound than on SiNW with native oxide.

Also Zhang et al. used hydrosilylation chemistry to coat SiNW devices with ss-DNA, although a different strategy was chosen^{61, 70}. The modification scheme starts with the UV-initiated attachment of 10-*N*-boc-

amino-dec-1-ene (Figure 7, alkene **7b**) to a device with H-terminated SiNWs. After the deprotection of the amino groups the surface was chemically modified with glutaraldehyde, allowing the covalent binding of amino-terminated compounds. Inspired by the work of others on devices with SiO_x nanowires^{37, 42, 73}, they subsequently immobilized PNA. The benefit of this approach over the method reported by Bunimovich et al. is twofold: PNA is not only neutral (see also §2.2.1), it is also bonded covalently. Although multivalent, ionic interactions might be stronger than one single covalent bond, the latter is independent of the salt concentration, making it more robust in wide range of chemically different environments.

As for sample characterization the research group was quite successful in depicting the chemistry performed on the SiNWs. Transmission electron microscopy (TEM) was performed for morphological study of non-oxidized SiNW surface. From the TEM data the authors concluded that the surface was nearly uniform, oxide free and did not show visible TEM-detectable defects. In addition, binding of fluorescently labeled, complementary DNA was used to demonstrate the selectivity of the non-oxidized SiNW surface chemistry and the specificity of PNA-DNA hybridization. Indeed, strong fluorescent signals on the SiNWs were obtained and the bright arrays of SiNWs were clearly visible (Figure 8).

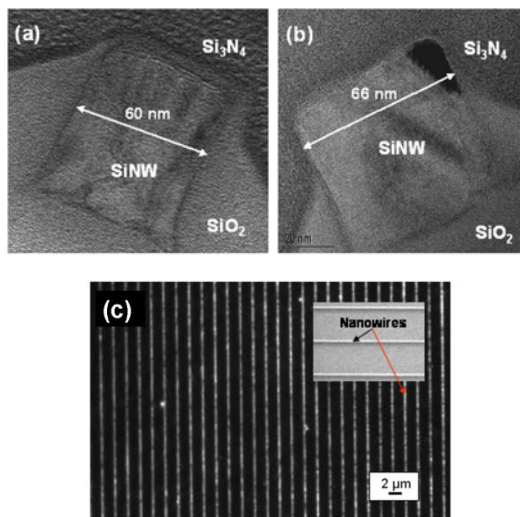
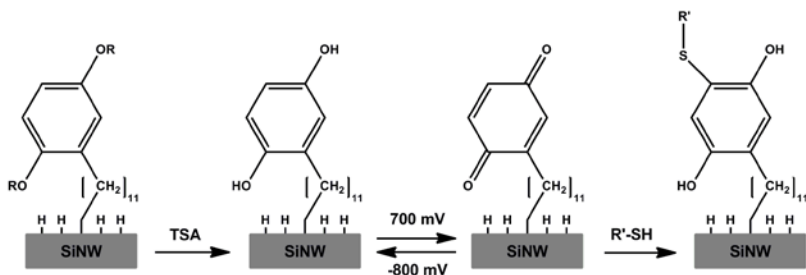


Figure 8. Cross-sectional TEM micrographs of SiNWs before and after HF and NH_4F etching: (a) SiO_x layer coated on the SiNW surface prior to etching, (b) hydrogen-terminated SiNW after etching. (c) Fluorescent images of Cy3-labeled complementary DNA hybridized to the PNA-functionalized SiNWs. Inset shows SEM micrograph of SiNW arrays. Figure from reference 59.

Earlier work by Zhang et al. focused on the sensing of alkali metal ions by the chemical modification of SiNW-based devices with crown ethers⁶⁹. Also in this case alkene **7b** was used, followed by the reaction with glutaraldehyde, resulting in an aldehyde-terminated monolayer. Subsequently, amine-terminated crown ethers were covalently attached. Based on the complexation selectivity of crown ether to alkali metal ions, the resulting functionalized oxide-free SiNW-based devices could detect Na^+ and K^+ .

The sensitivity of protein binding by oxide-free SiNW-based FETs was first reported by Stern et al. using biotin-avidin/streptavidin interactions and antibody-antigen sensing¹¹. Three different functionalized alkene derivatives were used in the UV-initiated reaction with H-terminated SiNW devices: 10-*N*-*boc*-amino-dec-1-ene (**7b**), 2-[2-(undec-10-

enyl)-4-(tetrahydro-2H-pyran-2-yloxy)phenoxy] tetrahydro-H-pyran containing a tetrahydropyran (THP) protecting group (**8**), and 1-decene (**9**). Only alkene **7b** could be realized for sensing purposes, whereas modification with alkene **8** was ineffective for sensing and alkene **9** aimed as a control. Using alkene **7b**, amino-terminated monolayers were obtained, followed by a common biotinylation protocol using N-hydroxysulfosuccinimide (sulfo-NHS) for capturing avidin and streptavidin. For antibody-antigen sensing the capture antibodies were bound to hydrosilylated SiNWs by NHS/ethylene dicarbodiimide coupling chemistry⁷⁴. The strategy for protein binding using alkene **8** is different and more complicated, yet very appealing. That is because it creates electrochemically active monolayers on top of the SiNWs. Such electro-active monolayers ensure not only the monolayer formation qualitatively, but they also allow the quantification of the surface coverage. This is based on the fact that the required electrons for the reduction of the electro-active moiety can be measured. The number of electrons is directly proportional to the number of the electro-active groups present and hence to the coverage. As a first step THP protected alkene **8** was photochemically bound to hydrogen-terminated SiNW. Removal of the protecting THP ethers under mild conditions of 1% toluene sulfonic acid (TSA) in methanol leads to the hydroquinone (Scheme 3). Cyclic voltammetry (CV) in PBS oxidized the hydroquinone to quinone. Finally, they aimed to couple thiolated biotin selectively to the thus formed quinone moieties, but this was not successful, most likely due to the degradation of the device performance that was observed upon chemical modification.



Scheme 3. The strategy reported by the Heath group⁶⁸ and also investigated by the Reed group⁷¹ for the selective immobilization of thiolated biotin ($R'-SH$) via a Michael addition. TSA stands for 1% toluene sulfonic acid. See text for further explanation.

While after UV-induced hydrosilylation with alkenes **7b** and **9** the devices experienced increased leakage, alkene **8** led to loss of gating behavior, most likely due to the formation of redox-active surface traps. For compound **7b** the authors report a device yield as low as <2% after the deprotection. The work of Stern et al. highlights the importance of validating the device performance after chemical modification.

Work done by the Simonato group covers an example of hydrosilylation using alkynes.^{72, 75} The reaction of H-terminated SiNWs and nanoribbons with alkyne **10** (Fig. 7) results in a sensor for sarin-like gases, as diphenylchlorophosphate (DPCP). Using this method the researchers demonstrated the fabrication of a portable sensor prototype for nervous gases exploiting SiNW FET devices.⁷²

2.3.4 Electrografting of Diazonium Salts

In addition to the hydrosilylation of alkenes and alkynes, electrografting of diazonium salts was reported as another method for the surface modification of oxide-free H-terminated Si surfaces. Electrografting of diazonium salts on oxide-free silicon was pioneered in 1997 by de Villeneuve et al.⁷⁶ An extensive review on different modification strategies with complex molecular assemblies lists (electro)grafting with diazonium

salts among the most popular developing routes for surface modification.⁷⁷ Very recently this type of chemistry was applied to the surface of SiNW-based devices by Azmi et al.⁷⁸ (Fig. 9).

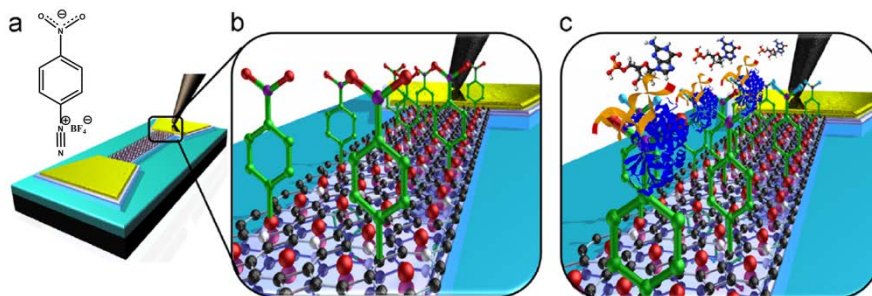


Figure 9. An illustration of a SiNW biosensor for detection of prostate cancer biomarker, adapted from reference 76. (a) A scheme of SiNW device with 4-nitrobenzenediazonium salt, (b) a monolayer of covalently attached 4-nitrobenzene, and (c) attachment of 8-OHdG to the amine-terminated SiNW surface.

The researchers used cyclic voltammetry (CV) to, firstly, electrograft 4-nitrobenzene diazonium to SiNWs and, secondly, to electroreduce the nitro groups to amino groups. For biosensing experiments amino-terminated SiNW devices were covalently modified with antibodies that target against the prostate cancer risk biomarker, 8-hydroxydeoxyguanosine (8-OHdG). Azmi and co-workers showed a set of XPS, AFM and contact angle results to follow the different steps in the surface modification scheme. Detection of the biomarker concentrations as low as 1 ng/ml (i.e. 3.5 nM) was demonstrated. Also, a portable hand-held read-out was introduced as an example of utilizing SiNW-based sensors in point-of-care (POC) diagnostics. This type of chemistry was extensively explored on planar silicon surfaces in Chapter 3 of this thesis.

2.3.5 Organic Monolayers on oxide-free SiNW devices: towards sensing

The observation of changes in device performance upon chemical modification of its sensing area has not only been reported by Stern et al., but also in a few other cases. Yet there is evidence that even non-charged molecules adsorbed on the nanowire alter the device characteristics. Haick et al. showed an improved conductance of the H-terminated SiNWs upon the chlorination/alkylation of the nanowire⁷⁹. They reported that methyl-terminated SiNWs exhibit higher source-drain conductance values, lower surface defect levels and higher on-off ratios than oxygenated SiNWs. Most recent work by the group of Haick explored detailed electrical characteristics of SiNW-based devices modified with butyl, 1,3-dioxane-2-ethyl, propyl-alcohol functionalities by the same chlorination/alkylation method.⁸⁰ The amounts of surface states and surface charge of the SiNW FET devices were significantly affected by the adsorption of molecular layers.

Another example of characterizing the surface passivation of a NW prior to sensing is the work of Masood et al.⁸¹. An improved device behavior after hydrosilylation on SiNW with 1-octadecene has been shown by means of capacitance-voltage and current-front-gate voltage electrical measurements. Based on other studies showing that H-Si (111) surfaces have the lowest reported surface recombination velocity and improved electronic performance as compared to Si (100) surfaces with SiO₂ interfaces, the authors stress the importance of using Si(111) surface to further improve the Si-NW biosensor performance.

2.4 Concluding Remarks and Outlook

In order to bind (bio)receptor molecules onto SiNW-based devices, most studies apply the silanization on the nanowire oxide layer. Clearly APTES is the most frequently used silane-based agent, enabling the subsequent immobilization of carboxylic acid- or aldehyde-terminated biomolecules. More often, further derivativization with glutaraldehyde has been applied to bind chemically amine-terminated biomolecules. A disadvantage of silane compounds is their ability to react with each other via cross-linking of the alkoxy units, resulting in rough, unordered multilayers. Based on the optimization studies on planar silica substrates that have become available⁴⁰ and reports on the quality differences between vapour- and wet chemistry-prepared APTES layers⁸², there is room for the improvement of silane chemistry on SiNW-based devices. Phosphonate monolayers are an interesting alternative for silane-based monolayers, due to their higher hydrolytical stability and the less critical pretreatment of the oxide surface that is required.

Apart from covalent functionalization of SiNW-based sensor devices also physisorption has been studied, which also enabled the detection of several compounds and ions. Covalent attachment of (bio)molecules to sensor surfaces may be appealing in terms of device stability, but some systems, e.g., membrane receptors require a more dynamic environment. It has been shown that a phospholipid monolayer can be covalently immobilized on SiO_x ⁸³ and Si-H ⁸⁴ surfaces, enabling the non-covalent immobilization of a second phospholipid layer. However, this strategy may hamper the fluidic properties of the bilayer, which is vital for the incorporation of biologically active structures into the membrane. The fusion of spherical unilamellar vesicles onto surfaces overcomes this problem. So far, only two different transmembrane ion channels on SiNW-based devices have been reported⁵², but lipid bilayers provide a matrix for

a virtually unlimited number of transmembrane proteins that can provide different functionalities.

Physisorbed PE layers are not covalently attached; nevertheless they are very stable, due to the multivalent character of the interaction. The multivalency is also beneficial regarding the detection of a PE that adsorbs onto the SiNW-based device. LbL films of PE have been employed for various applications, including electrochemical sensing and biosensing and they have also contributed to the investigation of fundamental studies in electrochemistry⁸⁵. The work of Ingebrandt and coworkers⁴⁸ can now be extended to the use of biologically relevant PEs and perhaps also the incorporation of nanoparticles.

An interesting candidate to replace SiO_x layers on silicon surfaces is found in alkene-prepared organic monolayers. There are a number of benefits for monolayers on oxide-free silicon over silane-based layers: a) no risk of oligomerization, resulting in a true monolayer, b) higher chemical stability, c) selective functionalization, i.e., the background surface is not functionalized, and d) a lower density of interface traps. Although a wide variety of preparation procedures for hydrosilylation surface chemistry are available, so far only UV-initiated methods have been used in the chemical modification of oxide-free H-terminated SiNW devices. This can be explained by the fact that the research in this direction is still in its early days, and it probably will not take long before some of the other available preparation methods will be explored on SiNW-based devices. An important issue in this regard is the surface orientation of the nanowire⁶⁸. In addition, a very good monolayer quality is needed, reducing the number of interfacial defects⁸⁶. In contrast to SiO_x-covered SiNW-based devices, the insulating properties in the case of oxide-free SiNW-based devices are exclusively to be realized by the organic monolayer itself. One possibility to improve the monolayer quality is by using alkynes instead of alkenes.⁸⁷⁻⁸⁹ Electrografting of diazonium salts is

another oxide-free modification strategy with great potential for biosensing applications especially for multi-array assays.

To conclude, selective functionalization of the nanowires is critical to retain sensitivity as the modification of the background oxide results in a reduced sensitivity. In addition, the modification of individual nanowires that are part of a larger array is essential to perform a multi-analysis using a single device. Continued advances in the preparation of well-defined, defect-free, organic-semiconductor interfaces will further improve the performance of SiNW-based devices. The combination of an increasingly growing number of interesting (bio)receptors, with sophisticated device fabrication methods, improved electrical characterization procedures and advanced organic surface modification does not only provide unlimited research opportunities, it will also contribute significantly to diverse, highly usable sensor applications in a variety of fields.

References

1. Y. Cui and C. M. Lieber, *Science*, **2001**, *291*, 851-853.
2. Y. Cui, Q. Q. Wei, H. K. Park and C. M. Lieber, *Science*, **2001**, *293*, 1289-1292.
3. J. Wan, S. R. Deng, R. Yang, Z. Shu, B. R. Lu, S. Q. Xie, Y. F. Chen, E. Huq, R. Liu and X. P. Qu, *Microelectron Eng*, **2009**, *86*, 1238-1242.
4. L. C. P. M. de Smet, D. Ullien, M. Mescher and E. J. R. Sudhölter, in *Nanowires - Implementations and Applications*, ed. A. Hashim, InTech, Rijeka, Croatia, **2011**, pp. 267-288.
5. M. Mescher, ISBN: 978-94-91909-00-9, TU Delft, **2014**.
6. N. S. Ramgir, Y. Yang and M. Zacharias, *Small*, **2010**, *6*, 1705-1722.
7. Y. Li, F. Qian, J. Xiang and C. M. Lieber, *Mater Today*, **2006**, *9*, 18-27.
8. E. T. Carlen and A. van den Berg, *Lab Chip*, **2007**, *7*, 19-23.
9. F. Patolsky, G. F. Zheng and C. M. Lieber, *Anal Chem*, **2006**, *78*, 4260-4269.
10. E. Stern, A. Vacic and M. A. Reed, *IEEE T Electron Dev*, **2008**, *55*, 3119-3130.
11. D. K. Aswal, S. Lenfant, D. Guerin, J. V. Yakhmi and D. Vuillaume, *Anal Chim Acta*, **2006**, *568*, 84-108.

12. M. Stutzmann, J. A. Garrido, M. Eickhoff and M. S. Brandt, *Phys Status Solidi A*, **2006**, *203*, 3424-3437.
13. R. J. Hamers, *Annu Rev Anal Chem*, **2008**, *1*, 707-736.
14. A. K. Wanekaya, W. Chen, N. V. Myung and A. Mulchandani, *Electroanalysis*, **2006**, *18*, 533-550.
15. J. N. Tey, I. P. M. Wijaya, J. Wei, I. Rodriguez and S. G. Mhaisalkar, *Microfluid Nanofluidics*, **2010**, *9*, 1185-1214.
16. M. W. Shao, D. D. D. Ma and S. T. Lee, *Eur J Inorg Chem*, **2010**, 4264-4278.
17. A. Cao, E. Sudhölter and L. de Smet, *Sensors*, **2014**, *14*, 245.
18. X. G. Zhang, *Electrochemistry of Silicon and its Oxide*, Kluwer Academic/Plenum Publishers, New York, **2001**.
19. J. Sagiv, *J Am Chem Soc*, **1980**, *102*, 92-98.
20. X. H. Wang, Y. Chen, K. A. Gibney, S. Erramilli and P. Mohanty, *Appl Phys Lett*, **2008**, *92*, 3.
21. Y. Chen, X. H. Wang, S. Erramilli, P. Mohanty and A. Kalinowski, *Appl Phys Lett*, **2006**, *89*.
22. Y. L. Bunimovich, Y. S. Shin, W. S. Yeo, M. Amori, G. Kwong and J. R. Heath, *J Am Chem Soc*, **2006**, *128*, 16323-16331.
23. Y. Ma, J. Zhang, G. Zhang and H. He, *J Am Chem Soc*, **2004**, *126*, 7097-7101.
24. M. C. Lin, C. J. Chu, L. C. Tsai, H. Y. Lin, C. S. Wu, Y. P. Wu, Y. N. Wu, D. B. Shieh, Y. W. Su and C. D. Chen, *Nano Lett*, **2007**, *7*, 3656-3661.
25. Z. Li, Y. Chen, X. Li, T. I. Kamins, K. Nauka and R. S. Williams, *Nano Lett*, **2004**, *4*, 245-247.
26. G. F. Zheng, F. Patolsky, Y. Cui, W. U. Wang and C. M. Lieber, *Nat Biotechnol*, **2005**, *23*, 1294-1301.
27. F. Patolsky, G. F. Zheng, O. Hayden, M. Lakadamyali, X. W. Zhuang and C. M. Lieber, *Proceedings of the National Academy of Sciences of the United States of America*, **2004**, *101*, 14017-14022.
28. W. U. Wang, C. Chen, K. H. Lin, Y. Fang and C. M. Lieber, *Proceedings of the National Academy of Sciences of the United States of America*, **2005**, *102*, 3208-3212.
29. G. J. Zhang, M. J. Huang, Z. H. H. Luo, G. K. I. Tay, E. J. A. Lim, E. T. Liu and J. S. Thomsen, *Biosens Bioelectron*, **2010**, *26*, 365-370.
30. A. Kim, C. S. Ah, H. Y. Yu, J. H. Yang, I. B. Baek, C. G. Ahn, C. W. Park, M. S. Jun and S. Lee, *Appl Phys Lett*, **2007**, *91*, 3.
31. P. E. Lobert, D. Bourgeois, R. Pampin, A. Akheyar, L. M. Hagelsieb, D. Flandre and J. Remacle, *Sens Actuators, B*, **2003**, *92*, 90-97.
32. F. Patolsky, G. F. Zheng and C. M. Lieber, *Nat Protoc*, **2006**, *1*, 1711-1724.
33. D. C. Li, P. H. Yang and M. S. C. Lu, *IEEE T Electron Dev*, **2010**, *57*, 2761-2767.

34. J. T. Sheu, C. C. Chen, P. C. Huang, Y. K. Lee and M. L. Hsu, *Jpn J Appl Phys* **1**, **2005**, *44*, 2864-2867.
35. L. B. Luo, J. S. Jie, W. F. Zhang, Z. B. He, J. X. Wang, G. D. Yuan, W. J. Zhang, L. C. M. Wu and S. T. Lee, *Appl Phys Lett*, **2009**, *94*, 3.
36. X. Y. Bi, W. L. Wong, W. J. Ji, A. Agarwal, N. Balasubramanian and K. L. Yang, *Biosens Bioelectron*, **2008**, *23*, 1442-1448.
37. X. Y. Bi, A. Agarwal, N. Balasubramanian and K. L. Yang, *Electrochem Commun*, **2008**, *10*, 1868-1871.
38. Y. Engel, R. Elnathan, A. Pevzner, G. Davidi, E. Flaxer and F. Patolsky, *Angew Chem Int Ed*, **2010**, *49*, 6830-6835.
39. E. T. Vandenberg, L. Bertilsson, B. Liedberg, K. Uvdal, R. Erlandsson, H. Elwing and I. Lundstrom, *J Colloid Interface Sci*, **1991**, *147*, 103-118.
40. J. A. Howarter and J. P. Youngblood, *Langmuir*, **2006**, *22*, 11142-11147.
41. M. H. Lee, K. N. Lee, S. W. Jung, W. H. Kim, K. S. Shin and W. K. Seong, *Int J Nanomedicine*, **2008**, *3*, 117-124.
42. J. Hahm and C. M. Lieber, *Nano Lett*, **2004**, *4*, 51-54.
43. A. Cattani-Scholz, D. Pedone, M. Dubey, S. Neppi, B. Nickel, P. Feulner, J. Schwartz, G. Abstreiter and M. Tornow, *ACS Nano*, **2008**, *2*, 1653-1660.
44. B. M. Silverman, K. A. Wiegand and J. Schwartz, *Langmuir*, **2005**, *21*, 225-228.
45. E. L. Hanson, J. Schwartz, B. Nickel, N. Koch and M. F. Danisman, *J Am Chem Soc*, **2003**, *125*, 16074-16080.
46. M. J. Schöning, M. H. Abouzar and A. Poghosian, *J Solid State Electrochem*, **2009**, *13*, 115-122.
47. G. Decher, *Science*, **1997**, *277*, 1232-1237.
48. X. T. Vu, R. Stockmann, B. Wolfrum, A. Offenhaesser and S. Ingebrandt, *Phys Status Solidi A*, **2010**, *207*, 850-857.
49. A. Poghosian, M. H. Abouzar, F. Amberger, D. Mayer, Y. Han, S. Ingebrandt, A. Offenhausser and M. J. Schöning, *Biosens Bioelectron*, **2007**, *22*, 2100-2107.
50. G. Decher and J. Schmitt, *Progr Colloid Polym Sci*, **1992**, *89*, 160-164.
51. J. A. Martinez, N. Misra, Y. M. Wang, P. Stroeve, C. P. Grigoropoulos and A. Noy, *Nano Lett*, **2009**, *9*, 1121-1126.
52. N. Misra, J. A. Martinez, S. C. J. Huang, Y. M. Wang, P. Stroeve, C. P. Grigoropoulos and A. Noy, *Proceedings of the National Academy of Sciences of the United States of America*, **2009**, *106*, 13780-13784.
53. S. C. J. Huang, A. B. Artyukhin, J. A. Martinez, D. J. Sirbully, Y. Wang, J. W. Ju, P. Stroeve and A. Noy, *Nano Lett*, **2007**, *7*, 3355-3359.

54. M. R. Linford and C. E. D. Chidsey, *J Am Chem Soc*, **1993**, *115*, 12631-12632.
55. M. R. Linford, P. Fenter, P. M. Eisenberger and C. E. D. Chidsey, *J Am Chem Soc*, **1995**, *117*, 3145-3155.
56. J. M. Buriak, *Chem Rev*, **2002**, *102*, 1271-1308.
57. S. Ciampi, J. B. Harper and J. J. Gooding, *Chem Soc Rev*, **2010**, *39*, 2158-2183.
58. S. Kar, C. Miramond and D. Vuillaume, *Appl Phys Lett*, **2001**, *78*, 1288-1290.
59. M. Calistri-Yeh, E. J. Kramer, R. Sharma, W. Zhao, M. H. Rafailovich, J. Sokolov and J. D. Brock, *Langmuir*, **1996**, *12*, 2747-2755.
60. S. F. Bent, *Surf Sci*, **2002**, *500*, 879-903.
61. G. J. Zhang, J. H. Chua, R. E. Chee, A. Agarwal, S. M. Wong, K. D. Buddharaju and N. Balasubramanian, *Biosens Bioelectron*, **2008**, *23*, 1701-1707.
62. E. J. Faber, L. C. P. M. de Smet, W. Olthuis, H. Zuilhof, E. J. R. Sudhölter, P. Bergveld and A. van den Berg, *ChemPhysChem*, **2005**, *6*, 2153-2166.
63. A. Vilan, O. Yaffe, A. Biller, A. Salomon, A. Kahn and D. Cahen, *Adv Mater*, **2010**, *22*, 140-159.
64. A. B. Sieval, R. Linke, G. Heij, G. Meijer, H. Zuilhof and E. J. R. Sudhölter, *Langmuir*, **2001**, *17*, 7554-7559.
65. A. B. Sieval, B. van den Hout, H. Zuilhof and E. J. R. Sudhölter, *Langmuir*, **2001**, *17*, 2172-2181.
66. A. B. Sieval, R. Linke, H. Zuilhof and E. J. R. Sudhölter, *Adv Mater*, **2000**, *12*, 1457-1460.
67. J. A. Streifer, H. Kim, B. M. Nichols and R. J. Hamers, *Nanotechnology*, **2005**, *16*, 1868-1873.
68. Y. L. Bunimovich, G. L. Ge, K. C. Beverly, R. S. Ries, L. Hood and J. R. Heath, *Langmuir*, **2004**, *20*, 10630-10638.
69. G. J. Zhang, A. Agarwal, K. D. Buddharaju, N. Singh and Z. Q. Gao, *Appl Phys Lett*, **2007**, *90*.
70. G. J. Zhang, G. Zhang, J. H. Chua, R. E. Chee, E. H. Wong, A. Agarwal, K. D. Buddharaju, N. Singh, Z. Q. Gao and N. Balasubramanian, *Nano Lett*, **2008**, *8*, 1066-1070.
71. E. Stern, J. F. Klemic, D. A. Routenberg, P. N. Wyrembak, D. B. Turner-Evans, A. D. Hamilton, D. A. LaVan, T. M. Fahmy and M. A. Reed, *Nature*, **2007**, *445*, 519-522.
72. S. Clavaguera, N. Raoul, A. Carella, M. Delalande, C. Celle and J. P. Simonato, *Talanta*, **2011**, *85*, 2542-2545.
73. T. Strother, R. J. Hamers and L. M. Smith, *Nucleic Acids Res*, **2000**, *28*, 3535-3541.
74. G. T. Hermanson, *Bioconjugate Techniques*, Elsevier Science & Technology Books, New York, 2nd Edition edn., **2008**.

75. V. Passi, F. Ravaux, E. Dubois, S. Clavaguera, A. Carella, C. Celle, J. P. Simonato, L. Silvestri, S. Reggiani, D. Vuillaume and J. P. Raskin, *IEEE Electr Device Lett*, **2011**, *32*, 976-978.
76. C. H. de Villeneuve, J. Pinson, M. C. Bernard and P. Allongue, *J. Phys Chem B*, **1997**, *101*, 2415-2420.
77. J. J. Gooding and S. Ciampi, *Chem Soc Rev*, **2011**, *40*, 2704-2718.
78. M. A. Mohd Azmi, Z. Tehrani, R. P. Lewis, K. A. Walker, D. R. Jones, D. R. Daniels, S. H. Doak and O. J. Guy, *Biosens Bioelectron*, **2014**, *52*, 216-224.
79. H. Haick, P. T. Hurley, A. I. Hochbaum, P. D. Yang and N. S. Lewis, *J Am Chem Soc*, **2006**, *128*, 8990-8991.
80. M. Y. Bashouti, M. Pietsch, K. Sardashti, G. Brønstrup, S. W. Schmitt, S. K. Srivastava, J. Ristein, J. Arbiol, H. Haick and S. Christiansen, in *Nanowires - Recent Advances*, ed. X. Peng, InTech, **2012**.
81. M. N. Masood, S. Chen, E. T. Carlen and A. v. d. Berg, *ACS Appl Mater Interfaces*, **2010**, *2*, 3422-3428.
82. S. Fiorilli, P. Rivolo, E. Descrovi, C. Ricciardi, L. Pasquardini, L. Lunelli, L. Vanzetti, C. Pederzoli, B. Onida and E. Garrone, *J Colloid Interface Sci*, **2008**, *321*, 235-241.
83. S. Heyssel, H. Vogel, M. Sanger and H. Sigrist, *Protein Sci*, **1995**, *4*, 2532-2544.
84. A. Charrier, T. Mischki and G. P. Lopinski, *Langmuir*, **2010**, *26*, 2538-2543.
85. F. N. Crespilho, V. Zucolotto, O. N. Oliveira Jr. and F. C. Nart, *Int J Electrochem Sci*, **2006**, *1*, 194-214.
86. O. Seitz, T. Bocking, A. Salomon, J. J. Gooding and D. Cahen, *Langmuir*, **2006**, *22*, 6915-6922.
87. L. Scheres, M. Giesbers and H. Zuilhof, *Langmuir*, **2010**, *26*, 10924-10929.
88. A. B. Sieval, R. Opitz, H. P. A. Maas, M. G. Schoeman, G. Meijer, F. J. Vergeldt, H. Zuilhof and E. J. R. Sudhölter, *Langmuir*, **2000**, *16*, 10359-10368.
89. E. J. Faber, L. C. P. M. de Smet, W. Olthuis, H. Zuilhof, E. J. R. Sudhölter, P. Bergveld and A. van den Berg, Veldhoven, the Netherlands, **2005**.

Chapter 3

Controlled Amino-functionalization by Electrochemical Reduction of Bromo and Nitro Azo Benzene Layers Bound to Si(111) Surfaces

Abstract

4-Nitrobenzenediazonium (4-NBD) and 4-bromobenzenediazonium (4-BBD) salts were grafted electrochemically onto H-terminated, p-doped silicon (Si) surfaces. Atomic Force Microscopy (AFM) and ellipsometry experiments clearly showed layer thicknesses of 2-7 nm, which indicates multilayer formation. Decreasing the diazonium salt concentration and the reaction time resulted in a smaller layer thickness, but did not prevent the formation of multilayers. It was demonstrated, mainly by X-ray Photoelectron Spectroscopy (XPS), that the diazonium salts do not only react with the H-terminated Si surface, but also with electrografted phenyl groups via azo-bond formation. These azo bonds can be electrochemically reduced at $E_{\text{red}} = -1.5$ V, leading to the corresponding amino groups. This reduction resulted in a modest decrease in layer thickness, and did not yield monolayers. This indicates that other coupling reactions, notably a biphenyl coupling, induced by electrochemically produced phenyl radicals, take place as well. In addition to the azo functionalities, the nitro functionalities in electrografted layers of 4-NBD were independently reduced to amino functionalities at a lower potential ($E_{\text{red}} = -2.1$ V). The presence of amino functionalities on fully reduced layers, both from 4-NBD- and 4-BBD-modified Si, was shown by the presence of fluorine after reaction with trifluoroacetic anhydride (TFAA).

This study shows that the electrochemical reduction of azo bonds generates amino functionalities on layers produced by electrografting of aryldiazonium derivatives. In this way multifunctional layers can be formed by employing functional aryldiazonium salts, which is believed to be very practical in the fabrication of sensor platforms, including those made of multi-array silicon nanowires.

This chapter was published in the following publication:

Daniela Ullien, Peter C. Thüne, Wolter F. Jager, Ernst J.R. Sudhölter, and Louis C.P.M. de Smet "Controlled Amino-functionalization by Electrochemical Reduction of Bromo and Nitro Azo Benzene Layers Bound to Si(111) Surfaces" Phys. Chem. Chem. Phys., 2014, 16, 19258-65.

3.1 Introduction

Proteins, antigens and DNA are the main target molecules for biosensors. An important aspect in achieving selectivity of such sensors is the attachment of the appropriate receptor molecules to the sensing layer. Depending on the field of application and type of sensor platform this may require chemical attachment. Amide bond formation is one of the most important strategies among different approaches for the chemical immobilization of receptors like antibodies or complementary DNA.¹ For example, receptors carrying a carboxylic acid group can be chemically attached to an amino-functionalized (sensor) surface via carbodiimide chemistry.²

Silicon-based electronic devices have found an increasing importance in sensor development since they can be built reproducibly at large scales and at low costs, using standard semiconductor technology. Moreover, by making use of different doping levels one can tune the semiconducting behavior of silicon. For example, silicon nanowire-based, field-effect transistors (SiNW FET) have shown a rapid, label-free, sensitive detection of biological and chemical species.^{3, 4} The surface modification strategies that have been explored on Si include silanization and hydrosilylation on oxide or H-terminated Si surfaces, respectively.^{5, 6} In this latter reaction, 1-alkenes or 1-alkynes react with Si-H groups at the surface to form Si-C bounds, which are more stable than the Si-O bond on silicon oxide surfaces as these are susceptible towards hydrolysis and are thermally labile.⁷ In addition, in the case of Si-C bond formation true monolayers are formed, and the sensing event (target/analyte interaction) takes place closer to the conducting surface, which increases the sensitivity of the device.⁵

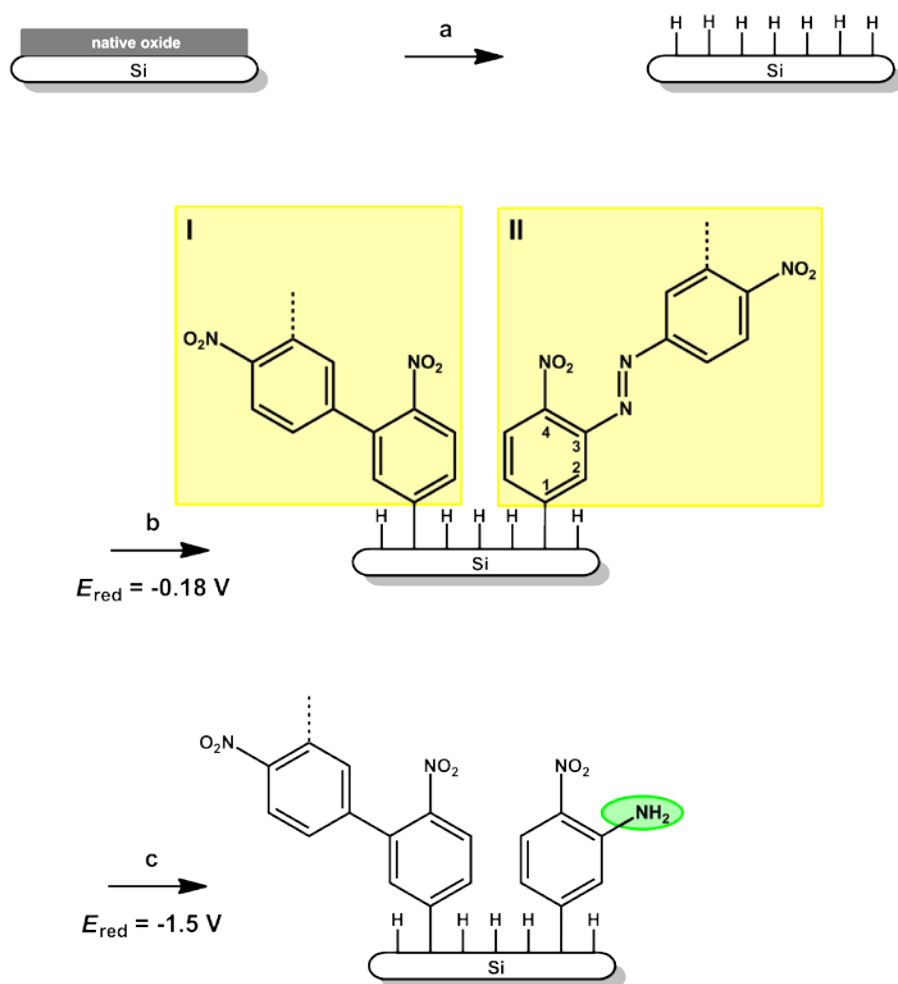
An interesting alternative to the hydrosilylation of 1-alkenes and 1-alkynes on H-terminated Si surface is the electrografting of aryl diazonium salts at these surfaces. In this reaction—which has been

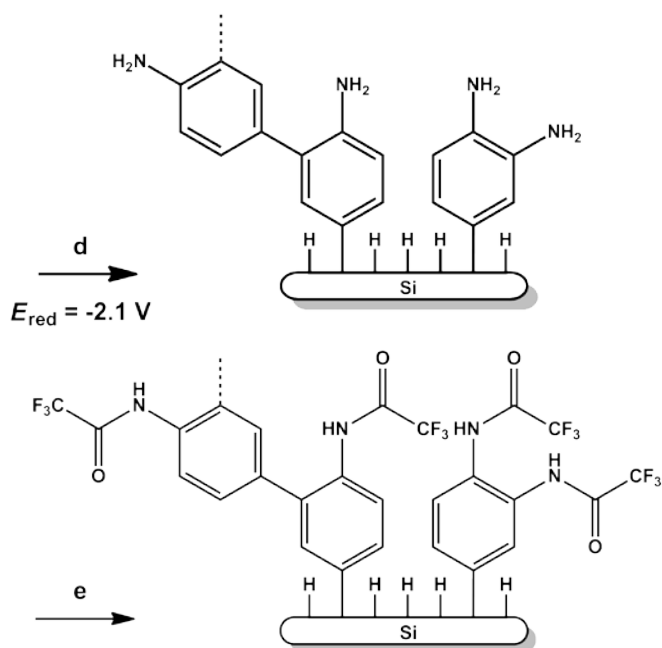
reported on carbon and metal surfaces as well—the diazonium salt is reduced via the uptake of an electron from the surface upon which N_2 is released. Subsequently, two resulting aryl radicals react with the surface, the first to abstract a hydrogen atom and the second to react with the thus formed surface radical, to form a stable Si-C bond.⁸ Very recently diazonium chemistry has been employed to graft antibodies targeted against a prostate cancer risk biomarker to SiNW surfaces, resulting in resistor-mode biosensors.⁹ In contrast to silanization and hydrosilylation, the diazonium electrochemical reaction allows one to attach organic molecules to specific areas of a surface. For example, adjacent wires that are part of multi-array devices can be modified with different functionalities by addressing individual nanowires electrochemically. Very recently, a novel method for the selective surface modification of SiNWs with metal particles by nanoscale Joule heating was demonstrated.¹⁰ With light-initiated hydrosilylation,¹¹ in combination with masking techniques also patterns can be made, but this templating cannot be performed at nm-level resolution.

Electrochemical grafting of diazonium salts on carbon materials¹², metals¹³ or semiconductors¹⁴ is known for more than 20 years.¹⁵ 4-Nitrobenzenediazonium (4-NBD) was electrografted for the first time on oxide-free silicon surfaces by de Villeneuve in 1997.¹⁴ Later, this type of functionalization was used to obtain aminobenzene-terminated Si surfaces via the chemical reduction of the nitro groups, enabling the chemical attachment of amine-terminated, single-stranded DNA via glutaraldehyde coupling, making the surface ready for hybridization experiments.¹⁶

The electrografting of diazonium salts on carbon, metal and semiconductor electrodes leads to the formation of layers that are thicker than one monolayer.^{15, 17, 18} Biphenyl coupling and the formation of azo bonds are common side reactions that have been demonstrated on Si(111) surfaces, metals and C-electrodes.¹⁹ X-Ray Photoelectron Spectroscopy

(XPS) studies of the N_{1s} emission, clearly indicate the presence of azo-bonds,^{19, 20} which point to the formation of phenyldiazene ('azo') structures. Recently, the electrochemical reduction of azo bonds to amines, was demonstrated for electrografted layers on gold.²¹

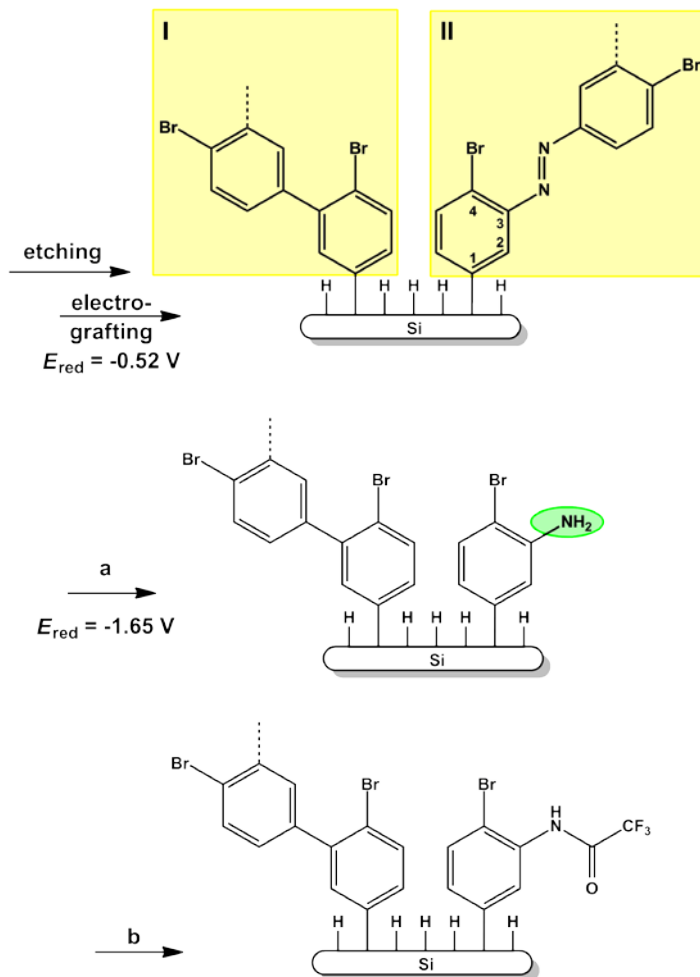




Scheme 1. Schematic representation of the surface etching of Si(111) (step a) and the electrografting of 4-NBD onto the H-terminated Si surface (step b), forming biphenyl-coupled (box I) and azo-coupled products (box II). The dashed lines indicate the further growth of the layers, both via biphenyl coupling and the formation of azo bonds. For matters of clarity, only one example of each coupling is drawn, but the attached structures can also be branched and contain both types of coupling. Next, a two-step electroreduction yields amino groups from the azo-bond (oval; step c) and from the nitro groups (step d). The formed amino groups are modified with TFAA, which results in amide formation (step e). The reported voltages represent the minimal voltages applied during the electrografting (step a) and the electroreduction (steps c and d). All values reported are relative to the standard calomel electrode (SCE).

Herein we describe the electrografting of 4-bromobenzenediazonium (4-BBD) and 4-NBD on H-terminated Si(111) surfaces and the independent electrochemical reduction of azo bonds that are present in these layers (Schemes 1 and 2). This methodology enables the fabrication of surfaces with amino functionalities in addition to the substituents at the 4-position

of the benzenediazonium compound that was grafted to the surface. We demonstrated the utility of the electrochemically generated amino functionalities by the reaction with trifluoroacetic anhydride.



Scheme 2. Schematic representation of the electrochemical reduction of 4-BBD-modified Si(111) surfaces (step a), followed by the functionalization of the resulting amino groups (step b). Boxes I and II represent the biphenyl and azo-coupled products, respectively. The oval highlights the amino functionality obtained from the electrochemical reduction of the azo bond. All values reported are relative to the standard calomel electrode (SCE).

3.2 Experimental Section

3.2.1 Materials and Reagents

4-Nitro and 4-bromobenzenediazonium tetrafluoroborate, sulfuric acid, and acetonitrile (ACN, HPLC grade, $\geq 99.9\%$) were purchased from Sigma-Aldrich. Ammonium fluoride, tetrabutylammonium tetrafluoroborate ($(\text{Bu}_4\text{N})\text{BF}_4$) and trifluoroacetic anhydride (TFAA) were purchased from Fluka. All chemicals were used as received. All aqueous solutions were prepared in MilliQ water (resistivity $> 10 \text{ M}\Omega$). Boron-doped ($0.001\text{--}0.005 \text{ }\Omega/\text{cm}$) silicon (Si) (111) wafers, with a thickness of $500\text{--}550 \text{ }\mu\text{m}$ and covered with native oxide were obtained from Siltronix.

3.2.2 Electrochemical Equipment

All 3-electrode electrochemical reactions were performed with a CH Instruments potentiostat (model CHI600D) equipped with a picoamp booster with Faraday cage (model CHI200B). In this configuration, Si(111) samples were used as the working electrode (WE) and mounted in a home-made Teflon cell with a Viton O-ring with an area of 0.25 cm^2 . The back contact (BC) was achieved via scratching InGa eutectic onto the back side of the Si sample. A Pt wire and a standard calomel electrode (SCE) were used as a counter electrode (CE) and reference electrode (RE), respectively.

3.2.3 Sample Treatment

Cleaning and etching of the surface (Scheme 1, step a)

Si dies of $\sim 1 \text{ cm} \times \sim 1 \text{ cm}$ were cleaned in acetone and water according to manufacturer specifications to remove the polymer coating preventing silicon chips from contaminants, followed by drying in a stream of nitrogen. The following steps were performed after the sample was mounted in the O-ring cell (see Section 2.2). Etching was performed in $40\% \text{ NH}_4\text{F}$ (aq) for 15 minutes to prepare a H-terminated Si surface. The etching

solvent was removed via a decanting step, which was followed by a rinsing step with MilliQ water and a drying step using a stream of nitrogen.

Electrografting (Scheme 1, step b)

A solution of 2.5 mM of diazonium salt in 25 mM (Bu₄N)BF₄ in ACN was added to the cell and electrografting experiments were carried out by applying a voltage scan from 0.20 V to -0.60 V at 0.05 V/sec (step b in Scheme 1). Afterwards, the samples were rinsed with ACN, ethanol, and water prior to analyses or further modification. In the experiments described in Section 3.1 three different concentrations of 4-BBD were used (0.025, 0.25 and 2.5 mM) and also different electrografting times have been used (5, 20 and 200 sec). The samples described in Section 3.2 were treated as described above using 2.5 mM diazonium salt and 200 sec of electrografting time. Samples modified with 4-NBD and 4-BBD without any post-treatment steps are referred to as 4-NBD- and 4-BBD-modified Si samples, respectively.

Electroreduction (Scheme 1, steps c and d; Scheme 2, step a)

Further electroreduction of the resulting samples was performed in 25 mM (Bu₄N)BF₄ in ACN by applying a voltage scan from -0.60 to -1.5 or -2.2 V at 0.05 V/sec. Subsequently, the samples were cleaned with ACN, ethanol, water and dried with a stream of dry nitrogen gas.

Reaction with TFAA (Scheme 1, step e; Scheme 2, step b)

A solution of 30 µL of TFAA in 1 ml of toluene was allowed to react with the electrochemically reduced samples for 2 h at room temperature. Then the samples were washed with toluene, ethanol and water and dried with a stream of dry nitrogen gas.

3.2.4 XPS

The XPS measurements were carried out on a Thermo Fisher Scientific, K Alpha model, equipped with a monochromatic Al K α X-ray source. XPS measurements were taken in normal emission with a spot size of 400 μm at a pressure of 10^{-9} mbar. During all XPS measurements the flood gun was enabled to compensate for the potential charging of surfaces. The spectra were analyzed using Avantage processing software.

3.2.5 Atomic Force Microscopy (AFM)

The AFM experiments were carried out in air using an NTEGRA AFM (NT-MDT) equipped with a NSG30 series silicon tip (resonance frequency 240-440 kHz, force constant 22-100 N/m). First, height images were collected in the tapping mode. Then the scratching mode was applied to remove the soft, grafted layers, followed by a tapping-mode measurement again. The thickness of the removed layer was determined by comparing the profile heights between scratched and unscratched areas (3 samples per modification condition).

3.2.6 Ellipsometry

Ellipsometry measurements were performed with an M-2000F spectroscopic ellipsometer (J.A. Woollam Co., Inc), equipped with a 75W Xe arc light source. The experiments were performed at an incident angle of 70° . The optical thickness was determined using a standard model available in the CompleteEase software, i.e. Si with a transparent film on top of it. This model makes use of the optical parameters for Si as reported by Herzinger et al.,²² while for the transparent film (modelled as a Cauchy film) the following values have been used: $n = 1.5$, $k = 0$.

3.3 Results and Discussion

3.3.1 Electrografting onto H-terminated Si(111)

4-NBD and 4-BBD were electrografted onto H-terminated Si(111) electrodes. Figure 1a presents the typical Cyclic Voltammetry (CV) results. Grafting of 4-NBD and 4-BBD takes place at -0.18 V and -0.52 V vs. SCE, respectively (Figure 1a, cycle i). The major contribution to the different electrografting potentials is the difference in the nature of the functional group of the diazonium salt: stronger electron withdrawing groups like nitro groups facilitate the reduction. When the samples were exposed to a subsequent second cycle using the same conditions, no electroreduction peaks were observed (Figure 1a, cycle ii). This suggests that no electrografting of diazonium takes place after the first CV cycle, which is in line with reports from others.¹⁴

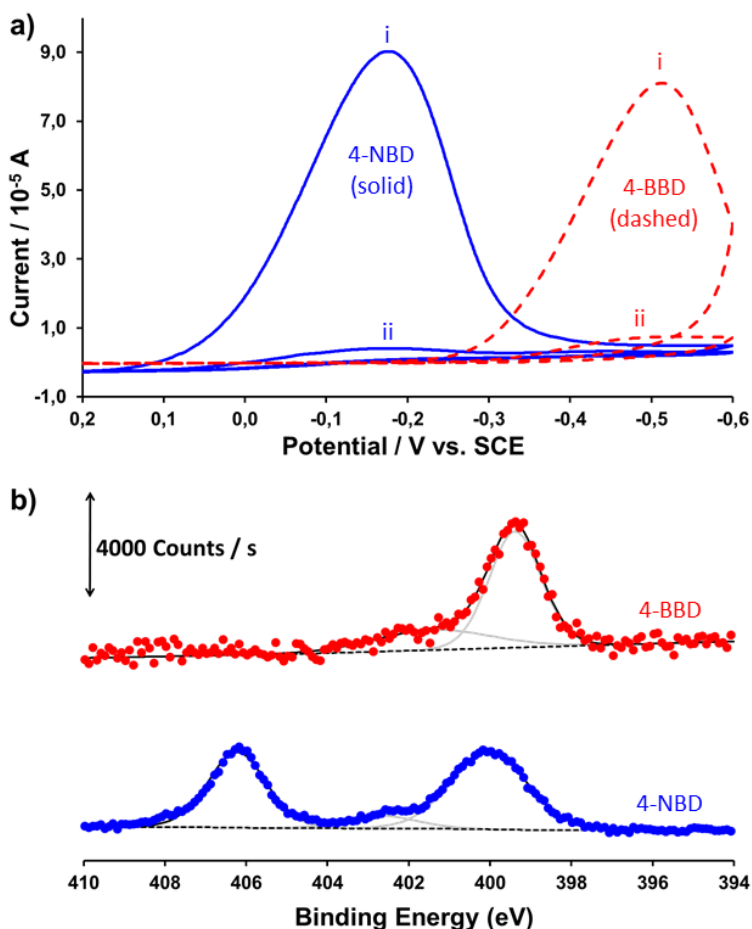


Figure 1. a) CV data on the electrografting of 4-NBD (blue solid) and 4-BBD (red dashed) in ACN on H-terminated Si(111), where i and ii refer to the cycle number, and b) XPS N1s region spectra of 4-NBD- and 4-BBD modified Si(111) (blue and red, respectively). The dashed line represents the baseline, the deconvoluted peaks are given in grey solid lines and the black solid line represents the envelope.

The electrografting of the 4-substituted benzenediazonium salts on Si was monitored by XPS, concentrating mainly on the N_{1s} region spectra. The N_{1s} binding energies for the salt [C₆H₅(N₂)]BF₄ are reported to be 405.1 and 403.8 eV.²³ After the grafting of 4-NBD to Si the N_{1s} region

spectrum shows three contributions at ~400, ~402 and ~406 eV, respectively (Figure 1b, blue circles). The major peak near 406 eV is attributed to the NO₂ functionality of 4-nitrobenzene grafted on Si. The minor peak near 402 eV is assigned to the tetrabutylammonium (TBA⁺) cation used in the procedure.²⁴ The peak near 400 eV is attributed to the azo group (-N=N-)²⁵ which is formed in a subsequent electrophilic aromatic substitution reaction of aryldiazonium ions with already grafted aryl moieties on the surface.¹⁹ In the literature multiple assignments for the 400 eV peak have been given. It is mainly referred to as the 'reduced form of nitrogen', or even to the amino groups that are formed upon the reduction of the nitro group during the electrografting procedure.^{14, 20, 26} Depending on the intensity of the X-ray source, the exposure time and likely also the photon energy, photoreduction of the nitro groups to amino groups can take place during XPS analysis.²⁷ We verified the N_{1s} signal under our experimental conditions and no detectable change was found (time-resolved data is provided in Figure A1 of the Supporting Information, Appendix A). Although the XPS peak of 4-aminobenzene appears around 400 eV, we have demonstrated that the reduction of nitro groups in ACN takes place at a more negative potential so that no amino groups are present at this stage, *vide infra*. Moreover, this peak is also present when 4-BBD is used, albeit at slightly lower binding energy (Figure 1b, red circles, 399.5 eV). This lower electron binding energy may be due to the difference in electron withdrawing properties of Br versus NO₂. In the case of Br the electron-withdrawing effect is smaller, making it easier to emit N_{1s} electrons, which results in a lower binding energy.

Since the 400 eV peak indeed reflects the presence of azo bonds, the N_{1s} region spectrum of grafted 4-BBD can be used to calculate the amount of azo bonds present in the grafted layer. Typical XPS results for standard electrografting conditions for 2.5 mM aryldiazonium salt and 200 sec of reaction time showed 24% Si, 56% C, 5.3% Br and 1.3% N₄₀₀. The averaged

ratio N_{400}/Br (measured for 5 samples with the same electrografting conditions) was found to be 0.24 ± 0.08 , i.e. 24 nitrogen atoms per 100 bromide atoms. Based on the structure depicted in Scheme 2, this means that on average 24% of all aryl groups present in 4-BBD-modified Si are attached via an azo bond.

In this work we performed experiments using different diazonium salt concentrations and electrografting reaction times and analyzed the thickness of the resulting layers with ellipsometry and AFM (Figure 2). The measurement of the layer thickness with AFM is possible by comparing the profile height of scratched vs. unscratched surfaces as described in Section 2.5.

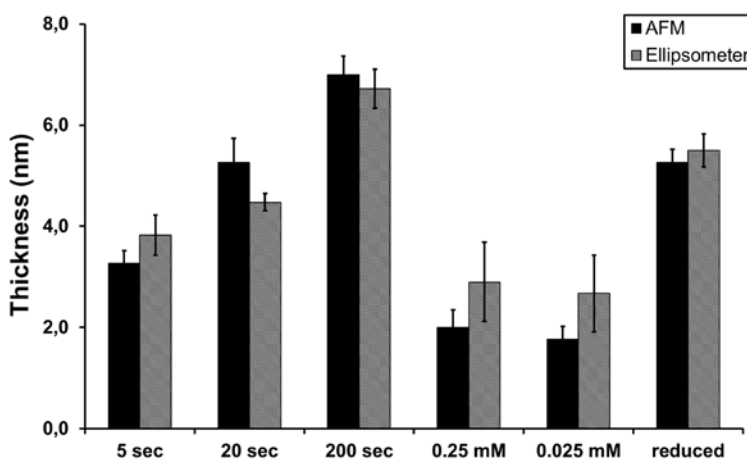


Figure 2. Concentration- and time-dependent data on the layer thickness from ellipsometric and AFM analysis of BBD-modified Si. In the cases of 5, 20 and 200 sec time of CV cycle, 2.5 mM of 4-BBD was used. In the cases of 0.25 and 0.025 mM of 4-BBD, 200 sec of electrografting time was applied. The ‘reduced’ sample shows the thickness after electroreduction, step a in Scheme 2 of the 2.5 mM 4-BBD for 200 sec of electrografting.

The layer thickness data obtained from AFM and ellipsometry measurements correlate well. The data show that the thickness of grafted

material decreases with decreasing electrografting times. In the conditions used by us we could not reduce the thickness to a sub-nanometer monolayer level, even by decreasing the concentration 100 times. Even for concentrations as low as 0.025 mM of 4-BBD, the observed layer thickness corresponds to 3 to 4 phenyl groups. The time-dependent results suggest that the grafting is not specific, i.e. before all possible Si-H sites are occupied, side reactions—biphenyl and azo coupling—already occur (boxes I and II in Schemes 1 and 2, respectively). In the next section we describe the results of the electroreduction of the azo bonds.

3.3.2 Electroreduction of Grafted Layers

After electrografting, the samples were immersed in ACN and exposed to a second CV cycle, during which a more negative potential was applied down to -2.2 V (Figure 3). The overall reduction is irreversible. In the reduction of 4-NBD grafted layers (Figure 3, blue solid) peaks are observed at -1.5 V and at -2.1 V. In the case of 4-BBD (Figure 3, red dashed) one peak at -1.65 V is observed. It is proposed from these observations to attribute the peak at -1.5/-1.65 V to the reduction of the azo linkage, and the peak at -2.1 V to the reduction of the nitro substituent to an amino group. The small difference in the reduction peak of the azo bonds in the 4-nitro and 4-bromo substituted molecules can be understood from the higher electron affinity originating from the nitro group. The thickness of the grafted layers has decreased after the reduction (Figure 2). For example, with AFM we measured average thickness of grafted layers of 7.0 ± 0.4 nm, and after the electroreduction the average layer thickness was 5.3 ± 0.3 nm, i.e. a reduction of 25%. Upon electroreduction the rms roughness value increased from 1.1 nm to 1.5 nm for a $1 \times 1 \mu\text{m}^2$ scan (Supporting Information Figure A2, Appendix A).

The electrochemical activity of the azo groups is thought to depend strongly on the layer structure and density. Previous studies of self-

assembled monolayers of azobenzenethiols on gold²⁸ and nitroazobenzene films on carbon¹⁸ suggest that densely packed layers severely inhibit the ion penetration into the layers and, in turn, reduce the accessibility of the azo groups, making them less electro-active. Our work on azobenzenes on Si and a recent study of Jung et al.²¹ on azobenzenethiols on gold show the possibility of electrochemical cleavage of azo groups that are present in films, most likely due to a lower layer packing.

By comparing the surface areas of the peaks in Figure 3 one can estimate the percentage of the azo-bond formation. The ratio between the surface area of the peak of the NO₂ to NH₂ reduction and the one of the azo-bond cleavage is ~7. Taking into account that the azo-bond and nitro reduction require 4 and 6 electrons,^{20, 29} respectively, the extent of azo-bond formation is 22%, assuming that both reduction processes are complete. This number is similar to the one obtained by the XPS results on 4-BBD, showing that 24% of the bromobenzene is attached via an azo bond.

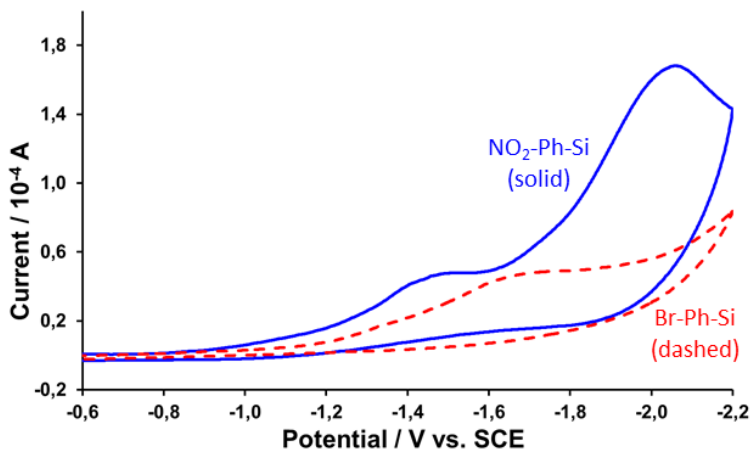


Figure 3. Electroreduction of electrografted layers on silicon (111) prepared from 4-NBD (blue solid) and 4-BBD (red dashed).

Electrografted Si samples that were exposed to subsequent reduction cycles to reduce the nitro and azo groups were also analyzed with XPS. Figure 4a shows typical Br_{3d} region spectra for 4-BBD-modified silicon samples. Upon reduction down to -2.2 V the intensity of the Br_{3d} XPS peak decreases, which indicates that Br-substituted aryl derivatives are released from the surface. The averaged degree of Br reduction was found to be 43% (Supporting Information, Figure A3, Appendix A). This decrease is attributed to the azo-bond reduction in the thin films of 4-BBD-modified Si samples.

While only ~25% of the linkages are azo bonds, up to 40% of the material is lost upon the electrochemical reduction. This may indicate that—on average—the azo bonds are closer to the surface than the biphenyl bonds. Another peculiar observation is that the 40% loss of layer material results in a layer thickness reduction of only ~25%. Presumably the layer is rather rigid as for fluid materials the layer thickness would be proportional to the amount of deposited material as the layer is expected to collapse in that case.

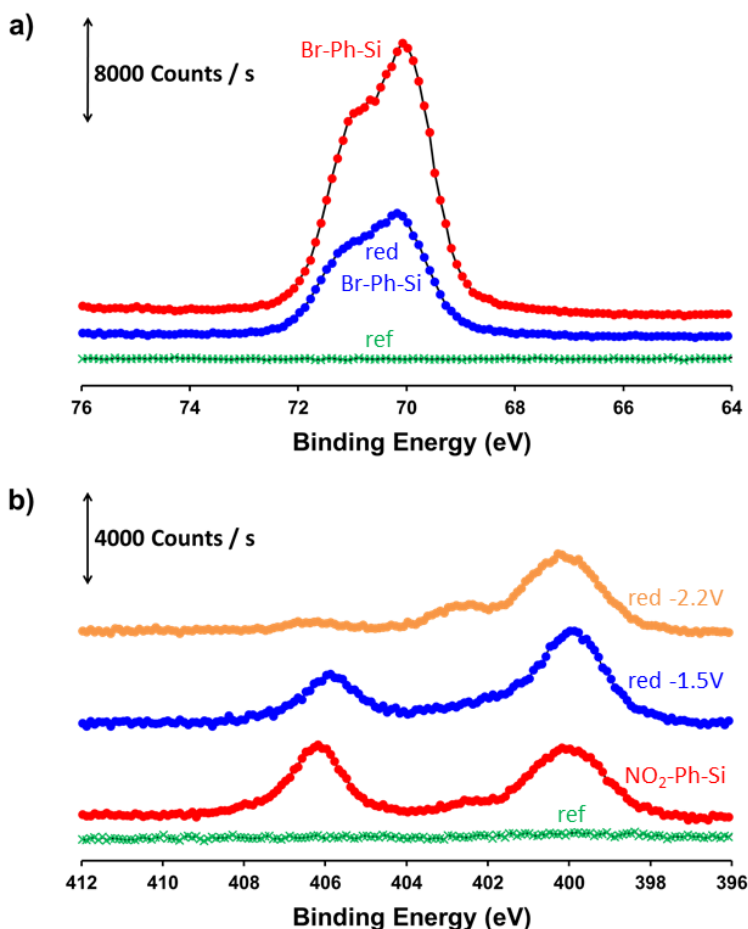


Figure 4. a) Br3d region spectra of 4-BBD-modified Si (red) and after the reduction down to -2.2 V (blue). The spectrum of the unmodified surface is also given (ref, green), b) N1s region spectra of the unmodified surface (ref, green), 4-NBD-modified Si (red), after the reduction down to -1.5 V (blue) and -2.2 V (orange).

The XPS results of 4-NBD-modified samples are presented in Figure 4b. As discussed in Section 3.1 the peak near 406 eV is attributed to the nitro group and the 400 eV peak is attributed to the azo and the amino groups. For the electrografted nitrobenzene that was not further reduced (Figure 4b, red) the N_{1s} peak ratio of 406 eV / 400 eV was found to be

-0.72 V. During the CV cycle down to -2.2 V (Fig. 4b, orange) we expect both reductions, i.e. azo to amino and nitro to amino, to happen. After this cycle the 406 eV / 400 eV ratio was found to be ~0.09. The decrease of the NO₂ peak is a signal for the loss of the NO₂-substituted aryl derivatives like in the case of 4-BBD-modified Si and also an indication for the transformation of the nitro group. The NO₂ signal does not disappear completely. Apparently a small amount of these groups - which may be connected to the surface via biphenyl coupling (Scheme 1, box I) - is not easily reduced.

Figure 4b also shows the result of the electroreduction of the 4-NBD-modified Si in the range between -0.6 and -1.5 V vs. SCE (blue), thus only the reduction of the azo units and no reduction of the nitro groups. First it is noted that the intensity of the 406 eV (NO₂) peak is higher compared to the one obtained after the reduction in the range between -0.6 and -2.2 eV vs. SCE. The peak ratio of 406 eV / 400 eV in this case was found to be ~0.47 (Fig. 4b, blue). This value is in between the results for the non-reduced and fully reduced 4-NBD-modified Si surface. Some of the originally present NO₂ groups that were connected to the surface via the azo bond are lost upon the reduction to -1.5 V. As shown by the XPS data the grafted layer still does contain NO₂ groups, which have not been reduced yet to amines. This is because the potential for the NO₂ to NH₂ reduction (i.e. -2.1 V) was not applied yet. In acetonitrile the two processes, the reduction of azo bonds and the nitro to amino conversion, can be separated. This confirms the earlier proposition that the two different types of reduction take place at different voltages.

Electrochemical analysis and XPS show that the reduction of nitro to amino groups and the azo cleavage can occur also in aprotic media such as ACN. These processes can only take place in the presence of protons. This may be explained by small amounts of water, possibly present in the ACN

as well as in a hydration layer of the grafted layers, which is sufficient to supply this demand for protons.

3.3.3 Functionalization of the Reduced Layers

The reduced layers were functionalized by a reaction with TFAA, yielding amides. Figure 5 summarizes typical XPS data on the TFAA modification of different samples. In Figure 5a we compare three samples treated with TFAA: 4-NBD- and 4-BBD-modified Si samples—which were further reduced in a voltage range of -0.6 to -2.2 V vs. SCE (red and blue, respectively)—and as a reference sample, 4-BBD-modified Si that was not further electroreduced (green). The F_{1s} region spectra shows significantly larger amounts of organic fluorine at 688 eV for the electroreduced samples treated with TFAA (red and blue circles) compared to the reference sample, which shows a peak at 686 eV (green). The last peak can be attributed to inorganic fluorine and indicated the presence of the tetrafluoroborate ion (BF_4^-) used in the procedure. In the red and blue plots this peak appears as a shoulder of the larger peak at 688 eV. The successful amide formation can also be seen by closely examining the C_{1s} region spectrum (Figure 5b), since carbon bound to elements with increased electronegativity like fluorine will give signals at increased binding energies. In more detail, the C_{1s} region of the electroreduced 4-NBD Si sample treated with TFAA shows two C_{1s} peaks at high bonding energies referred to as $-\underline{C}F_3$ and $-(\underline{C}=O)CF_3$ (Figure 5b, peaks D and C, respectively).³⁰ It is noticed that the ratio of the these two peak areas is not 1:1, which we contribute to small amounts of sample contamination before any aryldiazonium treatment (data not shown).

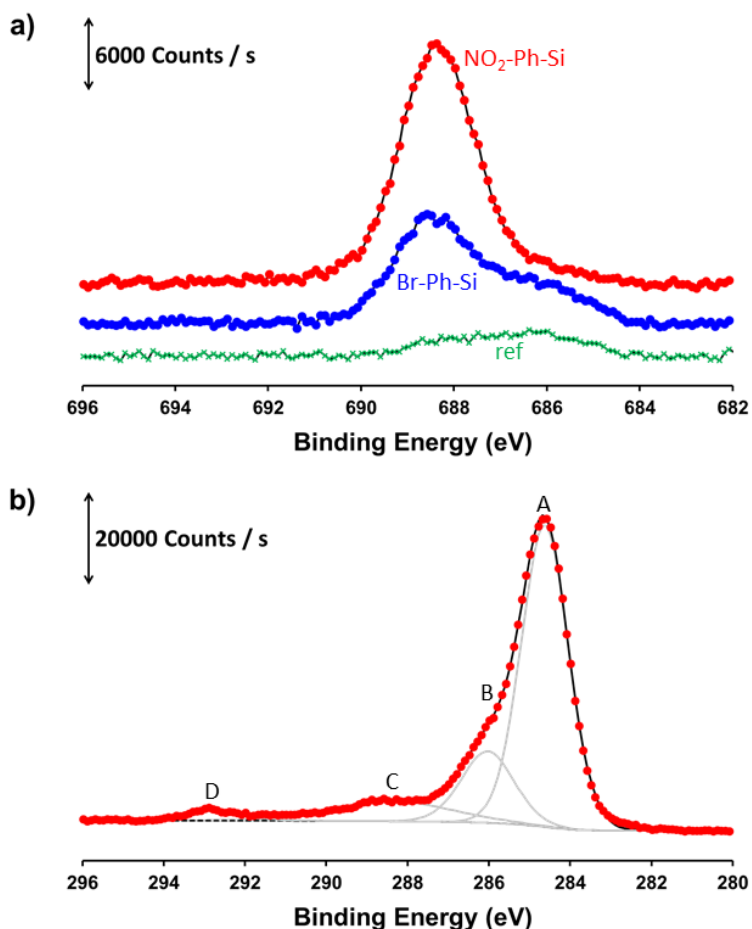


Figure 5. a) F1s region spectra of electrografted and electroreduced nitrobenzene (red) and bromobenzene (blue) on Si samples (down to -2.2 V) and a bromobenzene electrografted, but not reduced Si sample (ref, green, down to -0.6 V). All samples have been treated with TFAA; b) C1s region spectrum of an electrografted nitrobenzene on Si sample down to -2.2 V, followed by the treatment with TFAA. Peak A refers to $\underline{\text{C}}\text{-H}/\underline{\text{C}}\text{-C}$, B to $\underline{\text{C}}\text{-N}$, C to $(\underline{\text{C}}=\text{O})\text{CF}_3$ and peak D to $\underline{\text{C}}\text{-F}_3$. The dashed line represents the baseline, the deconvoluted peaks are given in grey solid lines and the black solid line represents the envelop.

The presence of a certain amount of TFA groups onto the treated 4-BBD-modified Si sample can be rationalized by formation of amino groups as a result of the azo-bond electroreduction at voltages around -1.5 V vs. SCE. Since both the nitro and azo group were reduced to amines in the case of 4-NBD-modified samples (Scheme 1, steps c and d), the amount of amino groups per attached aryl derivative is higher as compared to 4-BBD-modified samples, which is also observed by XPS as presented in Figure 5a.

3.4 Conclusions

The diazonium salts 4-NBD and 4-BBD were electrografted on H-terminated Si(111) at voltages of -0.18 and -0.52 V vs. SCE, respectively. The electrografting reaction is not specific, i.e. only forming Si-C bonds, and does not stop at the monolayer coverage. Instead, layers of 2-7 nm thickness are obtained. The layer thickness increases with increasing reaction time, but hardly with increasing aryldiazonium concentration. For both diazonium salts it was concluded that 22-24% of the aryl moieties are connected to the surface by azo-linkers. Electroreduction at potentials that were more negative than the grafting potential, reduced the azo units to amino groups. The required potentials were -1.5 and -1.65 V vs. SCE for 4-NBD and 4-BBD-modified Si, respectively. The reduction of the azo bonds leads to slightly thinner layers, due to scission. Monolayers, however, are not obtained due to the presence of the biphenyl bonds that are not susceptible to electroreduction. The nitro groups present in 4-NBD-modified Si have been reduced to amino groups at about -2.1 V vs. SCE. Since the azo groups can be reduced to amino groups, it is concluded that amino-functionalized surfaces can be obtained from electrografting of non-nitro containing aryldiazonium ions. The presence of reactive amino functionalities after electroreduction of the azo units, was proven by the formation of amide bonds by reaction with TFAA.

Our research demonstrates that multifunctional organic layers on Si surfaces can be formed by a straightforward and well-controlled electrochemical process. When applied to silicon nanowires that are part of multi-array devices, amino functionalities can be formed and functionalized individually. This would result in easy fabrication of arrays with different functionalities on the individual nanowires. In the case of BBD, multifunctionality on a single nanowire can be achieved. The aryl bromine can participate in reactions such as a Suzuki or a Sonogashira coupling, while the azo-derived amino functionality can be used in the formation of imines or amides.

Current research in our laboratory is directed towards the implantation of the described electrochemistry for the independent modification of SiNWs that are part of an array sensor platform.

References

1. M. Dufva, *Biomol Eng*, **2005**, *22*, 173-184.
2. M. J. E. Fischer, in *Surface Plasmon Resonance*, ed. N. J. de Mol, Humana Press, 1st edn., **2010**, vol. 627, pp. 55-73.
3. F. Patolsky, G. F. Zheng and C. M. Lieber, *Anal Chem*, **2006**, *78*, 4260-4269.
4. E. Stern, A. Vacic and M. A. Reed, *IEEE T Electron Dev*, **2008**, *55*, 3119-3130.
5. Y. L. Bunimovich, Y. S. Shin, W. S. Yeo, M. Amori, G. Kwong and J. R. Heath, *J Am Chem Soc*, **2006**, *128*, 16323-16331.
6. L. C. P. M. de Smet, D. Ullien, M. Mescher and E. J. R. Sudhölter, in *Nanowires - Implementations and Applications*, ed. A. Hashim, InTech, **2011**, pp. 267-288.
7. E. J. Faber, L. C. P. M. de Smet, W. Olthuis, H. Zuilhof, E. J. R. Sudhölter, P. Bergveld and A. van den Berg, *ChemPhysChem*, **2005**, *6*, 2153-2166.
8. R. Hunger, W. Jaegermann, A. Merson, Y. Shapira, C. Pettenkofer and J. Rappich, *J Phys Chem B*, **2006**, *110*, 15432-15441.
9. M. A. Mohd Azmi, Z. Tehrani, R. P. Lewis, K.-A. D. Walker, D. R. Jones, D. R. Daniels, S. H. Doak and O. J. Guy, *Biosens Bioelectron*, **2014**, *52*, 215-224.

10. J. Yun, C. Y. Jin, J. H. Ahn, S. Jeon and I. Park, *Nanoscale*, **2013**, *5*, 6851-6856.
11. F. Effenberger, G. Gotz, B. Bidlingmaier and M. Wezstein, *Angew Chem Int Ed*, **1998**, *37*, 2462-2464.
12. M. Delamar, R. Hitmi, J. Pinson and J. M. Saveant, *J Am Chem Soc*, **1992**, *114*, 5883-5884.
13. M. Couture, S. S. Zhao and J.-F. Masson, *Phys Chem Chem Phys*, **2013**, *15*, 11190-11216.
14. C. H. de Villeneuve, J. Pinson, M. C. Bernard and P. Allongue, *J Phys Chem B*, **1997**, *101*, 2415-2420.
15. J. Pinson and F. Podvorica, *Chem Soc Rev*, **2005**, *34*, 429-439.
16. A. Shabani, A. W. H. Mak, I. Gerges, L. A. Cuccia and M. F. Lawrence, *Talanta*, **2006**, *70*, 615-623.
17. P. Allongue, C. H. de Villeneuve, G. Cherouvrier, R. Cortes and M. C. Bernard, *J Electroanal Chem*, **2003**, *550*, 161-174.
18. P. A. Brooksby and A. J. Downard, *J Phys Chem B*, **2005**, *109*, 8791-8798.
19. P. Doppelt, G. Hallais, J. Pinson, F. Podvorica and S. Verneyre, *Chem Mater*, **2007**, *19*, 4570-4575.
20. S. S. C. Yu, E. S. Q. Tan, R. T. Jane and A. J. Downard, *Langmuir*, **2007**, *23*, 11074-11082.
21. H. J. Jung, H. Min, H. Yu, T. G. Lee and T. D. Chung, *Chem Comm*, **2010**, *46*, 3863-3865.
22. C. M. Herzinger, B. Johs, W. A. McGahan, J. A. Woollam and W. Paulson, *J Appl Phys*, **1998**, *83*, 3323-3336.
23. P. Finn and W. L. Jolly, *Inorg Chem*, **1972**, *11*, 1434-1435.
24. K. E. Lee, M. A. Gomez, T. Regier, Y. F. Hu and G. P. Demopoulos, *J Phys Chem C*, **2011**, *115*, 5692-5707.
25. M. Toupin and D. Belanger, *J Phys Chem C*, **2007**, *111*, 5394-5401.
26. J. Lyskawa, A. Grondein and D. Belanger, *Carbon*, **2010**, *48*, 1271-1278.
27. K. Roodenko, M. Gensch, J. Rappich, K. Hinrichs, N. Esser and R. Hunger, *J Phys Chem B*, **2007**, *111*, 7541-7549.
28. D. J. Campbell, B. R. Herr, J. C. Hulteen, R. P. VanDuyne and C. A. Mirkin, *J Am Chem Soc*, **1996**, *118*, 10211-10219.
29. P. Allongue, M. Delamar, B. Desbat, O. Fagebaume, R. Hitmi, J. Pinson and J. M. Saveant, *J Am Chem Soc*, **1997**, *119*, 201-207.
30. F. Pippig, S. Sarghini, A. Hollander, S. Paulussen and H. Terryn, *Surf Interface Anal*, **2009**, *41*, 421-429.

Chapter 4

Silicon Nanowire Field-Effect Transistors: Electrical Sensors for Biosensing Applications

Abstract

Electrical sensors like silicon nanowire field-effect transistors (SiNW FETs), have a great potential for biosensing. We evaluated this statement in our lab. SiNW devices from two different sources were used. Firstly, the design and fabrication of the SiNW devices are briefly discussed. Subsequently, the experimental set-ups are presented. Finally, the two different SiNW FET devices were investigated under different experimental conditions. The sensing capabilities of the devices are firstly checked in air, then in liquid, usually by changing the pH of the aqueous solution. Sensing with charged polyelectrolytes (PEs) was realized. In a last set of experiments we show preliminary biosensing results on influenza A antigen detection by SiNWs modified using the layer-by-layer method to deposit finally a specific biotinylated antibody on streptavidin attached to biotinylated polyallylamine (PAHb). From this research it is concluded that for stable and reproducible measurements in liquid, a reference electrode should define the liquid potential of the solution in contact with the SiNW.

4.1 Introduction

Influenza viruses are a major cause for a serious illness which potentially can cause millions of deaths¹. To eliminate this threat, first and foremost, effective surveillance of the ill population is needed by means of quick and reliable (bio)sensors. For a review on current state-of-the art sensing strategies for influenza surveillance we refer to Gopinath et al.² In addition, reviews by Grabowska et al.³ and Krejcova et al.⁴ cover the electrochemical methods for influenza virus detection.

Whole virus detection on SiNW-based devices was initially introduced by the Lieber lab⁵. The researchers were able to monitor single influenza A virus binding and dissociation events by tracing the source-drain conductance of SiNW FETs with time. To enable the use of SiNW FETs in point-of-care (POC) diagnosis of the flu, these devices should be, firstly, compatible with current large-scale production techniques of semiconductors. Secondly, they should be easily modified by chemical-biological methods for antigen capturing, allowing facile fabrication. Thirdly, they should be sensitive to small markers of the disease and not necessarily to the whole virus.

SiNW-based FETs are not commercially available. Over the past years many different fabrication processes have appeared⁶ and they are mainly the result of efforts of academic groups and research institutes. Two of our collaborators provided us with SiNW FET devices produced by well-known complementary metal-oxide semiconductor (CMOS) techniques. An overview of possible chemical modification techniques of SiNWs was introduced in Chapter 2. One of the perspective non-covalent approaches for antibody-antigen immobilizations on sensor devices is by making use of polyelectrolytes (PEs) using the layer-by-layer deposition (this thesis, Chapter 2, Section 2.2.1). Responses of SiNW FETs to the immobilization of PEs from aqueous solutions was demonstrated for the first time by the research group of Ingebrandt^{7, 8}. On the basis of this report, and also our own work on polyelectrolyte multilayers on plane silica surfaces⁹, we

decided to immobilize PE layers using polyethylenimine (PEI) and polystyrene sulfonate (PSS), where the last layer is biotinylated polyallylamine hydrochloride (PAHb)*. This layer was subsequently modified with streptavidin, which allowed the next modification with a specific biotinylated antibody to detect influenza A antigen.

4.2 DIMES/TU Delft SiNW FETs

4.2.1 Design and Fabrication

The first source of SiNW FETs was from a collaboration with DIMES/TU Delft through the lab of Prof. P. M. Sarro (PhD project Thomas Moh). The thesis work of Thomas Moh concentrated on top-down processing for fabrication of the SiNW FETs on a large-scale, compatible with known CMOS techniques. In this process expensive nanolithography methods were avoided. Moh applied new techniques as (1) direct patterning and (2) wet etching to make SiNW FET devices. Direct patterning utilizes the conventional photolithography by exploring its limits in the nano dimension. Wet etching makes use of the time-controlled etching to develop nano-sized structures. For further details the reader is referred to the thesis of Thomas Moh^{6, 10, 11}.

* The synthesis of biotinylated polyallylamine is described in Chapter 5, Section 2.4 of this thesis.

The layout of the devices produced by the two before-mentioned techniques is quite similar and is shown in Fig. 1. Figure 1a shows a scheme of a 15 mm × 15 mm die with the nanowire area circled in red. The rest of the lines and squares are individual contact pads for the drain and the common source, which is indicated by "0". Figure 1b reveals a cross-section of a silicon nanowire, employing an Al-Si back-gate to tune the nanowire properties. On a single die of 15 mm × 15 mm and made by the direct patterning method 12 nanowires are present. Making use of the wet etching method, a single die of 10 mm × 15 mm have 7 nanowires present. In addition, in this design 3 FET devices were actually nanowire arrays. Overall we have investigated 3 dies made by direct patterning and 9 dies made by wet etching. These devices were evaluated and compared by us.

All NWs were of p-type (boron doped) silicon. By direct patterning the nanowires (batch 1) had a thickness of 80 nm, a width of 400 nm, and a length of 5-10 μm. For that reason these 'wires' were called nanosheets. However, in this thesis, for reasons of convenience we only use the name of nanowire. By wet etching patterning (batch 2) the nanowires had a thickness of 300 nm, a width of 100 nm, and a length of 5-10 μm.

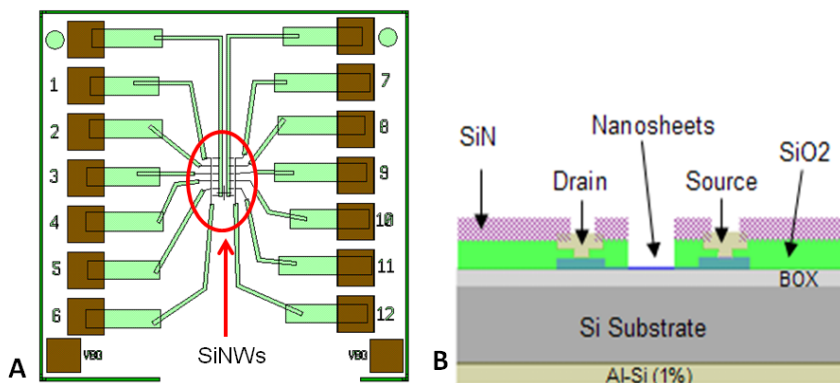


Figure 1. (a) Scheme of the DIMES/TU Delft SINW FET chip, showing an area with 12 NWs circled in red; (b) cross-section of the FET device with back-gate contact (Al-Si). This figure was provided by Thomas Moh.

The buried oxide (BOX) layer has a thickness of 400 nm. The doping density of SiNWs is around 10^{15} - 10^{17} cm⁻³ and the source/drain areas around 10^{19} cm⁻³.

4.2.2 Experimental Set-up

The electrical measurements were performed using a probe station (Suss MicroTec, Germany) and a standard Keithley 4200 semiconductor characterization system (Keithley Instruments, the Netherlands). All dies had electrical back-contact (Fig. 1b). Each die was placed on the probe station metal base, called 'chuck', and the contact pads on the chip were touched with tungsten needles. A fixed source-drain voltage of 50 mV was applied. The varying drain-source current (I_{ds}) was measured while the back-gate potential (V_{bg}) was swept between 0 and -10 V.

After the evaluation in air, the nanowires were exposed to an aqueous environment, making use of a homemade Teflon flow-cell. A scheme is depicted in Fig. 2a and in Fig. 2b a photograph of the flow cell is shown. Only a small area around the nanowires was exposed to the liquid, while the contact pads were left outside and approachable for tungsten needles of the probe station (Fig. 2b). The back-gate contact was achieved through T-shaped Cu plate underneath the SiNW FET chip embedded in Teflon, but with a hole in the lower part of the Teflon to realize contact with a metal 'chuck' of the probe station.

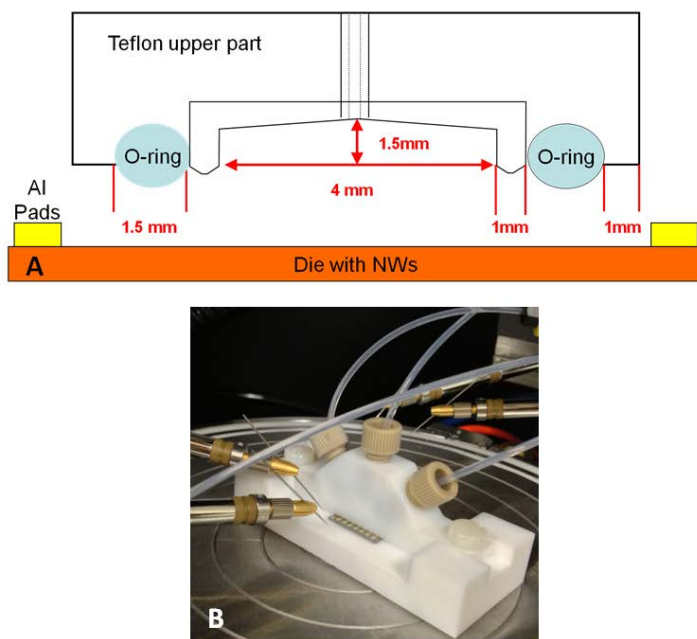


Figure 2. (a) Schematic of the cross section of a custom-made Teflon flow-cell applied in this study, and (b) a photograph of a SiNW FET chip inserted into the flow-cell placed on the metal base of the Probe station.

4.2.3 Results and Discussion: Electrical Characterizations

Initial measurements performed on batch 1 nanowires (prepared by direct patterning method) exposed to air showed FET characteristics typical for p-type devices (Fig. 3a). SiNW FETs were closed at positive potentials, and started to conduct currents by applying negative potentials. In sensing experiments an important parameter is the threshold voltage (V_t) and its relative shift. The most sensitive area for small signal detection is the depletion region¹², where the majority charge carriers are filled to a large extend and do not contribute to the current (I_{ds}).

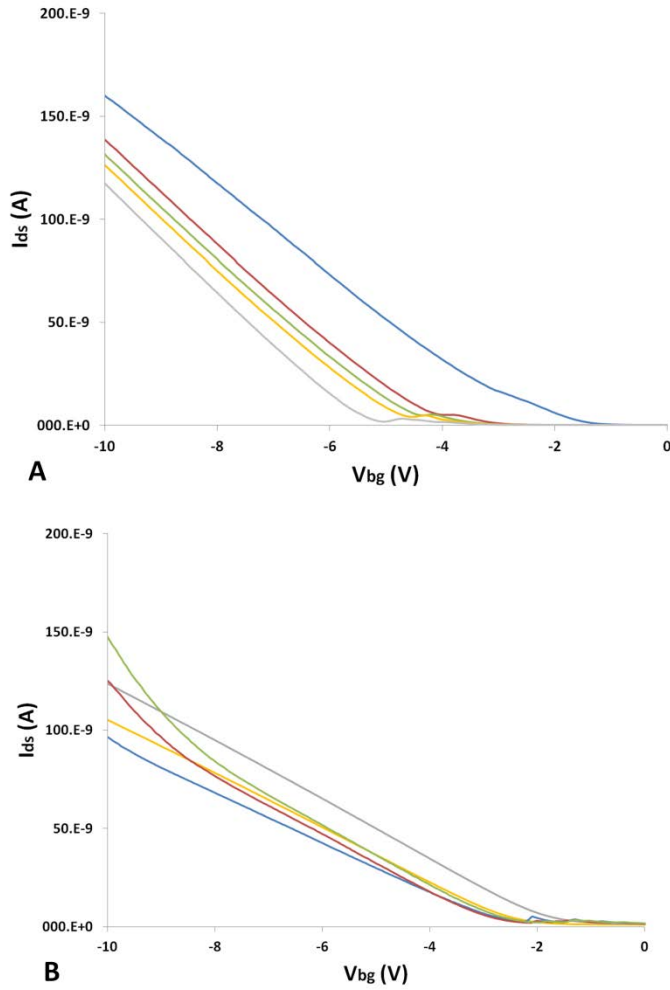


Figure 3. Typical electrical I_{ds} - V_{bg} characteristics in air of p-type SINW FETs from batch 1 (a) and batch 2 (b).

Initial experiments performed on batch 2 nanowires (prepared by the wet etching method) exposed to air showed that all the NW that were organized in an array have resistor behaviour, and only 4 single NWs per die showed FET characteristics (Fig. 3b). In comparison to batch 1, devices from batch 2 required the application of less negative potentials. V_t in batch 2 deviated less between the nanowires: average of ~ 0.5 V compared

to ~ 1.5 V in batch 1. SiNW FET devices from batch 2 gave lower currents, I_{ds} . In both batches, blocked NWs were present with zero FET characteristics, further decreasing the number of usable devices. The reasons for deviations in electrical characteristics, V_t and I_{ds} , may be flaws in the fabrication process, such as a non-uniform doping of the wafer. The process of SiNW FETs fabrication was not yet optimized.

After the characterizations in air, the SiNWs were investigated in aqueous solutions of varying pH value. Since the SiNWs are covered with native oxide layer, the extent of dissociation of the present surface SiOH groups varies with pH and has an effect on the number of charge carriers in the nanowire. In theory in p-type SiNWs, at higher pH values (more basic solutions) more surface silanol groups are dissociated and a higher negative surface potential is present. This negative surface potential expels the electrons in the nanowire, and thus increases the number of holes, i.e. the majority charge carriers. The drain-source current (I_{ds}) therefore increases at fixed back gate potential. In order to keep the current constant at increasing pH, the threshold voltage shifts to less negative values. However, typical results from batch 1 devices demonstrate no such behaviour (Fig. 4a).

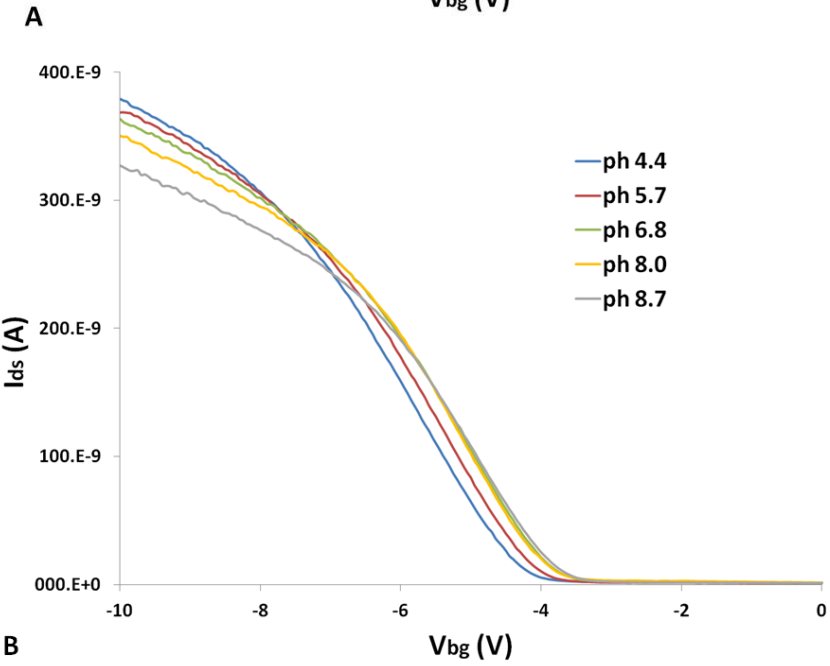
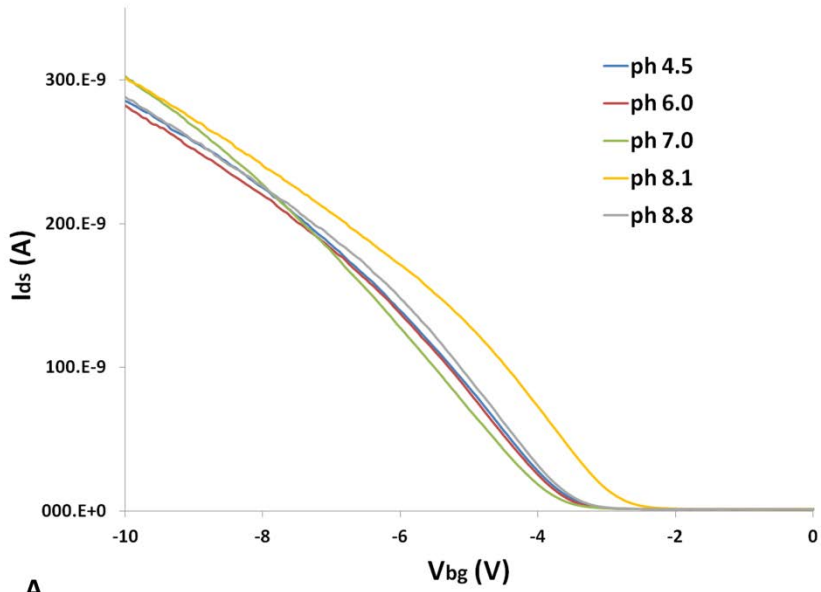


Figure 4. Drain-source current vs. back gate potential on SiNW FET varying different buffer solutions (a) batch 1 and (b) batch 2.

In fact, for batch 1 there is no clear pH dependence of SiO_x surface. However, in batch 2 the dependence of SiNW FET electrical characteristics on different pH solutions was more clear. Starting from a V_{bg} bias of -2 V initially a good correlation was observed upon lowering the bias, i.e. threshold voltages decreases with decrease in pH. The sensitivity of the device from Fig. 4b was calculated to be 36 mV/pH. This value is lower than the Nernstian limit of 59 mV/pH. This is in line with the sub-Nernstian response that has been reported for SiO_2 via a site-binding model¹³. Also the data is comparable to the 50 mV/pH sensitivity found by Moh^{6, 10}. In addition, at gate voltage around -7 V a switch in the behaviour is observed. Earlier measurements on these devices by Moh et al. did not show such a behaviour. The difference between the two measurement set-ups is related to the use of a reference electrode. In the previous work at DIMES a grounded Ag/AgCl reference electrode was used to stabilize the liquid potential in the flow-cell during back-gate voltage sweep. Previously, instabilities and drifts were a well-known issue in liquid measurements of planar FET devices.^{14, 15} Comparable instabilities are observed in NW FETs.¹⁶⁻¹⁸ Such a switch in behaviour and other instabilities can be referred to the poorly defined liquid potential near the NW surface, which can be solved by using reference electrode during measurements in liquid.

4.2.4 Conclusions

The DIMES SiNW devices were characterized in air and in liquid using back-gate configuration. Initial measurements in air showed typical p-type FET characteristics. However, measurements in liquid were less conclusive. Results on batch 1 (direct patterning method) did not show expected pH dependence. At the same time results on batch 2 (wet etching method) revealed a device sensitivity of 36 mV/pH, although not very stable. In addition, the reproducibility of the results was low. The number of SiNW devices was not sufficient to fully investigate the issue of instabilities.

Our initial measurements were done by using back-gate configuration. Comparable measurements on the same devices by Moh et al. using a grounded reference electrode were more successful. It is concluded that liquid potential should be well defined. This can be realized either by grounding the reference electrode and applying voltage through back-gate or by grounding the back-gate and the use of a reference electrode as front-gate potential. Thus, we come to the important conclusion to improve the measurement set-up by adding reference electrode which can control the potential in the liquid. It was further implemented in following work with Philips SiNW FETs as described in the next part of this chapter.

4.3 Philips SiNW FETs

4.3.1 Design and Fabrication

The second source of SiNW FETs was from a collaboration with Philips Research through Dr. J. H. Klootwijk (PhD project Marleen Mescher). The fabrication of the Philips SiNW FETs was also based on a top-down processing, using typical CMOS techniques as in the case of DIMES/TU Delft devices. The method was described by Mescher et al.¹⁹ Using this simple and robust method, 28 NW devices per 1 chip (or die) were fabricated. The devices consist of p-type (boron-doped) NWs connected between two highly-doped Si contact leads, which in turn are connected to aluminum contact pads. The layout of one die is presented in Fig. 5a, showing aluminium as yellow parts, while silicon is given in red. Fig. 5b shows a magnification of the NW FET region, where dark blue refers to the low-doped Si nanowire. The schematic cross-section of one device can be seen in Fig. 5c. The NWs dimensions range 20-2000 nm in width, 3 μm in length and the thickness is between 50 and 100 nm. For the experiments described in Section 4.3.3 nanowires with the following dimensions were used: 3 μm in length, 300 nm in width and 40 nm in thickness. In addition, 8 nm thick thermal oxide was grown on top of a NW for better insulation

while in contact with liquids. From this collaboration 15 chips were received with 2 SiNW FETs per chip wire-bonded to the electrical base for characterizations (30 NWs in total).

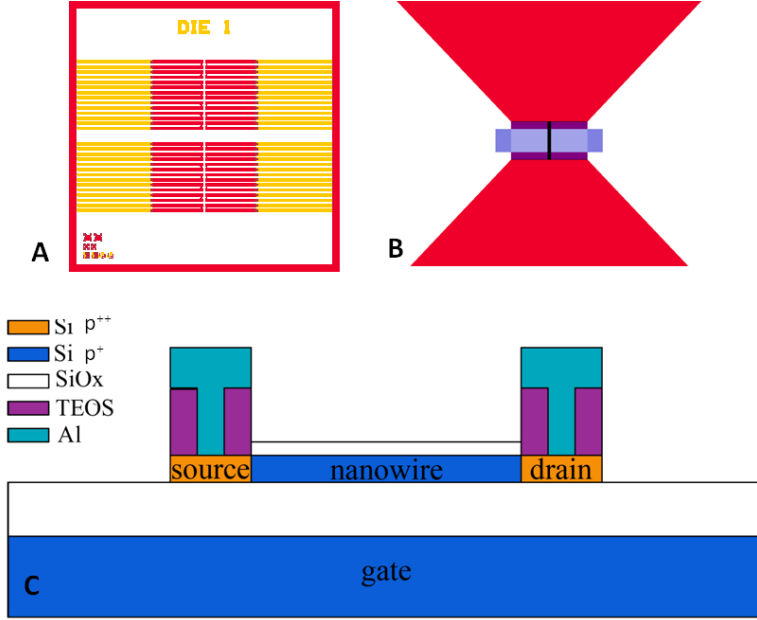


Figure 5. (a) Top view of the SiNW FET chip layout, (b) zoom in on a NW FET region, (c) Schematic not to scale. This figure is courtesy of Marleen Mescher.

4.3.2 Measurement Set-up

The measurement set-up for the experiments on the devices from Philips consists of a die glued to the electrical base (Fig. 6a). The contact pads of the NWs are wire-bonded to the electrical base, such as by applying voltage to the legs of the base, NWs are effected accordingly. The electrical base is placed on top of the black interface box²⁰ (Fig. 6b) with connectors to a Keithley 4200 semiconductor characterization system (Keithley Instruments, the Netherlands).

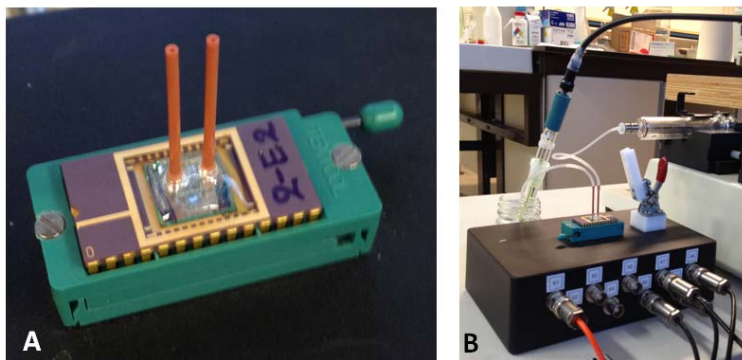


Figure 6. Photographs of (a) the measurement set-up consisting of a die glued to the electrical base with flow cell on top, and (b) the microfluidic system with syringe connected to the pump from right, flow cell with tubing and a beaker with the reference Ag/AgCl electrode at the left-hand side of the image. In (b) the electrical box with connectors to the Keithley characterization system is also shown.

The microfluidic system consists of a flow cell (Zeonex E48R, Philips Research, the Netherlands) glued on top of the die and Silastic Q7-4750 tubing (Dow Corning, Midland, MI, USA). The solution was sucked from the beaker with a front gate reference electrode (Fig. 6b) by a syringe pump (Harvard Apparatus, Holliston, MA, USA).

For electrical characterizations a fixed 50 mV source-drain bias was applied. The drain-source current (I_{ds}) is measured while the gate potential is swept (V_g). During the measurements in air the potential of the back gate was swept. For electrical characterizations in the aqueous phase the back gate was grounded and the front gate was swept by means of an Ag/AgCl reference electrode.

4.3.3 Results and Discussion: Electrical Characterizations

The typical electrical characterizations in air (I_{ds} vs. V_g) are shown in Fig. 7. The devices are closed at positive voltages and start to conduct at negative potentials, showing representative p-type behaviour. The Philips SiNW FETs opened easily by applying small voltage around -1 V. The results show two I_{ds} - V_g graphs, since in our set-up two SiNW devices can be checked simultaneously (Fig. 7, blue). In addition, the gate current (I_g) parameters are checked for possible current leakage through the back gate (Fig. 7, red). The I_g values are at least 3 orders of magnitude lower than I_{ds} . The device reliability in air was investigated previously by Mescher et al.^{19, 21} and was found to be sufficient for sensor applications. The variation in electrical characteristics, such as V_t , of the device within a single die was small (<0.5 V).¹⁹

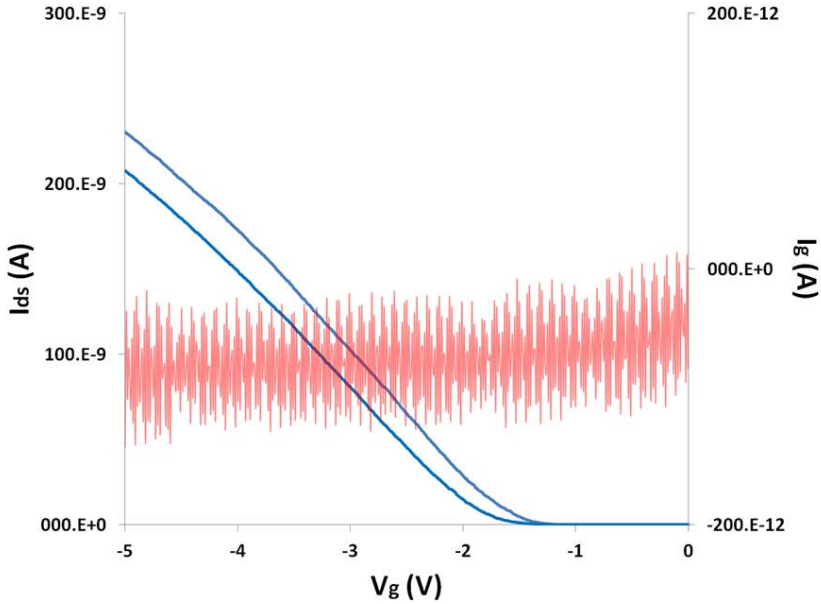


Figure 7. Typical result of the I_{ds} - V_g SiNWs characteristics in air (blue data). The gate current (I_g) is also shown in red (y-axis on the right-hand side). Two devices are measured simultaneously.

Typical result for liquid measurements in 50 mM HEPES/ 50 mM NaCl buffer pH = 7.1 on bare SiO_x is presented in Fig. 8. As can be seen from the comparison of Fig. 7 and 8, the results are the same and typical for p-type SiNWs, i.e. a more negative gate potential (V_g) increases drain-source current (I_{ds}). In liquid measurements, the noise levels are a bit higher compared to the electrical characterizations in air. A current leakage through the back gate, traced by I_g , and breakdown of the devices sometimes happened and decreased the number of working devices.

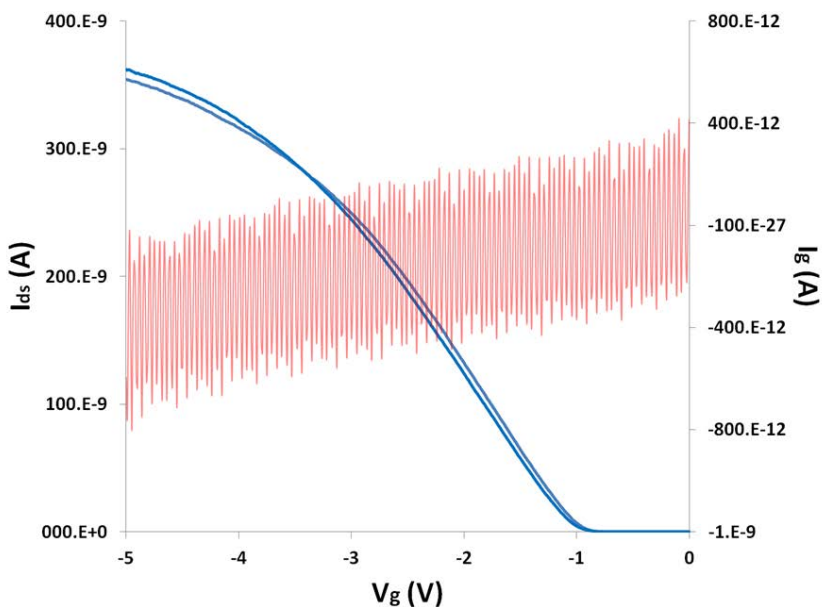


Figure 8. Typical electrical result of the bare SiNWs exposed to HEPES/ NaCl buffer pH=7.1. Two devices are measured simultaneously. The gate current is shown in red.

The evaluation of Philips devices in liquid was checked previously by Mescher et al. by pH sensing experiments¹⁸, and by assessing the influence of conductivity and dielectric constant of water-dioxane mixtures on the electrical response of SiNW FETs²⁰ and by Cao et al. by using siloprene-based ion-selective membranes for potassium and sodium sensing.²²

Modification of the SiNWs by polyelectrolyte multilayers

Modification of the SiNWs by polyelectrolyte layer-by-layer adsorption is one of the chemical modification techniques possible for protein detection (this thesis, Chapter 2). To our knowledge a combination of PEs and proteins for antigen detection on nanowires was not yet reported. In this section SiNWs were modified by alternating positive and negative PEs and a protein, here streptavidin. Initially, a shift in threshold voltage (V_t) of the SiNW FETs as a response to the addition of PEs was measured. Later, the change in electrical characteristics of SiNWs to the addition of streptavidin, was verified.

A stack of PEI/PSS/PAHb was built on SiNW surface by flushing the device with PEs in 1 mg/ml concentration in 50 mM HEPES/ 50 mM NaCl buffer pH=7.1 for 4 min. After each PE deposition, a rinsing step was introduced by flushing with only HEPES/NaCl buffer solution for 4 min. After the rinsing step electrical measurements on modified NWs were performed. As in all experiments in aqueous phase, the back gate was grounded while the front gate was swept between 0 and -10 V. The potential between the source and the drain was fixed, 50 mV. The threshold voltage was defined as voltage at 1 nA drain-source current.

The results of these measurements are presented in Fig. 9. As can be seen from Fig. 9, an addition of the polycation shifts V_t to more negative voltages, and an addition of the polyanion shifts V_t to more positive values. The addition of a polycation results in more attraction of electrons to the nanowire, thus more depletion and less current I_{ds} . In order to compensate V_t has to become more negative. Figure 9 shows the response of the threshold voltage shift on 3 chips. Two NWs on each chip were measured simultaneously. One NW on chip #3 did not give any response, and hence the results of only 5 NWs are presented. 4 out of 5 NWs show a clear alternating signal, however the changes upon each layer addition are very small compared to literature reports. In more detail Vu

et al. (whose system is similar to ours) reported deposition of alternating PAH and PSS, starting with 0.11 V for first PE deposition, followed by a decrease to 0.06 V for the fourth layer.⁷ Dorvel et al. adsorbed poly-L-lysine (although on a SiNWs covered with different dielectric) with the V_t shift of 0.16 V, followed by a deposition of a single stranded DNA and V_t shift of 0.09 V.²³ Maximum shift recorded by us was 0.1 V, however typical shift was around 0.02 V. One of the possible reasons for lower changes in threshold voltage can be related to the thickness of the silicon oxide layer on top of SiNW: 8 nm in our case vs. 6 nm in the case of Vu et al.⁷ The additional 2 nm of oxide move away the sensing surface from the NW core. Comparison to the research of Dorvel et al.²³ from this point of view is problematic since in that work a thin layer of a different dielectric, i.e. hafnium oxide, was deposited on top of SiNWs covered with native oxide. In addition, the Debye screening effect²⁴ could play a role. Vu et al.⁷ used 10 mM phosphate buffer for characterisations and Dorvel et al.²³ used 20 mM saline-sodium citrate buffer, while we used 50 mM HEPES buffer. Additional decrease of the salt concentration might help to prevent screening of the signal, and increase in the threshold voltage shifts during alternating PE deposition.

The addition of PEs was expected to give higher responses.⁷ Still, qualitatively the alternating response was according to expectations with more negative threshold potentials for positively charged PEs, and more positive threshold potentials for negatively charged PSS. Before performing the experiments of influenza A antigen detection, the response of NWs to streptavidin binding was checked. Streptavidin at pH = 7.1 has negative charge too (it has an isoelectric point of ~5), and a shift of 0.02 V to more positive threshold voltages was observed (Fig. 9). These findings were encouraging to perform the next step of biotinylated antibody attachment and consequent detection of influenza A antigen.

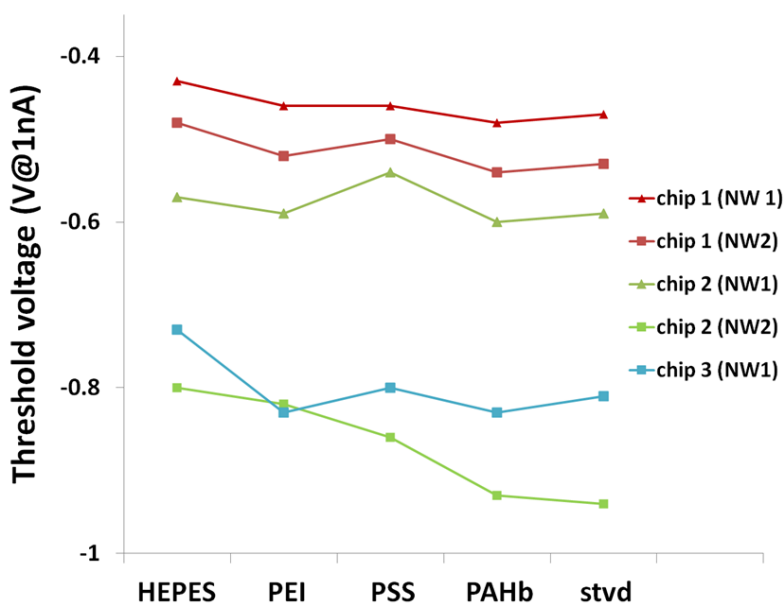


Figure 9. Threshold voltage change during the PEs deposition, including the last step of streptavidin addition.

Influenza A antigen sensing

After the initial evaluation of PE adsorption onto the SiNW devices, the next step of antibody-antigen immobilization was performed and followed by studying the changes in V_T . The top layer of SiNW covered with silicon oxide was modified with PEI, PSS and biotinylated PAH. For antigen detection biotinylated PAH reacted with streptavidin, which allowed binding of the biotinylated antibody (HB65) specific to influenza A antigens. In our experiments we have made use of biotinylated antibody (HB65) and antigen related to recombinant influenza A protein (Imgenex) and were obtained from the Department of Virology, Erasmus Medical Center, Rotterdam, the Netherlands.

The experiments followed the same protocol for PEs adsorption as described in the previous section. However, to avoid non-specific binding of the proteins to the walls of the microfluidic system, rinsing with BSA

was introduced. BSA is frequently used in biochemical assays, such as an enzyme-linked immunosorbent assay (ELISA), as a blocking agent. BSA is a negatively charged protein in immobilization pH with an isoelectric point of $\sim 4.7^{25, 26}$, thus it should not bind to negatively charged PSS. As a result of BSA insertion into the PE layers, the sequence of deposition changed to PEI, PSS, and BSA. Afterwards, biotinylated PAH was flushed through the system, followed by the addition of streptavidin, biotinylated specific antibody (HB65) and influenza A antigen in 10 $\mu\text{g/ml}$ concentration in HEPES/ NaCl buffer pH = 7.1 (for all the proteins).

Preliminary results on influenza A sensing with SiNW FETs are presented in Fig. 10. Figure 10 shows results measured on 2 different chips, with 2 NWs measured simultaneously (4 SiNWs in total). Interestingly, these devices show different responses to the chemical-biological modification leading to capturing of influenza A. However, the shift of the negatively charged BSA to more negative potential is not expected. Nonetheless, it is present in 3 NW devices out of 4 (most vividly in chip 1, NW 2; Fig. 10). In general, we observe non-reproducible results from the sensing experiments. Due to the limited availability of SiNW devices we were unable to perform more experiments.

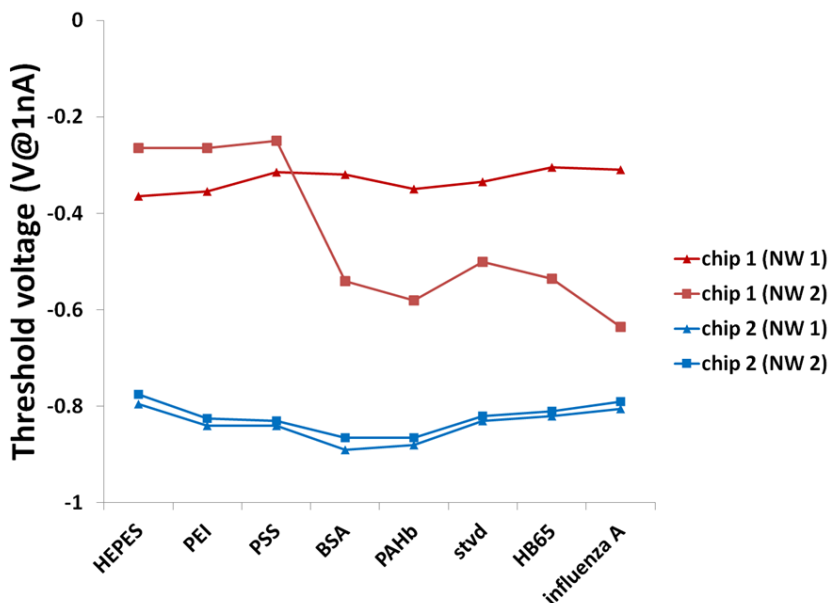


Figure 10. Threshold voltage shift upon addition of PEs, where last PE, namely biotinylated polyallylamine, allows capturing of streptavidin and consequently biotinylated specific antibody (HB65) to sense influenza A.

4.3.4 Conclusions

Philips SiNW FETs were initially characterized in air and in HEPES buffer, and showed p-type FET behaviour as expected. The modification of SiNW FETs with polyelectrolytes gave moderate results. The responses were lower than values reported in literature, although a direct comparison on the sensitivity is difficult due to the different device characteristics.

While PE sensing by SiNW FETs is somewhat positive, preliminary results on influenza A sensing by these devices are uncertain at the moment. So far, no reproducibility upon influenza A antigen sensing was observed. Intercalation of the BSA step in the process disturbed habitual pattern of PEs deposition. It remains unclear why negatively charged BSA shifts threshold voltage to more negative potentials and not to the opposite direction. However, the small amount of available devices

prevented us from further investigating the matter. In the next chapters an alternative optical resonator platform was used.

References

1. WHO, *World Health Statistics*, Report 978 92 4 156444 1, **2012**.
2. S. C. Gopinath, T. H. Tang, Y. Chen, M. Citartan, J. Tominaga and T. Lakshmipriya, *Biosens Bioelectronics*, **2014**, *61*, 357-369.
3. I. Grabowska, K. Malecka, U. Jarocka, J. Radecki and H. Radecka, *Acta Biochim Pol*, **2014**, *61*, 471-478.
4. L. Krejcova, D. Hynek, P. Michalek, V. Milosavljevic and R. Kizek, *Int J Electrochem Sci*, **2014**, *9*, 3440-3448.
5. F. Patolsky, G. Zheng, O. Hayden, M. Lakadamyali, X. Zhuang and C. M. Lieber, *Proc Natl Acad Sci USA*, **2004**, *101*, 14017-14022.
6. T. S. Y. Moh, ISBN: 978-90-5335-773-6, TU Delft, **2013**.
7. X. T. Vu, R. Stockmann, B. Wolfrum, A. Offenhäusser and S. Ingebrandt, *Phys Status Solidi A*, **2010**, *207*, 850-857.
8. M. H. Abouzar, A. Poghosian, A. M. Pedraza, D. Gandhi, S. Ingebrandt, W. Moritz and M. J. Schoning, *Biosens Bioelectron*, **2011**, *26*, 3023-3028.
9. G. Z. Garyfallou, L. C. P. M. de Smet and E. J. R. Sudhölter, *Sens Actuators, B*, **2012**, *168*, 207-213.
10. T. S. Y. Moh, Y. Maruyama, C. Shen, G. Pandraud, L. C. P. M. de Smet, H. D. Tong, C. van Rijn, E. J. R. Sudhölter and P. M. Sarro, *Proceeding IEEE Transducers*, Beijing, China, **2011**, pp. 1590-1593.
11. T. S. Y. Moh, S. K. Srivastava, S. Milosavljevic, M. Roelse, G. Pandraud, H. W. Zandbergen, L. C. P. M. de Smet, C. J. M. van Rijn, E. J. R. Sudholter, M. A. Jongsma and P. M. Sarro, *Proceeding IEEE MEMS*, Paris, France, **2012**, pp. 1344-1347.
12. H. D. Tong, S. Chen, W. G. van der Wiel, E. T. Carlen and A. van den Berg, *Nano Lett*, **2009**, *9*, 1015-1022.
13. L. Bousse, N. F. De Rooij and P. Bergveld, *IEEE T Electron Dev*, **1983**, *30*, 1263-1270.
14. P. Bergveld, presented in part at the IEEE Sensor, Toronto, **2003**.
15. E. E. Krommenhoek, M. van Leeuwen, H. Gardeniers, W. M. van Gulik, A. van den Berg, X. Li, M. Ottens, L. A. van der Wielen and J. J. Heijnen, *Biotechnol Bioeng*, **2008**, *99*, 884-892.
16. Y. Cui and C. M. Lieber, *Science*, **2001**, *291*, 851-853.
17. F. Patolsky, G. Zheng and C. M. Lieber, *Nanomedicine*, **2006**, *1*, 51-65.
18. M. Mescher, B. Marcellis, L. C. P. M. de Smet, E. J. R. Sudhölter and J. H. Klootwijk, *IEEE T Electron Dev*, **2011**, *58*, 1886-1891.
19. M. Mescher, L. C. P. M. de Smet, E. J. R. Sudhölter and J. H. Klootwijk, *J Nanosci Nanotechnol*, **2013**, *13*, 5649-5653.
20. M. Mescher, A. G. Brinkman, D. Bosma, J. H. Klootwijk, E. J. R. Sudhölter and L. C. P. M. de Smet, *Sensors*, **2014**, *14*, 2350-2361.

21. M. Mescher, ISBN: 978-94-91909-00-9, TU Delft, **2014**.
22. A. Cao, M. Mescher, D. Bosma, J. H. Klotwijk, E. J. R. Sudhölter and L. C. P. M. de Smet, *Anal Chem*, **2015**, *87*, 1173-1179.
23. B. R. Dorvel, B. Reddy, Jr., J. Go, C. Duarte Guevara, E. Salm, M. A. Alam and R. Bashir, *ACS Nano*, **2012**, *6*, 6150-6164.
24. E. Stern, R. Wagner, F. J. Sigworth, R. Breaker, T. M. Fahmy and M. A. Reed, *Nano Lett*, **2007**, *7*, 3405-3409.
25. F. Macritchie, *J Colloid Interface Sci*, **1972**, *38*, 484-488.
26. L. Medda, B. Barse, F. Cugia, M. Bostrom, D. F. Parsons, B. W. Ninham, M. Monduzzi and A. Salis, *Langmuir*, **2012**, *28*, 16355-16363.

Chapter 5

Protein Detection on Biotin-derivatized Polyallylamine by Optical Microring Resonators

Abstract

Silicon optical microring resonators (MRRs) are sensitive devices that can be used for biosensing. We present a novel biosensing platform based on the application of polyelectrolyte (PE) layers on such MRRs. The top PE layer was covalently labeled with biotin to ensure binding sites for antibodies via a streptavidin-biotin binding scheme. Monitoring the shift in the microring resonance wavelength allows real-time, highly sensitive detection of the biomolecular interaction.

This chapter is based on the following work:

Daniela Ullien, Peter J. Harmsma, Shahina M. C. Abdulla, Bart M. de Boer, Duco Bosma, Ernst J. R. Sudhölter, Louis C. P. M. de Smet, and Wolter F. Jager "Protein detection on biotin-derivatized polyallylamine by optical microring resonators" Optics Express, 2014, 22, 16585-16594.

5.1 Introduction

Microring resonator (MRR) based sensing¹ is one of the optical label-free technologies available now for highly sensitive detection of biomolecules like proteins or DNA^{2, 3}. One of the advantages of MRRs is their compatibility with wafer-scale semiconductor fabrication technologies. Essentially, the MRR is a periodic passive wavelength filter, which transmits or absorbs optical signals at specific resonance wavelengths. A fraction of the light in the MRR extends from the MRR surface, decaying exponentially with distance. Changes in the refractive index associated with binding phenomena to the MRR surface cause a shift in the resonance wavelengths, which can be accurately measured. Photons travel multiple roundtrips in the MRR, and consequently have many interactions with the analyte, providing high sensitivity.

This type of devices will reach its full sensing potential for (bio)sensing applications only with highly optimized surface chemistry^{3, 4}. For silicon-based optical biosensing, simple physisorption of proteins to the sensor surface has been reported, but for advanced applications surface modification is required. So far, surface modification for biosensing has almost exclusively achieved by covalent functionalization using silane chemistry. Bailey and coworkers have demonstrated real-time monitoring of several surface modifications on microring resonators, such as polymerization reactions⁵ and layer-by-layer (LbL) deposition of polyelectrolytes (PE)⁶⁻⁸. The LbL electrostatic polymer deposition was used for evanescent decay profiling, showing a decay length of 63 nm⁶.

In this Chapter, a novel method is presented for capturing analyte molecules based on LbL deposition of PEs. This method is based on electrostatic interactions and is very general, as it will work on all charged surfaces. Due to the large decay length of the MRR, around 65 nm, this method allows for the construction of extensive multilayer systems without losing sensitivity. In our approach, the last PE layer is functionalized and

this covalent labeling enables the incorporation of a large variety of functional groups at different degrees of functionalization. To the best of our knowledge surface modification using labeled polyelectrolytes has not been reported for biosensing applications using a MRR or another optical measuring platform. For the biosensing application demonstrated here, biotinylated polyelectrolyte is used, allowing the subsequent capture of streptavidin as a model protein, see Fig. 1. Figure 1 also gives the structures of polyethyleimine (PEI), poly(allylamine hydrochloride) (PAH) and poly(sodium styrene sulfonate) (PSS), which were used to prepare the PE stack yielding PEI(PSS/PAH)₃.

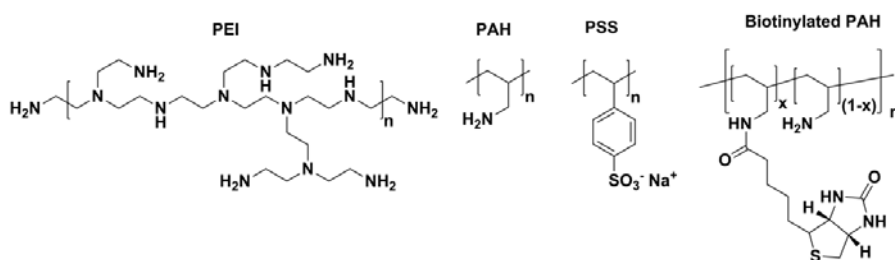


Figure 1. Polyelectrolytes deposited on MRR device for streptavidin capture.

5.2 Material and Methods

5.2.1 Materials

Polyethyleimine (PEI, Mw~25kDa, branched), poly(allylamine hydrochloride) (PAH, Mw~15kDa), poly(sodium styrene sulfonate) (PSS, Mw~70kDa), biotin, N-hydroxysuccinimide (NHS), 1-Ethyl-3-(3-dimethylaminopropyl)carbodiimide (EDC), and streptavidin were obtained from Sigma-Aldrich.

5.2.2 Microring Resonator

Silicon-On-Insulator (SOI) microring resonators were fabricated in the framework of ePIXfab⁹ using a 193 nm deep-UV lithography process. Waveguides are located on a 2.0 μm thick SiO₂ bottom cladding, and have

dimensions of 220 nm (height) by 450 nm (width) to support a single transverse electric (TE)-polarized mode at a wavelength of 1550 nm. Optical coupling between access waveguide and ring is provided by Multimode Interference (MMI) couplers having a 50/50 split ratio. The total ring length is 1040 μm , of which 840 μm consists of the waveguide structure described above. The remaining 200 μm is occupied by the MMIs and MMI tapers, and contributes only little to the sensitivity. The ring is folded to a semi-circle, see Fig. 2. To ensure maximum sensitivity, no top layer was applied to the samples, so that only a thin native oxide layer covers the waveguides. Wafers were thinned to 250 μm thickness.

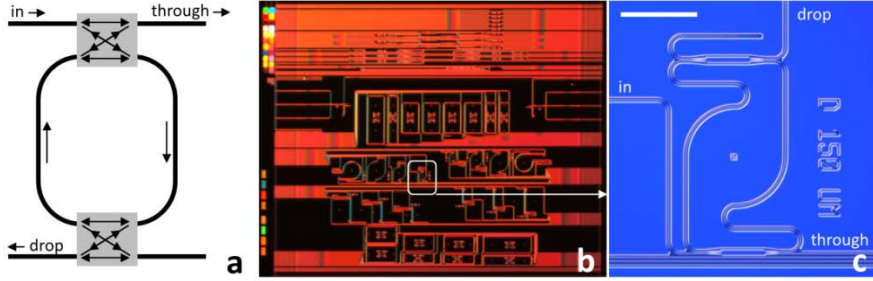


Figure 2. (a) Schematic representation of MRRs, showing a ring-shaped waveguide, with optical couplers to input, ‘through’ output and ‘drop’ output. (b) Microscopic photograph of generic MRR test chip (6x6 mm). (c) Microscope photograph of the device selected for these tests. The scale bar indicates 100 microns.

We use out-of-plane grating couplers¹⁰ to couple light in and out of the MRR. These grating couplers, designed to couple TE polarized light into the chip, are mature and standardized building blocks in the ePIXfab platform. At the time of design, TM couplers were not yet validated, which was the main reason to design our system for TE polarization only. To permanently mount fibers to the chip, we use fibers having 40° angled facets mounted in-plane with the chip¹¹, see Fig. 3a. A thermal conductive glue is used for bonding the chip to an aluminum plate for temperature

stabilization and assembly robustness. A home-built flow cell made from PMMA, see Fig. 3b is glued on top of the chip using a UV curable glue (NOA61, Norland Products). With a pumping rate of $90 \mu\text{l} / \text{minute}$, the flow rate of the liquid at the resonator sensing area is 1 mm/sec , which is in the laminar flow regime for water.

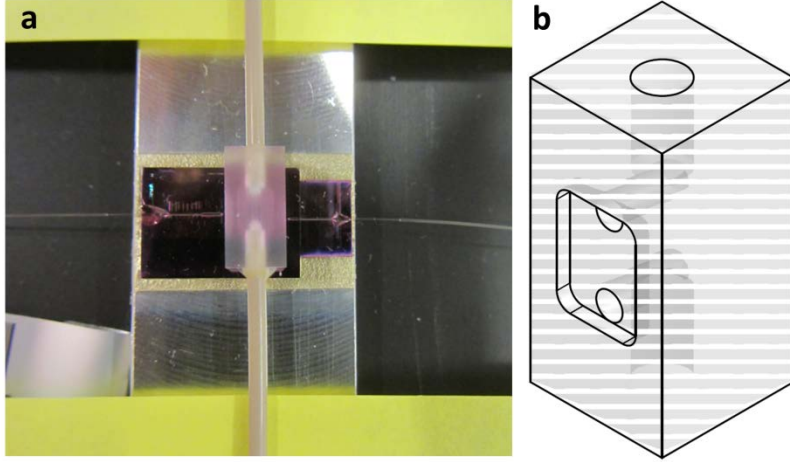


Figure 3. Top view of assembled MRR sensor (a), showing the flow cell glued on the chip, with tubing extending upwards and downwards, and in-plane mounted fibers extending to the left and right, and (b) schematic of the flow cell.

Figure 4 shows typical MRR transmission spectra before and after fiber mounting. Fiber mounting introduces about 3 dB extra loss of optical power per fiber connection due to non-optimal alignment. Upon mounting the spectra become cleaner because the transparent UV epoxy between fiber and grating coupler suppresses residual reflections. Ring performance parameters such as Free Spectral Range (FSR, 500 pm) and the on-off ratio (14 dB) remain the same. The FSR agrees well with the estimated 520 nm as follows from $\text{FSR} = \lambda^2/n_g L$, with λ the wavelength (1531 nm), n_g the waveguide group index (4.337), and L the ring length (1040 μm). The small

deviation can be explained by small waveguide width deviations, and by the different effective group index of the MMI couplers.

The overall loss is in the order of 21 dB. Each grating coupler causes 5 dB loss, and the 7 mm of access waveguides another 2 dB loss in air. The MRR insertion loss is 1 dB, a 3-dB fiber-optic splitter, see Fig. 5, adds up to an expected loss of 16 dB. The remaining 5 dB is caused by extra waveguide loss due to absorption by the water, and by non-optimal alignment even prior to gluing.

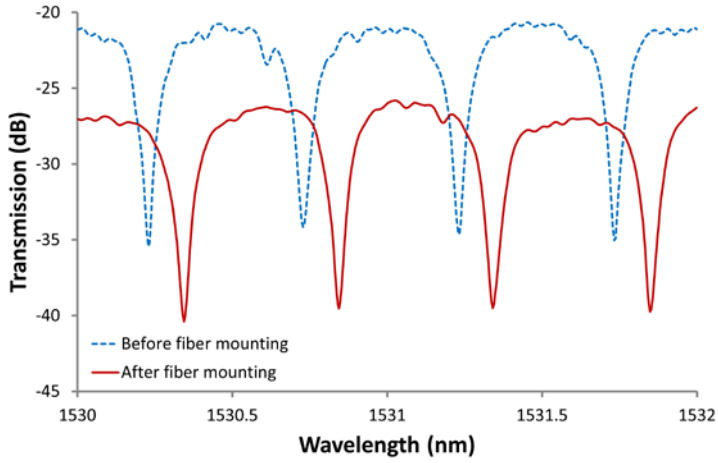


Figure 4. Transmission spectra of the MRR.

5.2.3 Optical Set-up

During the binding experiments, we continuously measure the MRR spectra, and post-process the data to obtain the resonance wavelengths as a function of time. The spectra are measured by scanning the wavelength of a tunable laser (Agilent 81960A), and measuring the power transmitted by the MRR using a detector (Agilent N7744), see Fig. 5a. A polarization controller (HP 11896A) sets the polarization to TE at the chip, thereby

maximizing the transmission. A typical measurement over 2 nm takes 0.7 seconds or more, depending on the laser settings.

In order to verify that the MRR response did not shift rapidly by more than the Free Spectral Range within a measurement interval, we optionally include a second laser (New Focus 6262), see Fig. 5b and fix its wavelength to match the reflection wavelength (1529.8 nm) of a temperature insensitive Fiber Bragg Grating (FBG). The signal from this second laser 2 is reflected by the FBG, and routed to detector 2 by the optical circulator. The scanning range of tunable laser 1 is chosen not to include the FBG reflection wavelength, and this signal is transmitted by the FBG to detector 1. This system provides two independent simultaneous measurements:

- 1) A wavelength scan (laser 1, detector 1), providing accurate MRR wavelength shifts. Data acquisition rate is in the order of 1 Hz.
- 2) A transmission measurement at fixed wavelength (laser 2, detector 2). Each MRR wavelength shift by one FSR causes a minimum and maximum of the detector signal. Data acquisition rate is in the order of 50 kHz, so that high-speed large shifts can be monitored by counting the detector signal minima and maxima.

Combining the result of these two datasets, accurate wavelength shifts are obtained in which a full FSR shift will be spotted accurately.

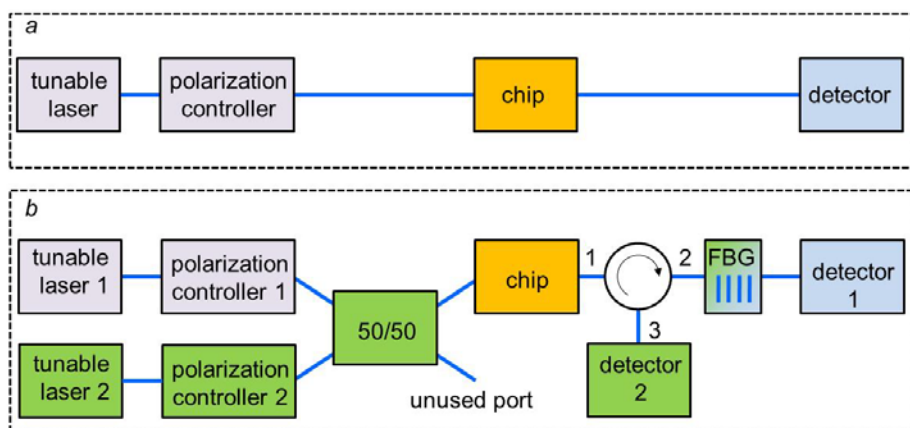


Figure 5. Optical setup: using a single scanning laser source (a) and using an additional fixed laser source, with the optical path indicated in green (b). FBG stands for Fiber Bragg Grating.

5.2.4 Synthesis of Biotinylated PAH

Biotinylated PAH was synthesized by covalent attachment of biotin to PAH via a carbodiimide-activated coupling reaction (Supporting Information, Fig. B1, Appendix B). The synthesis was adapted from Tsai et al.¹². 6% biotinylated PAH was synthesized by adding 500 mg PAH, 130 mg biotin, 166 mg EDC, and 61.5 mg NHS in 70 ml deionized water (DI) and reacting at room temperature for 3 days while stirring. The unreacted biotin was removed by dialysis (Mw cut off ~7 kDa) against DI water for 2 days with refreshing every 12 h. To evaluate the biotin grafting density, biotinylated PAH was freeze dried and analyzed by proton nuclear magnetic resonance (¹H-NMR). Using the integrated values of the two peaks at 4.4 and 4.6 ppm in the proton NMR spectrum, which originate from the two bridgehead protons of biotin, the labeling was calculated to be 2.5%, 6% and 9% biotin load of the PAH polymer (Supporting Information, Fig. B2, Appendix B).

5.2.5 Polyelectrolyte Deposition and Streptavidin Immobilization

PE layers were formed by subsequently flushing the flow-cell with 1 mg/ml PEI, PSS and PAH in 150 mM NaCl pH=5.5 solution for 4 min at a pumping rate of 90 μ l/min. The last bound PE layer was a biotinylated PAH added using a concentration of 1 mg/ml in 150 mM NaCl pH=5.5. After each polymer deposition, the chip was flushed with 150 mM NaCl for 4 min. The constant flow conditions were maintained with a syringe pump model 33 from Harvard apparatus.

If the flow for the first PSS layer deposition is continued for 15 min., then the following layers exhibit a very unstable behavior. The optimum deposition time was found to be 4 min.

After PE deposition, 1 or 10 μ g/ml of streptavidin in NaCl pH=5.5 was flushed through the flow-cell for 1 h. NaCl solutions were adjusted to the required pH by adding small amounts of concentrated NaOH (aq.) or HCl (aq.). The solution pH was monitored (and re-adjusted when required) with a Metrohm 827 pH Lab meter (Metrohm Applikon, The Netherlands).

5.3 Results

5.3.1 MRR Sensitivity

Using the setup shown in Fig. 5b we counted the transmission minima and maxima while the ring resonator becomes wet. When aqueous NaCl reaches the MRR device, first the optical power drops a bit due to losses of the wetted input waveguide. The solution reaches the ring at 11.3 sec, shifting the resonances, see Fig. 6. The wetting of the ring resonator takes about 0.3 sec. The fringes are generated at a rate of up to 2 fringes per ms, the typical total number of fringes is 50, see Fig. 6. This corresponds to a wavelength shift of 25 nm for an ambient refractive index change of 0.33, or a sensitivity of 75 nm/RIU. A commercial waveguide simulation tool (Photon Design Fimmwave) predicts a sensitivity of $dn_{eff}/dn_{amb} =$

0.197, with n_{eff} the effective index of the waveguide, and n_{amb} the ambient refractive index. Using $d\lambda/dn_{\text{amb}} = (\lambda/n_g) \cdot dn_{\text{eff}}/dn_{\text{amb}}$ with λ the wavelength and n_g the group index, we expect a sensitivity of 70 nm/RIU. The observed value is slightly higher, in spite of the fact that the MMI couplers do not contribute significantly to the sensitivity. Higher sensitivity values reported in literature (for example 163 nm/RIU¹³) can only be achieved using TM polarization. We calculate a TM sensitivity in the order of 220 nm/RIU for our waveguide structure.

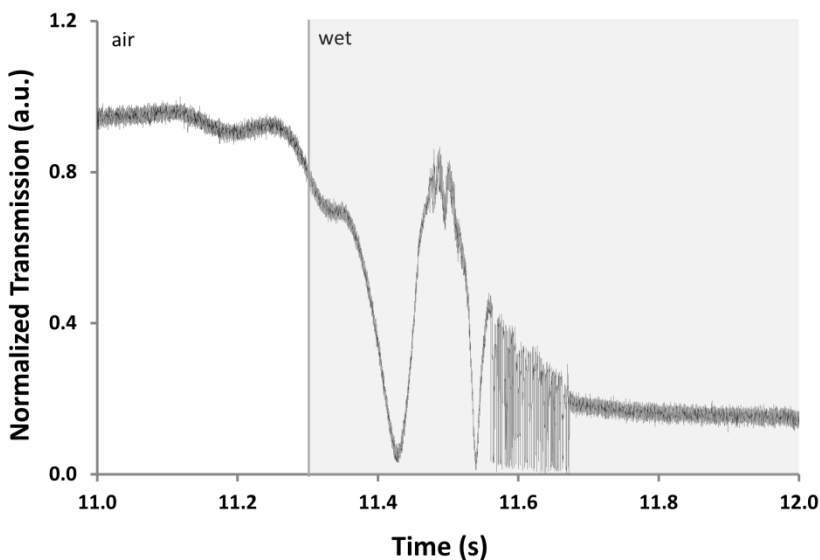


Figure 6. Fringe counting during the transition of MRR from air to NaCl solution.

5.3.2 MRR Response to PEs Deposition

The wavelength shift of the MRR upon the addition of PE layers is shown in Fig. 7. In Figure 7a the sequential addition of the different polyelectrolytes, being PEI, PSS, PAH, PSS, PAH, PSS and biotinylated PAH is shown. On the horizontal-axis we plot the time when the PEs or 0.15 M NaCl aqueous solution were added to the flow-cell as indicated by the vertical lines in the Fig. 7a. It takes 1.5 min. to observe the shift in the

case of PEs, due to the time for the solution to pass through the tubing to reach the flow-cell (dead volume $\approx 135 \mu\text{l}$). Wavelength shifts observed upon polyelectrolyte addition are typically in the order of 0.3 to 0.6 nm, which is significantly larger than values reported earlier with the same polymers⁶. Measurements of the thickness of dry PAH/PSS bilayers by ellipsometry, also indicate a significantly larger layer thickness of 5.4 nm, see Fig. B4 in the Supporting Information, Appendix B. Also noteworthy, and different from previously reported cases, is the very small 0.02 nm shift that is observed upon rinsing with aqueous NaCl solution. This indicates that the polyelectrolyte layers are firmly attached and are not easily washed away.

The wavelength shifts inflicted by each PE attachment from 6 different experiments are represented in Fig. 7b. Figure 7b clearly shows that wavelength shifts induced by the first two PE attachments, from the first PEI layer and the first PSS layer, exhibit large variations. These variations exceed the variation in sensitivity between individual MRRs, which is in the order of 10% (measured with NaCl solution), and may be due to the initial cleanliness of the oxide surface. The variations in wavelength shifts decrease with the attachment of the following layers, with a notable exception for the last PAHb layer, *vide infra*. It is clearly visible that the wavelength shifts upon attachment of PSS layers ($0.50 \pm 0.05 \text{ nm}$) are substantially larger than those observed for PAH layers ($0.29 \pm 0.04 \text{ nm}$). The wavelength shift induced by the addition of biotinylated PAH ($0.44 \pm 0.08 \text{ nm}$) is significantly larger than the typical PAH shift. There is a clear difference between the 2.5% biotinylated PAH (the two lower points) which have an average response of 0.34 nm and the rest of the biotinylated series with an average of 0.49 nm. This implies that the covalent attachment of biotin to the PAH has a positive effect on the binding of this polyelectrolyte, despite the decreased charge density of this polymer.

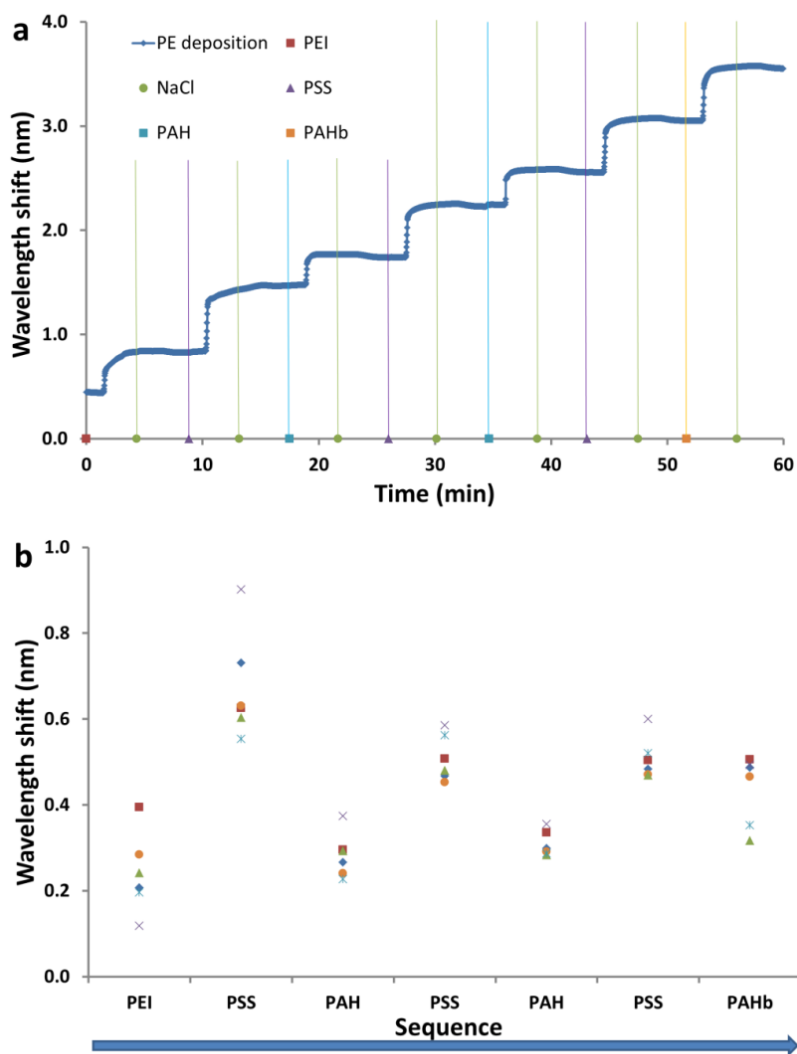


Figure 7. (a) Optical response of the MRR to the addition of PE layers. (b) Wavelength shifts of MRRs upon PEs addition for 6 individual devices.

5.3.3 Biotinylated PAH/ Streptavidin

The last layer of PE on the MRR was biotinylated PAH, which can bind streptavidin. We used streptavidin as a model protein for measuring the binding event between the analyte and the underlying surface. The response of the ring resonator upon injection of streptavidin solutions is shown in Supporting Information, Fig. B3, Appendix B. Figure B3 clearly shows that the time at which the streptavidin starts to attach, does not correlate with the injection time. While the polyelectrolytes all started to grow at exactly 1.5 minutes after injection, streptavidin growth starts much later, at 7 to 15 minutes after injection. This phenomenon is attributed to non-specific binding of the protein to the tubing and the interior of the flow cell, which consumes the protein before it reaches the active surface of the ring resonator.

In Fig. 8 we have normalized the data from Fig. S3 by starting all traces at the origin at the moment the streptavidin attachment begins. Figure 8 clearly demonstrates that the magnitude of the wavelength shift, ranging from 0.45 to 0.9 nm is comparatively large. This wavelength shift, which is proportional to the amount of streptavidin attached, is a function of the degree of biotinylation of the underlying PAH layer and, to a lesser extent, to the streptavidin concentration. The best results, implying faster growth, and the formation of a denser streptavidin layer, are obtained by using PAH with 6% biotin attached. When 10 $\mu\text{g/ml}$ streptavidin is injected the layer growth is fast and 80% is finished within 5 minutes. Using a 1 $\mu\text{g/ml}$ streptavidin solution the growth is much slower, and clearly divided in two regimes; fast growth during the first 15 minutes, and a much slower growth afterwards. Nevertheless, the total wavelength shift approaches the same value after 1 hour, indicating that the amount of streptavidin attached is independent of the streptavidin concentration. It was also demonstrated that rinsing with aqueous NaCl solution did not remove the bound streptavidin (not shown).

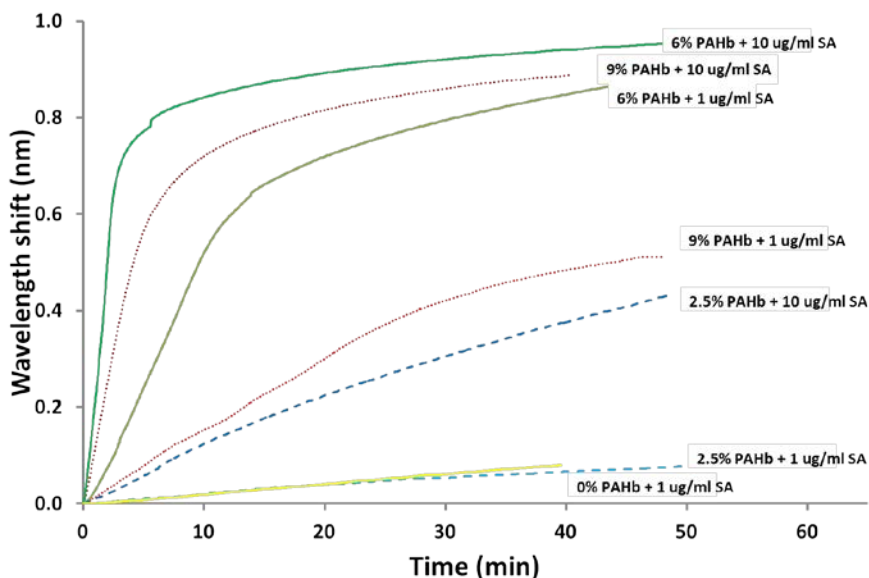


Figure 8. Normalized MRR shifts as a response to the addition of 1 and 10 $\mu\text{g/ml}$ streptavidin. Data was taken at a sampling rates between 0.8 and 1.4 Hz, clearly faster than the timescale of the binding process.

For the 9% biotinylated PAH layer, the amount of streptavidin attached, and the rate of streptavidin attachment are lower. Using 10 $\mu\text{g/ml}$ streptavidin solutions a fast growth was observed during the first 5 minutes, followed by a much slower growth afterwards like in the case with 6% biotinylated PAH. Using 1 $\mu\text{g/ml}$ streptavidin solutions, the growth is slower and the amount of streptavidin attached after one hour is much lower when lower concentrations of streptavidin are used. Whether the final degree of loading depends on the streptavidin concentration cannot be concluded from our data.

For the 2.5% biotinylated PAH layers the slowest streptavidin attachment was observed. Using the 10 $\mu\text{g/ml}$ streptavidin solution, the slowest growth was observed among different percentages of biotinylation. For the 1 $\mu\text{g/ml}$ streptavidin solution the rate and the extend of

streptavidin attachment were very low, and similar to those of non-specific binding to a blank, non-biotinylated, PAH sample.

These results clearly indicate that efficient and strong streptavidin binding to the biotinylated PAH can be achieved, but that streptavidin also binds non-specifically to other surfaces. This non-specific binding may also explain why the initial slope during the streptavidin binding does not scale with the streptavidin concentration, as expected¹⁴. In order to make devices that do not waste precious proteins by non-specific binding, it is necessary to prevent this binding of streptavidin by blocking the non-specific binding sites by an inactive protein, e.g. bovine serum albumin or other bio-repellent species.

5.4 Discussion

We have shown that a 7-layer polyelectrolyte film, composed of PEI, PSS, PAH, PSS, PAH, PSS and biotinylated PAH can be produced in a reproducible fashion. The observed wavelength shifts upon PE deposition are large and the deposited layers are very stable. Layer detachment by rinsing with aqueous NaCl is hardly observed. This is in contrast to the case of Luchansky et al.⁶, where rinsing with Tris buffer causes substantial detachment of PE layers, in particular the PAH layer. This is most likely due to competition of the ammonium ions of the Tris buffer and those of the attached PAH molecules.

The covalent attachment of biotin to the upper PAH layer, turns out to be a versatile and efficient method for producing a biotin-functionalized surface. Streptavidin attachment was observed for PAH with a 2.5, 6 and 9% degree of functionalization. However, kinetics of streptavidin binding and final layer density were not proportional to the degree of PAH biotinylation. Remarkably, the best results, in terms of rate and extent of streptavidin attachment, were obtained with the intermediate degree of biotin functionalization, i.e. 6%.

Non-specific binding of streptavidin to exposed surfaces is significant and has a pronounced effects on our experiments. Due to non-specific streptavidin binding, the streptavidin concentration profile in the solution above the ring resonator is not known. Therefore the initial slope during the streptavidin binding does not scale with the administered streptavidin concentration. Also, subsequent binding events to obtain a useful biosensor by immobilization of antibodies against a clinically-relevant analyte will take place on the non-specifically bound streptavidin and lead to waste of precious materials and loss of sensitivity.

5.5 Conclusions

We have demonstrated that the silicon optical microring resonator (MRR) is a highly sensitive, reliable and user friendly device for investigating surface modification and the subsequent construction of biosensors. Using this device we demonstrated that PEs deposition from aqueous NaCl solution results in stable PE layers, which exhibit negligible PE detachment during the rinsing step. We have shown that a stable 7-layer polyelectrolyte film, composed of PEI and alternated layers of PSS and PAH can be produced in a reproducible fashion. Employing biotinylated PAH as the last PE layer in this architecture, has been demonstrated as a suitable technique for protein deposition on MRRs.

Deposition of streptavidin on these biotinylated surfaces, based on kinetics and final layer density, worked best for PAH layers with an intermediate, 6%, degree of biotinylation. For follow-up experiment we intend to use the streptavidin functionalized PE architecture as a universal platform for the development of biosensors.

References

1. W. Bogaerts, P. De Heyn, T. Van Vaerenbergh, K. De Vos, S. K. Selvaraja, T. Claes, P. Dumon, P. Bienstman, D. Van Thourhout and R. Baets, *Laser Photonics Rev*, **2012**, *6*, 47-73.
2. A. J. Qavi, A. L. Washburn, J. Y. Byeon and R. C. Bailey, *Anal Bioanal Chem*, **2009**, *394*, 121-135.
3. M. S. Luchansky and R. C. Bailey, *Anal Chem*, **2012**, *84*, 793-821.
4. M. J. Banuls, R. Puchades and A. Maquieira, *Anal Chim Acta*, **2013**, *777*, 1-16.
5. F. T. Limpoco and R. C. Bailey, *J Am Chem Soc*, **2011**, *133*, 14864-14867.
6. M. S. Luchansky, A. L. Washburn, T. A. Martin, M. Iqbal, L. C. Gunn and R. C. Bailey, *Biosens Bioelectron*, **2010**, *26*, 1283-1291.
7. G. Decher, *Science*, **1997**, *277*, 1232-1237.
8. R. R. Costa and J. F. Mano, *Chem Soc Rev*, **2014**, *43*, 3453-3479.
9. <http://www.epixfab.eu/>
10. D. Taillaert, F. Van Laere, M. Ayre, W. Bogaerts, D. Van Thourhout, P. Bienstman and R. Baets, *Jpn J Appl Phys* *1*, **2006**, *45*, 6071-6077.
11. P. O'Brian, presented in part at the ECOC, Amsterdam, **2013**.
12. W. B. Tsai, C. Y. Chien, H. Thissen and J. Y. Lai, *Acta Biomater*, **2011**, *7*, 2518-2525.
13. M. Iqbal, M. A. Gleeson, B. Spaugh, F. Tybor, W. G. Gunn, M. Hochberg, T. Baehr-Jones, R. C. Bailey and L. C. Gunn, *IEEE J Sel Top Quant*, **2010**, *16*, 654-661.
14. B. Johnsson, S. Lofas and G. Lindquist, *Anal Biochem*, **1991**, *198*, 268-277.

Chapter 6

Influenza A Detection by Free-space Coupled Optical Microring Resonators

Abstract

The optical microring resonator (MRR) is one of the developing sensing platforms that can provide a rapid and sensitive solution to influenza A detection. We present here research on influenza A detection using a free-space coupled MRR. A chemical-biological system based on polyelectrolytes (PEs) for selective capturing of influenza A was developed. In this system, the top PE layer is biotinylated for subsequent coupling with streptavidin, enabling the coupling of a biotinylated antibody. The thus-modified MRR showed response to the addition of clinically relevant concentrations of influenza A nucleoprotein, with a response time of about 15 min. The response time can be decreased by flushing the flow system with Bovine Serum Albumin to prevent nucleoprotein binding to the inner walls of the system. In addition, both pre- and post-treatment of the flow system with bleach improves the reproducibility between different devices and also facilitates their reuse.

This chapter is based on the following work:

Daniela Ullien, Peter J. Harmsma, Bart M. de Boer, Duco Bosma, Ernst J. R. Sudhölter, Louis C. P. M. de Smet, and Wolter F. Jager "Influenza A detection by free-space coupled optical microring resonator", manuscript in preparation.

6.1 Introduction

Influenza spreads throughout the world in seasonal epidemic outbreaks and can potentially cause millions of deaths in pandemic years, especially in poor and overcrowded areas.¹ Substantial progress has been achieved in the development of diagnostic assay for viral detection² and influenza sensing strategies³⁻⁵ over the past decades. Nevertheless there is an ongoing demand for faster, cheaper and reliable assays for the early detection of influenza. Proximity ligation assays (PLA)⁶, biosensor-based methods⁷⁻⁹, Förster/fluorescence resonance energy transfer (FRET)-based methods¹⁰, microarray assays¹¹, and nanoparticle-based techniques^{12, 13} are among those as reviewed by Shojaei et al.², who concentrated on the specific case of avian influenza virus. Sensors with a wider influenza virus variety have been reviewed by Gopinath et al.³, overviewing not only different sensor platforms, such as surface plasmon resonance, quartz crystal microbalance, interferometry, silicon nanowires, etc., but also different biological recognition elements, such as glycan ligands, aptamers and antibodies.

An interesting class of assays are label-free biosensor immunoassays which are the closest to the point-of-care (POC) rapid diagnostics, as they do not rely on highly trained personnel and costly procedures. Label-free methods use proteins without any attachment of additional chemical compounds, e.g. fluorophores for light-emitting analysis. Thus, no valuable resources are spent on the development of a labelled protein with equivalent characteristics as an unlabelled one. Moreover, label-free methods fulfil the high sensitivity and high selectivity requirements of POC. A good example of a label-free biosensor immunoassay^{3, 14, 15} using optics is the work of Xu et al.⁷ showing the detection of poultry avian influenza virus by an interferometric biosensor immunoassay.

We present here a different approach for influenza A virus detection using an integrated optical biosensor. In our work, influenza A was

detected by means of a free-space coupled silicon-on-insulator (SOI) microring resonator (MRR). This work is a continuation of the research described in Chapter 5 of this thesis and explores protein binding on the MRR platform covered with biotinylated polyallylamine hydrochloride (PAHb). The MRR platform has been used for detecting model proteins like immunoglobulin G (IgG) antibody-antigen pairs¹⁶ and cancer biomarkers for clinically relevant diagnostics.^{17, 18} Virus detection using silicon photonic microring resonator was previously shown by McClellan et al.¹⁹ on the bean pod mottle virus. Our approach complies best with the POC demands for low-cost, high-speed and high-sensitivity detection of influenza A by utilizing free-spaced coupled photonic resonator.

In the MRR technique the laser inserted into the SOI waveguide is coupled to the microring structure on the device and generates resonances going through the ring structure. The formed evanescent field in MRR is sensitive to refractive index changes in the medium above its surface up to ~60 nm.²⁰ Detection is possible by utilizing the direct relation between the wavelength shift of the resonances and the effective refractive index of the surrounding medium. Free-space coupled MRR²¹ does not exploit permanent fibre-chip coupling, making it extremely easy to replace chips in a fast and reliable fashion. In addition, reuse of the chip is possible. The platform given in Fig. 1 schematically illustrates the chemical-biological coupling of the influenza A antibody (dark blue) to the surface of the MRR. The principal of the protein immobilization is based on the biotinylated polyelectrolyte attachment previously shown by us²² and described in Chapter 5 of this thesis.

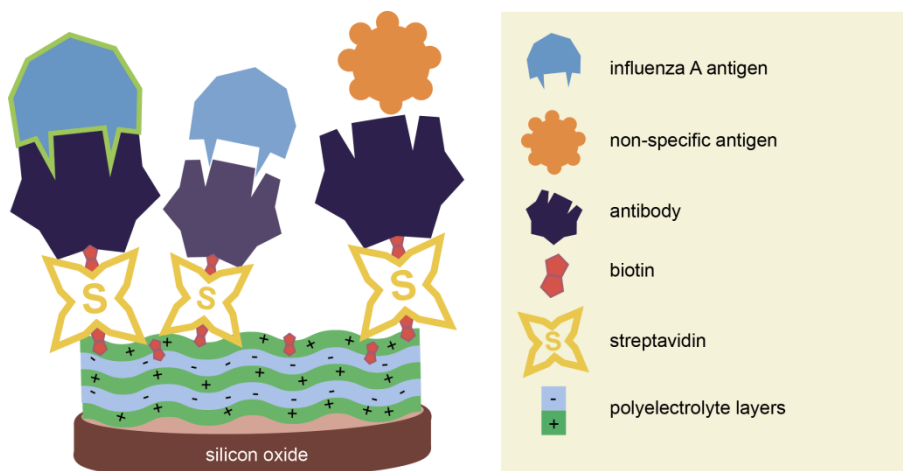


Figure 1. Schematic representation of the chemical-biological stack for influenza A detection based on biotinylated polyelectrolyte attachment.

6.2 Materials and Methods

6.2.1 Materials

Polyethyleneimine (PEI, $M_w = \sim 25\text{kDa}$, branched), poly(allylamine hydrochloride) (PAH, $M_w = \sim 15\text{kDa}$), poly(sodium styrene sulfonate) (PSS, $M_w = \sim 70\text{kDa}$), biotin, 1-hydroxy-2,5-pyrrolidinedione (NHS), 1-ethyl-3-(3-dimethylaminopropyl)carbodiimide (EDC), streptavidin and 4-(2-hydroxyethyl)-1-piperazineethanesulfonic acid (HEPES) were obtained from Sigma-Aldrich and used as received. Recombinant influenza A protein was purchased from Imgenex. Influenza A antibodies (specific-HB65, and nonspecific-HB64) were purchased at European Veterinary Laboratory (EVL, the Netherlands) and were biotinylated with a biotinylated kit (Lightning-Link Type B Biotin Antibody Labeling Kit, Novus Biologicals). Bovine Serum Albumin (BSA), IgG from rabbit serum, sodium chloride and sodium hydroxide were purchased from Sigma-Aldrich. Sodium hypochlorite was obtained from Brenntag (Germany).

6.2.2 MRR layout

Figure 2 (left) shows the schematic layout of a microring resonator.²³ The MRR is fabricated in a multi-project wafer run in the ePIXfab framework²⁴, using the standardized waveguide stack of 220 nm thick silicon on 2000 nm oxide. The waveguide width is 450 nm. The MRR consists of a ring-shaped waveguide, connected to bus waveguides A-B and C-D by means of directional couplers. We use a 180 nm gap over a length up to 5 microns and a bend radius of 10 microns to achieve approximately 10% power transfer between the bus and ring waveguides, resulting in well-defined wavelength resonances (Fig. 2, right). The ring length is 1120 microns, resulting in a free spectral range of 500 pm.

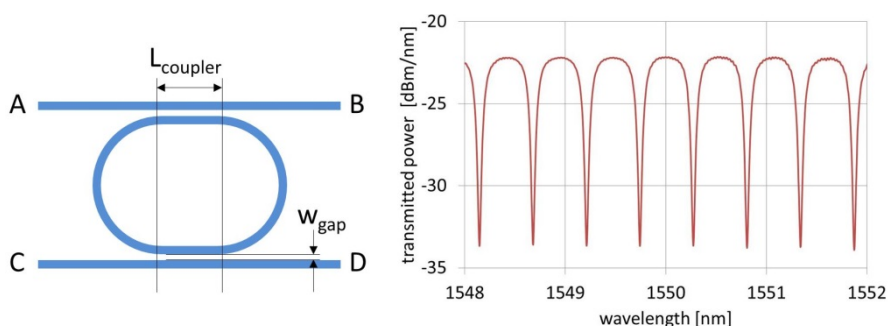


Figure 2. Schematic top view on the microring resonator (left), and a typical wavelength response (right).

6.2.3 Free-space coupling

Our collaborators from TNO have developed a portable desktop tool²¹ (Fig. 3) to conveniently achieve single-channel input, multi-channel output optical coupling to a chip. Light from a tunable laser source (Agilent 81960A) is provided via a polarization-maintaining single-mode fibre. An optical system images this fibre onto the out-of-plane grating couplers²³ on the chip, so that no fragile fibres need to be in close proximity to the

chip. The chip output signals are imaged onto multi-mode fibres by the same optical system, providing tolerant alignment, and directed to a detection system (Agilent N7744). A lab analyst can easily replace and align sensor chips in a matter of minutes by means of visual alignment, without the risk of causing damage to sensor or optical coupling system. This setup enables ring resonator sensing experiments outside conventional optics labs.

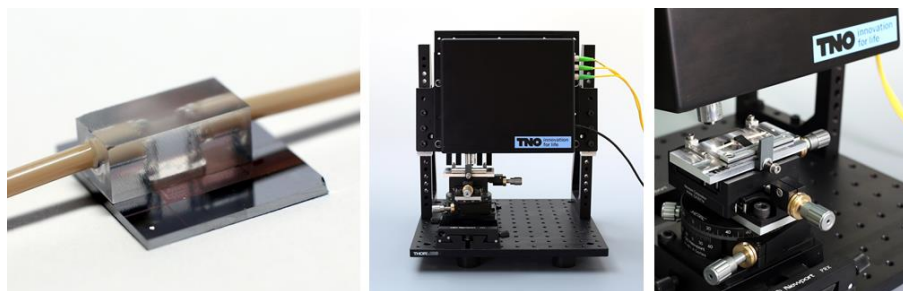


Figure 3. MRR chip with a flow cell (left), optical coupling setup (centre), and zoom-in of a chip inserted in the setup (right). Courtesy: Dr. Harmsma, TNO, The Netherlands.

6.2.4 Chemical-biological layer deposition

Layer deposition was performed by flushing the solution containing the adsorbent through the flow-cell glued onto the MRR chip. Firstly, polyelectrolyte (PE) layers were formed by rinsing alternating the chip with 1 mg/ml solutions of PEI, PSS and PAH in 100 mM HEPES/150 mM NaCl (hereafter referred to as HEPES buffer) at pH = 7.1. To prevent non-specific binding on the tubing and the flow-cell, 0.3 mg/ml of BSA in HEPES buffer was delivered through the flow-cell. The final PE was a 6% biotinylated PAH derivative, synthesized according to our previously published protocol.²² In short, biotin was covalently attached to PAH by carbodiimide chemistry. The biotin percentage was obtained from ¹H-NMR data (Supporting Information, Fig. C1, Appendix C). For the PE layers a

rinse of 3 min with a constant pump speed of 90 $\mu\text{l}/\text{min}$ (with 1 mm/sec laminar flow rate of the liquid at the resonator sensing area) was sufficient to build a layer, i.e. a plateau value was reached. Each PE adsorption step was followed by a HEPES buffer rinse for 3 min. This way the following PE stack was made: $\text{PEI}/(\text{PSS}/\text{PAH})_2/\text{PSS}/\text{PAHb}$, with intercalated BSA in it.

After the deposition of biotinylated PAH, 10 $\mu\text{g}/\text{ml}$ of streptavidin followed by 10 $\mu\text{g}/\text{ml}$ of biotinylated antibody—both in HEPES buffer—were flushed at the same pumping speed, but increased time of 15 min for optimal adsorption. Afterwards an additional BSA step was performed to minimize non-specific binding of the nucleoprotein (10 $\mu\text{g}/\text{ml}$ of BSA in HEPES for 15 min). Influenza A detection was verified by flowing solution of the virus protein in HEPES buffer at different concentrations. Non-specific responses were tested with two control experiments. First, the biotinylated non-specific antibody (HB64) was attached to the layers and influenza A stayed as the antigen. Second, layers with a specific antibody to influenza A were prepared to expose them to a reference antigen, i.e. rabbit IgG (with same variation in concentrations of the antigen).

6.2.5 Ellipsometry measurements

The thicknesses of PE layers were measured by ellipsometry using planar Si substrates. The conditions for PE deposition on planar Si were exactly as described in Section 6.2.4. The measurements were obtained by an M-2000F spectroscopic ellipsometer (J.A. Woollam Co., Inc), equipped with a 75W Xe arc light source. The experiments were performed at an incident angle of 70° . The optical thickness was determined using a standard model available in the CompleteEase software, i.e. Si with a transparent film on top of it. This model makes use of the optical parameters for Si as reported by Herzinger et al.²⁵, while for the transparent film (modelled as a Cauchy film) the following values have been used: $n = 1.5$, $k = 0$.

6.3 Results and Discussion

6.3.1 Layer-by-layer deposition

With free-space coupled MRR it is extremely easy to obtain reproducible results with PE multilayer deposition. In Fig. 4 we present typical results of such an experiment. Figure 4a shows the step-by-step PE adsorption. The steps are clearly visible and the observed shifts range between 120-250 pm depending on the PE in question. Even biotinylated PAH with a degree of functionalization of only 6% gives a different MRR response, since it has a different adsorption capability compared to its non-biotinylated analogue. This difference in absorption has been monitored thanks to the high sensitivity of the optical MRR set-up. The HEPES buffer rinse occurs between each PE flush and does not show removal of the PE layers from the MRR surface.

To prevent non-specific binding of streptavidin and subsequent antibody-antigen pair formation at the tubing and the walls of the flow-cell, a solution of the anti-fouling BSA protein in high concentration was flushed through the microfluidic system. A certain amount of BSA protein is expected to be adsorbed on the tubing, the flow-cell and between PE layers and saturate (block) unoccupied, non-specific binding sites.²⁶ Figure 4a shows the BSA response during the adsorption on MRR. In Fig. 4a it is visible that some addition of the negatively charged BSA to the surface of the MRR is happening, even though the top layer is also negatively charged PSS. We can attribute this addition to the attachment of BSA molecules in between the PE chains or to the attachment of BSA to PSS due to its amphoteric nature.²⁷ The kinetics of BSA binding is slower than those of PE layers, which can be detected due to the sensitivity of these devices.

The next step of immunoassay formation is flushing with 10 µg/ml of streptavidin and the biotinylated antibody (Fig. 4b, in this case specific antibody). This leads to an additional wavelength shift of 300-400 pm for

each step, again depending on the protein. The specific response of the proteins starts at ~1.5 min after the injection into the flow-cell system. This delay time is slightly larger compared to the PE delay-time of 1.1 min, but consistent and much smaller compared to our previously reported delay-time of 7-15 min.²² This has been accomplished by the addition of the BSA step in the process of building the chemical-biological stack for antigen detection.^{26, 28} This result implies that adding BSA during the build-up of the PE layers prevents protein fouling on the tubing and other surfaces that are accessible for injected proteins on their way to the MRR surface.

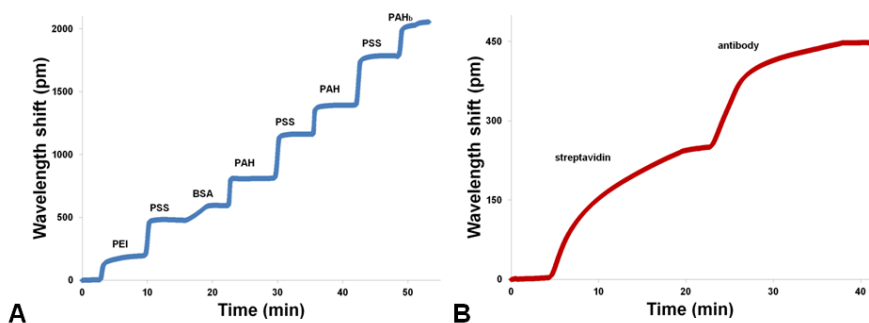


Figure 4. Representative results of an MRR experiment a) layer-by-layer deposition of PEs, b) protein adsorption on a PAHb-terminated PE multilayer.

6.3.2 Antigen detection

After the attachment of the biotinylated antibody and the BSA blocking of the non-specific sites, the resulting stacks were tested for antigen detection. Figure 5a shows duplicate results for the influenza A detection at relatively high analyte concentrations of 10 and 1 $\mu\text{g/ml}$. While there is some variation in results of the duplicate, it is clear that the total wavelength shift as well as the kinetics of the adsorption increase for higher concentrations of influenza A.

However, we did not notice any reliable dependence between the concentration of injected analyte and the MRR response for lower antigen concentrations, as expected in such measurements^{17, 19} (Fig. 5b). Figure 5b shows the total wavelength shift after 15 min of exposure to influenza A protein for 6 individual MRR sensors. For all these measurements the chemical-biological stack was built using the same conditions. The analyte was measured directly on biotinylated specific antibody. An assumption was made that the lack of a concentration dependency is due to the high non-specific binding of the antigen to the MRR surface which is still present in our system. To circumvent this non-specific binding, a second BSA treatment was introduced after the antibody step prior to the antigen insertion into the sensor. The second BSA addition led to a 95 pm MRR shift, on average. This indicates additional BSA binding on the active surface of the MRR, which should result in the blockage of the non-specific sites by BSA.

The results of the influenza A sensing experiments at low antigen concentrations of 10 and 100 ng/ml after the addition of the second BSA treatment are presented in Fig. 6a, in red. The second BSA step was introduced to reduce the non-specific binding of the antigen to the surface of the MRR by blocking the non-specific sites. Our initial assumption was to expect a lower wavelength shift for lower influenza A concentration.^{17, 19} However, no such concentration dependency was observed, since both 10 and 100 ng/ml antigen concentration give similar results for total wavelength shifts (5 to 40 pm shift). This implies that the above-made assumption that BSA sufficiently treats non-specific binding of the antigen is not correct and that it does not resolve this issue. In addition, Fig. 6a allows comparison between second BSA treated and untreated experiments (red vs. blue). For 100 ng/ml influenza A case, the capacity of the system decreased with the addition of the second BSA step. However, for the 10 ng/ml case this trend is not clear, because only

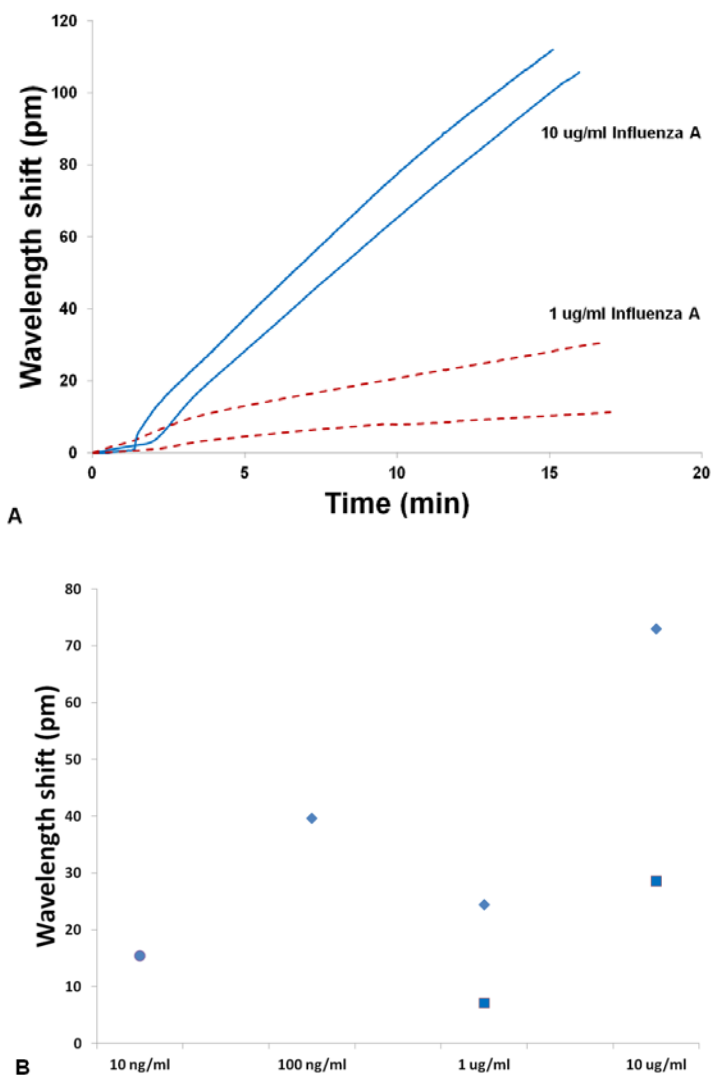


Figure 5. (a) Wavelength shifts during the addition of 10 and 1 µg/ml influenza A to specific antibody attached via biotin-streptavidin chemistry to PEs deposited on the surface of the MRR device; (b) total wavelength shift of 6 individual immunoassays with different concentrations of the influenza A antigen, taken after 15 min of exposure of the MRR surface. The real-time graphs are presented in the Supporting Information, Fig. C2, Appendix C.

2 out of 3 experiments show the same trend. Obviously, more experiments are needed and the work may benefit from exploring alternative anti-fouling agents.

Figure 6b shows an example of influenza A detection at 10 ng/ml concentration together with two control experiments. In Fig. 6b, the green line rises with a value of 42.5 pm within 15 min upon the addition of 10 ng/ml influenza A. Subsequent addition of different concentrations of the antigen shows additional increases in the signal, followed each time by a relatively flat response of the buffer rinse step. For this device we again do not observe a concentration-dependent response, even by increasing concentrations step by step on one device. We note that the detection limit of our sensor is reliant on two factors. The baseline drift, seen clearly in Fig. 6b (initial 10 min), and the sensitivity deviations between devices, addressed below in Section 6.3.3, make it difficult to compare between responses to different concentrations and to see a clear correlation between them. Although the kinetics correlation is not clear, the devices show a response to influenza A nucleoprotein addition as low as 10 ng/ml (Fig. 5b and Fig. 6).

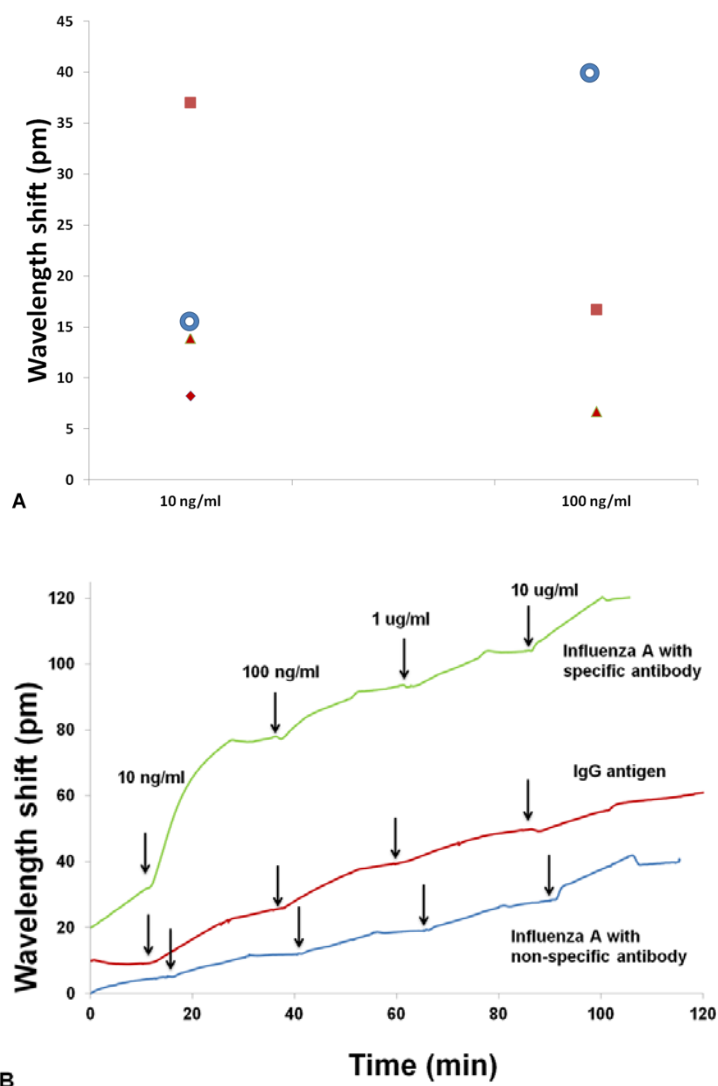


Figure 6. (a) Total wavelength shift vs. low concentrations of influenza A specific antigen. Duration of exposure is 15 min. Comparison between BSA (second) treated (red, solid) and untreated (blue, hollow) experiments. The real-time graphs are presented in the Supporting Information, Fig. C3, Appendix C.; (b) MRR response of the chemical-biological stack to the addition of influenza A nucleoprotein to specific (green) and non-specific (blue) antibody; and the response to the addition of different rabbit IgG antigen (red) to specific antibody of influenza A.

In Fig. 6b the results of two control experiments are presented. One control (Fig. 6b, red) was done using a widely abundant, but not specific IgG of the immune system as an antigen. Although the initial background was rather flat and hence promising, upon addition of the IgG antigen to the system, the picture changed with time. Firstly, we do not observe big wavelength shift as in case of the influenza A addition. Moreover, a constant drift appears during the buffer rinse steps, which makes it extremely difficult to distinguish between potential non-specific IgG adsorption and the background signal. The background drift can be attributed to the instability of the relatively large stack of PEs and proteins. For instance, if there would be swelling or shrinkage of the layer stack with time, the MRR system will observe this. In the case of swelling, more water will penetrate into the PE layers and the refractive index will decrease ($n_{\text{water}} = 1.33$ and $n_{\text{polymer}} = 1.5$). Shrinkage of the PE layers will cause increase in the refractive index. As the MRR wavelength shift is proportional to the change in the refractive index, the MRR drift upwards or downwards will reflect shrinkage or swelling, respectively. Both cases were observed for our system.

The second control experiment (Fig. 6b, blue) was performed by introducing non-specific antibody in the chemical-biological stack on the ring resonator. The MRR wavelength shift of the non-specific antibody was comparable to the shift of the specific antibody adsorption (Supporting Information, Fig. C4, Appendix C). The assumption is that both have the same amount of material on the MRR surface capable of antigen binding. The response of the influenza A in different concentrations to the MRR covered by non-specific antibody is small compared to the system with specific antibody and it follows the background drift. The kink upon addition of the 10 $\mu\text{g/ml}$ influenza A to the non-specific antibody may be referred to the non-specific binding of the antigen. However, the kink

goes away with buffer flushing, suggesting the removal of physically adsorbed molecules.

To conclude, we observe specific interaction of influenza A with the antibody, since only addition of the specific antibody (the green line in Fig. 6b) gave a strong MRR response. Some non-specific interaction is present, as can be seen from the two control experiments (Fig. 6b red and blue lines), but it is markedly smaller. The system, however, is unreliable when it comes down to measuring low concentrations of the influenza A antigen.

6.3.3 Pre- and post-treatment of the MRR devices

Deviations between MRR devices that are observed during the influenza A experiments may be partly due to the initial difference in sensitivity of each device. Figure 7 illustrates the statistical deviation in sensitivity of a set of 7 different non-treated vs. treated MRR devices. It was checked by measuring the response of each device to 1 M NaCl solution. Pre-treatment of the surface of the ring resonator with a 1% bleach solution at pH = 9 improved the sensitivity deviation to ~10%. Pre-treatment with bleach removes eventual organic contaminants from the surface of the sensor ring, while the rather thick resist layer on the reference ring remains intact as becomes clear from its insensitivity to the addition of PE. Devices with higher sensitivity to 1 M NaCl reveal higher wavelength shifts during influenza A experiments. However, no concentration-dependent trend was observed (Fig. 5b and 6a).

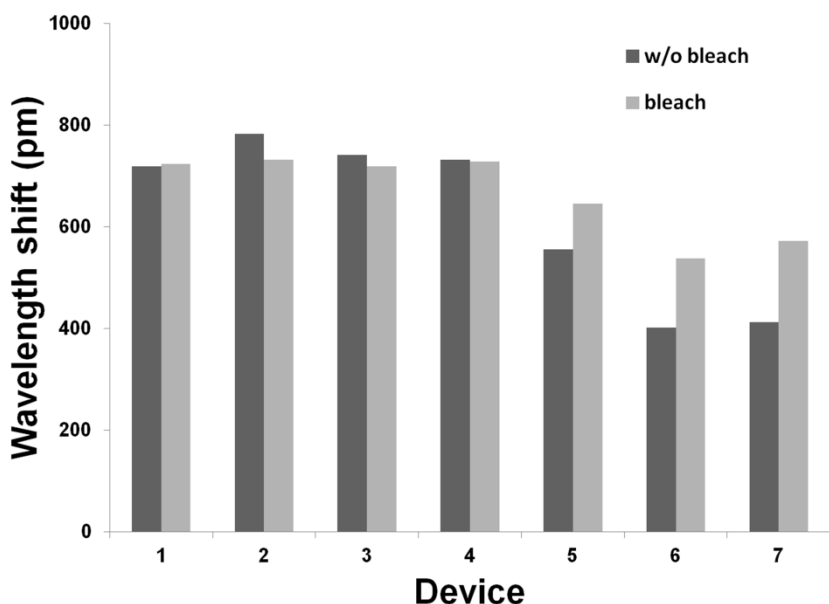


Figure 7. Sensitivity deviation between MRR devices in response to rinse with 1 M NaCl after pre-treatment with bleach (light grey) and without bleach treatment (dark grey). The size of the complete bar is a total MRR wavelength shift upon addition of 1M NaCl.

Post-treatment of the MRR devices was done with 1% bleach at pH values of 9 and 11. Figure 8 shows the results of treatment with bleach at pH = 11. The total wavelength shift during the complete build-up, i.e. PE depositions together with streptavidin, antibody and influenza A for this experiment was ~2500 pm. After finishing the influenza A detection, the solution with 1% bleach at pH = 11 was flushed over the MRR surface for 20 min. During this step the signal decreased as much as ~4000 pm (Fig. 8). The first 2500 pm of the signal change was attributed to layers removal, while the remaining part could be related to SiO_x removal, as reported for strong alkaline conditions.^{29, 30} Surprisingly, these findings were not confirmed by ellipsometry experiments done on planar silicon substrates separately. In more detail, the full chemical-biological stack had an

optical thickness of 10.8 ± 0.9 nm, and was reduced to ~ 7 nm after 15 min of bleach treatment at pH = 11. In separate experiments the PE layers were found to have an optical thickness of 7.8 ± 1 nm, which were reduced to ~ 1.5 nm within 15 min of treatment with bleach at pH = 11. Next, for bleach times from 30 min and higher an increase in the optical thickness was observed (up to ~ 20 nm after 12 h).

In an attempt to explain this discrepancy, we first looked more into the silicon/silica-related chemistry of hypochlorite. Hypochlorite solution was reported to be an etching and texturing reagent for SiO_x surfaces.^{29, 30} Lounas et al.³⁰ reported solvent-dependent effects of sodium hypochlorite solutions on the nature of the surface structure upon etching. The use of aqueous solutions without ethanol was found to induce the formation of nanostructures, like nanoneedles, on the Si surface. Hence, it can be reasoned that the optical thickness data as obtained by ellipsometry measurements is affected by changes in the surface roughness, making the optical thickness data unreliable.

To further investigate the effect of the pH, the post-treatment was also performed in 1% bleach at lower alkaline conditions (pH = 9, data not shown). During the bleach experiments at pH = 9 we observed decrease of ~ 1800 pm of the MRR signal, which is not only lower than the change at pH = 11 (~ 4000 pm), but also lower than the change established during the layer build-up (~ 2500 pm). This may indicate that only the top-layer is removed, i.e. the protein layer, while the PE layers remained onto the surface at pH = 9. Also, the ellipsometry tests showed only ~ 2 nm decrease in layer thickness after 15 min of bleach treatment at pH = 9. The MRR data on bleaching/etching suggest that hypochlorite is less potent at pH = 9 compared to pH = 11.

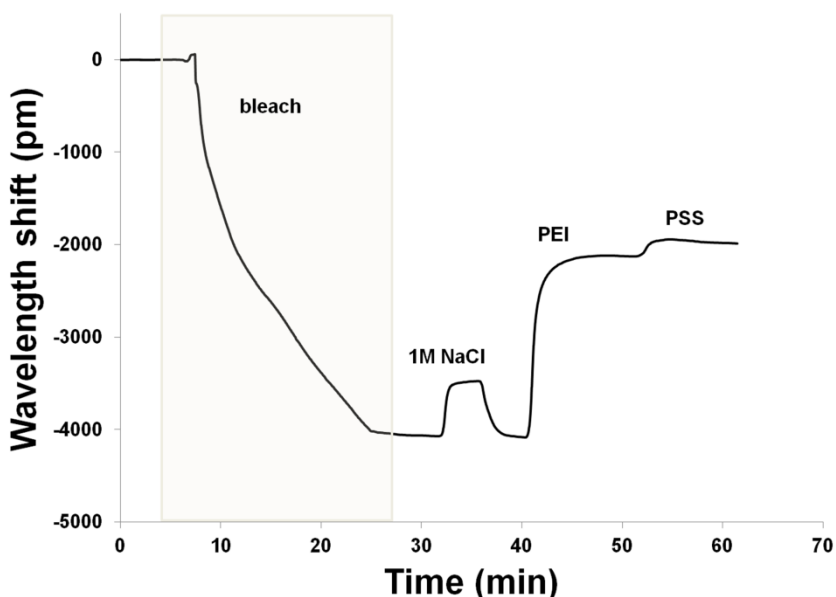


Figure 8. Wavelength shift during the addition of bleach pH = 11 in the post-treatment process. Further inspection for sensitivity with 1 M NaCl and building of PE layers on the regenerated device.

Finally we report and discuss the observations related to Fig. 8 at ~30 min. This part of the plot demonstrates that PEs can be adsorbed onto the device after the post-treatment bleach. In more detail, the addition of 1 M NaCl resulted in a signal increase of about 160 pm (39%), compared to the original sensitivity of the device. This increase may be attributed to the increase in the surface roughness of silicon, which was proposed after discussing the ellipsometry data. Next, at ~36 min, a rinse step was applied to establish the experimental buffer concentration, before adding PE in the same manner as the initial experiments. Upon the addition of a PEI solution the signal increased about 2000 pm, which is a factor of about 25 higher than the PEI response observed in the beginning of the experiment. Again, this increased sensitivity may be attributed to the

increased surface roughness of the MRR. Lastly, the signal change upon the subsequent addition of PSS was also higher than the one observed before bleaching. Although the bleach post-treatment may have changed the silicon MRR surface morphology, it did not alter the device sensing capability. In fact, it increased MRR sensitivity.

6.4 Conclusions

Free-space coupled MRRs simplify the use of optical ring resonator systems and anticipates future utilization of such devices in POC diagnostics. Fouling of the proteins was reduced by introducing BSA to the flow system during the PE layers formation and on the finished device. We observed specific responses of the chemical-biological stack, built with a biotinylated polyelectrolyte, to addition of influenza A as low as 10 ng/ml within 15 min. However, a concentration-dependent response, i.e. increase of the signal with increase of the antigen concentration, was only observed within the 1-10 $\mu\text{g/ml}$ influenza A range. As the realization of such a system in clinical trials demands sensitivities at lower concentrations, further improvements are required. One such an improvement was realized by decreasing the sensitivity variations between devices to 10% by pre-treatment with bleach. Post-treatment with bleach after antibody-antigen experiments allow the regeneration of used devices, leading to the possibility of multiple usage of the same chip and, in turn, decreasing the costs. Bleaching with hypochlorite at $\text{pH} = 11$ resulted in higher device sensitivities, which may be related to an increase in the surface roughness due to etching. More experiments, including for instance Atomic Force Microscopy imaging, are needed to further investigate this.

References

1. WHO, *World Health Statistics*, Report 978 92 4 156444 1, 2012.
2. T. R. Shojaei, M. Tabatabaei, S. Shawky, M. A. Salleh and D. Bald, *Mol Biol Rep*, 2015, 42, 187-199.
3. S. C. Gopinath, T. H. Tang, Y. Chen, M. Citartan, J. Tominaga and T. Lakshmipriya, *Biosens Bioelectron*, 2014, 61, 357-369.
4. L. Krejcova, D. Hynek, P. Michalek, V. Milosavljevic and R. Kizek, *Int J Electrochem Sci*, 2014, 9, 3440-3448.
5. I. Grabowska, K. Malecka, U. Jarocka, J. Radecki and H. Radecka, *Acta Biochim Pol*, 2014, 61, 471-478.
6. J. Schlingemann, M. Leijon, A. Yacoub, H. Schlingemann, S. Zohari, A. Matyi-Tóth, I. Kiss, G. Holmquist, A. Nordengrahn, U. Landegren, B. Ekström and S. Belák, *J Virol Methods*, 2010, 163, 116-122.
7. J. Xu, D. Suarez and D. Gottfried, *Anal Bioanal Chem*, 2007, 389, 1193-1199.
8. D. Guo, M. Zhuo, X. Zhang, C. Xu, J. Jiang, F. Gao, Q. Wan, Q. Li and T. Wang, *Anal Chim Acta*, 2013, 773, 83-88.
9. D.-G. Ahn, I.-J. Jeon, J. D. Kim, M.-S. Song, S.-R. Han, S.-W. Lee, H. Jung and J.-W. Oh, *Analyst*, 2009, 134, 1896-1901.
10. S. K. Poddar, *J Virol Methods*, 2003, 108, 157-163.
11. J. Zhao, S. Tang, J. Storhoff, S. Marla, Y. P. Bao, X. Wang, E. Y. Wong, V. Ragupathy, Z. Ye and I. K. Hewlett, *BMC Biotechnology*, 2010, 10, 74-74.
12. J. D. Driskell, C. A. Jones, S. M. Tompkins and R. A. Tripp, *Analyst*, 2011, 136, 3083-3090.
13. J. Li, M. Zou, Y. Chen, Q. Xue, F. Zhang, B. Li, Y. Wang, X. Qi and Y. Yang, *Anal Chim Acta*, 2013, 782, 54-58.
14. A. A. M., K. R. and S. G., *Indian J Med Microbiol*, 2008, 26, 297-301.
15. X. Fan, I. M. White, S. I. Shopova, H. Zhu, J. D. Suter and Y. Sun, *Anal Chim Acta*, 2008, 620, 8-26.
16. A. Ramachandran, S. Wang, J. Clarke, S. J. Ja, D. Goad, L. Wald, E. M. Flood, E. Knobbe, J. V. Hryniewicz, S. T. Chu, D. Gill, W. Chen, O. King and B. E. Little, *Biosens Bioelectron*, 2008, 23, 939-944.
17. A. L. Washburn, L. C. Gunn and R. C. Bailey, *Anal Chem*, 2009, 81, 9499-9506.
18. K. W. Kim, J. Song, J. S. Kee, Q. Liu, G. Q. Lo and M. K. Park, *Biosens Bioelectron*, 2013, 46, 15-21.
19. M. S. McClellan, L. L. Domier and R. C. Bailey, *Biosens Bioelectron*, 2012, 31, 388-392.
20. M. S. Luchansky, A. L. Washburn, T. A. Martin, M. Iqbal, L. C. Gunn and R. C. Bailey, *Biosens Bioelectron*, 2010, 26, 1283-1291.

21. P. J. Harmsma, B. M. de Boer, D. Ullien, E. J. R. Sudhölter, L. C. P. M. de Smet, W. F. Jager, S. M. C. Abdulla, A. A. and R. A. J. Hagen, *Proceedings of the 19th Annual Symposium of the IEEE Photonics Society Benelux Chapter*, **2014**, Enschede, 71-74.
22. D. Ullien, P. J. Harmsma, S. M. Abdulla, B. M. de Boer, D. Bosma, E. J. R. Sudhölter, L. C. P. M. de Smet and W. F. Jager, *Opt Express*, **2014**, *22*, 16585-16594.
23. W. Bogaerts, D. Taillaert, B. Luyssaert, P. Dumon, J. Van Campenhout, P. Bienstman, D. Van Thourhout, R. Baets, V. Wiaux and S. Beckx, *Opt Express*, **2004**, *12*, 1583-1591.
24. <http://www.epixfab.eu/>.
25. C. M. Herzinger, B. Johs, W. A. McGahan, J. A. Woollam and W. Paulson, *J Appl Phys*, **1998**, *83*, 3323-3336.
26. J. W. Haycock, *Anal Biochem*, **1993**, *208*, 397-399.
27. K. K. Vijai and J. F. Foster, *Biochemistry*, **1967**, *6*, 1152-1159.
28. J. T. Kirk, N. D. Brault, T. Baehr-Jones, M. Hochberg, S. Jiang and D. M. Ratner, *Biosens Bioelectron*, **2013**, *42*, 100-105.
29. L. Sun and J. Tang, *Appl Surf Sci*, **2009**, *255*, 9301-9304.
30. A. Lounas, A. N. Bouda, H. Menari, Y. Belkacem and N. Gabouze, *Surf Eng*, **2014**, *30*, 148-151.

Chapter 7

Conclusions and Outlook

7.1 Conclusions

This thesis describes research aiming for selective and sensitive influenza A detection using two sensing devices, i.e. (electrical) silicon nanowire field-effect transistors (SiNW FETs) and (optical) microring resonators (MRRs). To obtain selectivity, the surfaces of the sensing devices were functionalised. Firstly, surface functionalization using diazonium chemistry was investigated to enable the specific functionalization of an individual nanowire in an array. Secondly, the surfaces were functionalised by layer-by-layer deposition using (functionalised) polyelectrolytes.

Electrografting (Chapter 3) of the diazonium salts 4-NBD and 4-BBD on H-terminated Si(111) shows to be non-specific, i.e. not only surface Si-aryl moieties are formed, but also aryl-aryldiazonium and diazo couplings occur, leading to the formation of 2-7 nm thick surface layers. Part of these diazo groups could be electrochemically reduced, leading to thinner surface layers, and also to the formation of amino groups. These groups were formed by reduction of the aforementioned azo groups and also by reduction of present nitro groups (only for 4-NBD). Monolayers, however, are not obtained due to the presence of the biphenyl bonds that are not susceptible to electroreduction. Since the azo groups can be reduced to amino groups, it is concluded that amino-functionalized surfaces can be obtained from electrografting of non-nitro containing aryldiazonium ions.

Our research demonstrates that multifunctional organic layers on Si surfaces can be formed by a straightforward and well-controlled electrochemical process. When applied to silicon nanowires that are part of multi-array devices, amino functionalities can be formed and functionalized individually.

In Chapter 4 the performance of the p-type silicon nanowires made at DIMES (thesis of Thomas Moh, TU Delft, 2013) showed varying responses. The wet-etched devices revealed a device sensitivity of 36 mV/pH, however showing some instability. It was shown that besides a back-gate electrode, the additional use of a liquid-gated, front-gate electrode,

improves the stability of the measurements. Further experiments were done using p-type silicon nanowires fabricated at Philips Research (thesis of Marleen Mescher, TU Delft, 2014). Layer-by-layer modification of these nanowires using polyelectrolytes of opposite charge, showed an alternating shift of the threshold voltage of the devices. Preliminary research was performed on these silicon nanowires to detect influenza A. However, the results showed poor reproducibility. This research was not extended due to the lack of available devices. As a result, we made a shift to the optical resonator detection.

In Chapter 5 we have demonstrated that the silicon optical microring resonator (MRR) is a highly sensitive, reliable and user-friendly device for investigating surface modifications and the subsequent construction of biosensors. Using this device we demonstrated that PE deposition from aqueous NaCl solutions results in the formation of stable PE layers, which exhibit negligible PE detachment during rinsing steps. The employment of biotinylated PAH as the last PE layer in this architecture has proven to be a suitable technique for protein deposition on MRRs. Deposition of streptavidin on these biotinylated surfaces worked best for PAH layers with 6% degree of biotinylation.

The method is extended in Chapter 6 on the influenza A detection. The use of free-space coupled MRR simplifies the use of optical ring resonator systems and anticipates future utilization of such devices in POC diagnostics. Fouling of the proteins was solved by introducing BSA to the flow system during the PE layers formation and on the finished device. Using a chemical-biological stack built on a biotinylated PE, a specific response was observed to addition of influenza A as low as 10 ng/ ml within 15 min. However, for the realization of such system in clinical trials further improvements should be made to obtain clear concentration-dependent trends. One such improvement was realized by decreasing the sensitivity variations between devices to 10% by the application of a pre-treatment of the MRR surface with bleach. Meanwhile post-treatment with

bleach, i.e. after antibody-antigen experiments, allow regeneration of the device, leading to multiple usage of the same chip and decrease of the costs.

7.2 Outlook

By performing biosensing experiments on SiNW FETs as well as on MRRs, a better understanding of the pros and cons of each system was obtained. Both systems need more improvements to be practical as a viable POC device.

The use of silicon nanowires for biosensing applications is still very challenging. To get an amount of devices that is required for a thorough and statistically sound bioassay sensor study is difficult and depends on collaborations with other labs, since SiNW devices are not yet commercially available. The chip layout and SiNW characteristics need improvements. Firstly, in the case of SiNW FETs a micron-sized reference electrode should be embedded in the chip layout, since it is a necessary factor for stable measurements. Secondly, routes for better SiNW isolation can be explored to prevent current leakages. However, thick isolations should be avoided, since it decreases sensitivity of the device, as can be seen from the results of Chapter 4. Isolation with alternative oxides to SiO_x can be further explored. Thirdly, for the realization of multi-functionalized SiNW FETs, serial electroreduction of 4-nitrobenzene attached to SiNWs can be implemented.

The use of the microring resonator technique has its benefits. The MRR platform is simpler to handle, especially when equipped with a free-space coupled system. There are no undesired leakages (with a proper flow-cell construction) which destroy a device performance. There is no detrimental effect of higher salt concentration as in the case of SiNW FET devices, which are highly sensitive to Debye screening effects. The optical signal senses antibody-analyte interaction tens of nanometers away from the surface of the ring resonator. With MRR technique we were able to

show influenza A sensing of 10 ng/ml concentration. Influenza A recognition can potentially be realized in lower limit of detection then reached by us, by optimizing the system and removing redundant drift. First, the sensitivity deviation between MRR devices can be improved. Secondly, the temperature correction of the reference ring needs further enhancement. And finally, the optimization of the biological system for the elimination of the non-specific binding is required. With explored platform different other virus systems can be also sensed providing the existence of a biotinylated antibody.

Appendix A

Supporting Information to Chapter 3:

*Controlled Amino-functionalization by Electrochemical
Reduction of Bromo and Nitro Azo Benzene Layers
Bound to Si(111) Surfaces*

Constant N_{1s} signal upon XPS illumination

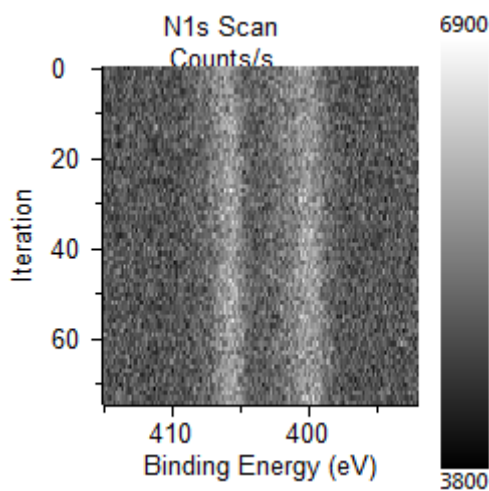


Figure A1. XPS N_{1s} spectra taken during 15 min (75 iterations) upon illuminating a sample of 4-nitrobenzenediazonium electrografted on Si with a pass energy of 50 eV. No significant changes were observed in the peak intensities with X-ray exposure time.

RMS roughness of the samples in AFM

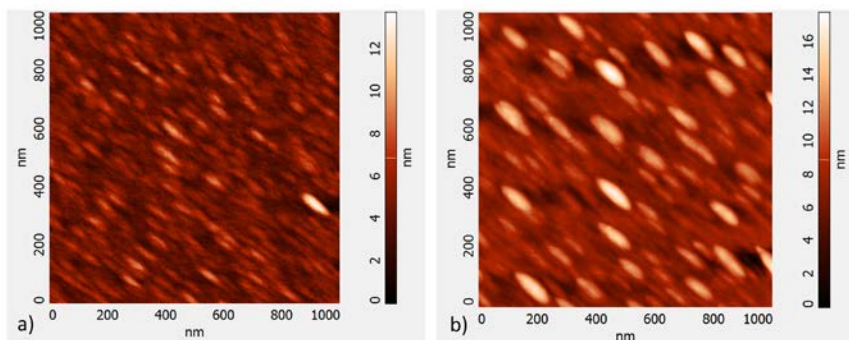


Figure A2. AFM topography scans of the samples before (a) and after (b) the electroreduction of 4-bromobenzenediazonium on Si. Upon electroreduction the rms roughness value increased from 1.1 nm to 1.5 nm for a $1 \times 1 \mu\text{m}^2$ scan.

Electroreduction of 4-BBD-modified Si (Azo-bond cleavage)

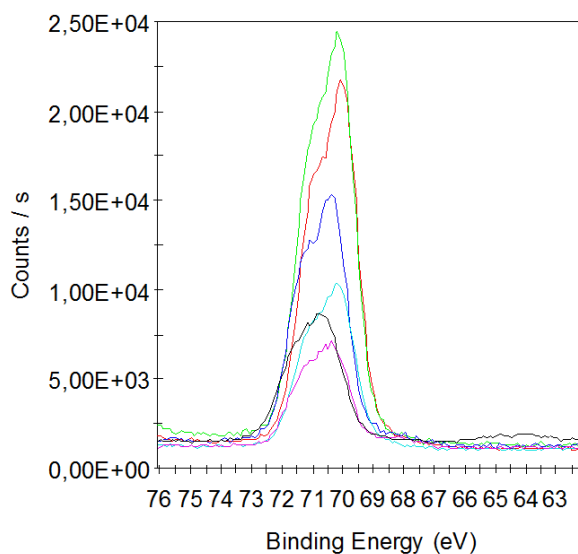


Figure A3. XPS Br_{3d} spectra of bromobenzene electrografted on Si (3 upper graphs), and bromobenzene after the reduction of azobenzene on Si (3 lower graphs). On average the reduction is 43%.

Appendix B

Supporting Information to Chapter 5:

*Protein Detection on Biotin-Derivatized Polyallylamine by
Optical Microring Resonator*

Carbodiimide coupling to produce biotinylated poly(allylamine)

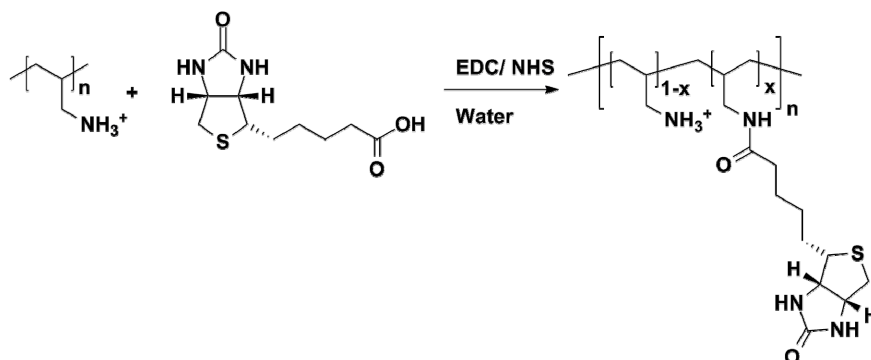


Figure B1. EDC - 1-Ethyl-3-(3-dimethylaminopropyl)carbodiimide, NHS - N-hydroxysuccinimide.

^1H -NMR spectra of 6% biotinylated PAH

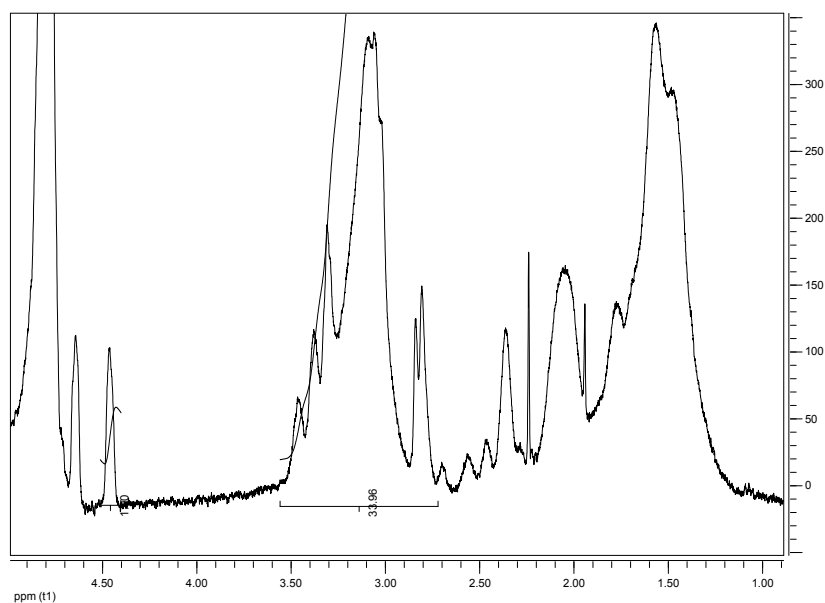


Figure B2. Using the integrated value of the peak at 4.4 ppm as donated from one biotin proton and comparing it to the peaks ~ 2.7-3.5 pm which originate from 2 protons of a PAH polymer and 3 protons of biotin, the labeling was calculated to be 6%.

MRR shifts

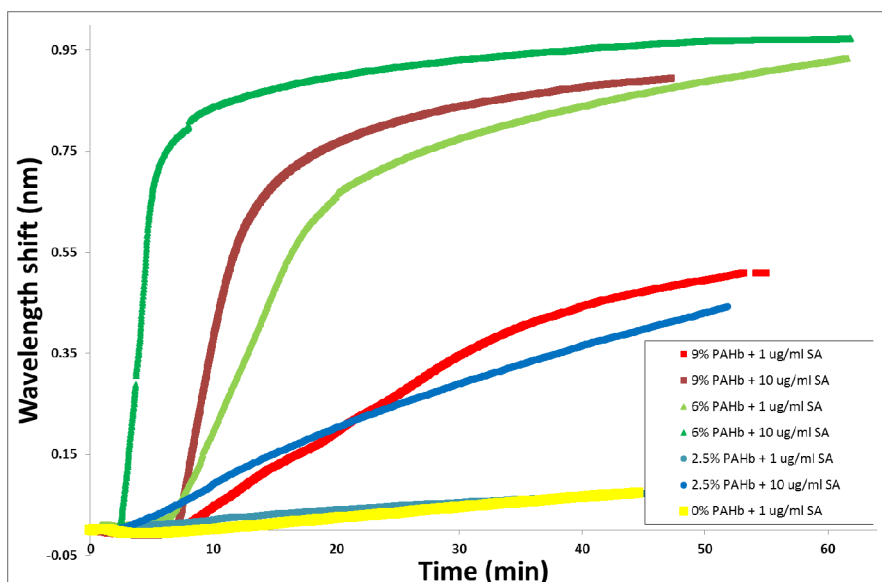


Figure B3. MRR shifts as a response to the addition of 1 and 10 ug/ ml streptavidin.

Layer thickness

The thickness of PAH/PSS bilayers made in NaCl solutions was measured by ellipsometry to be 5.42 nm for dry layers. This value is substantially larger than the 2.44 nm reported for PAH/PSS layers made in Tris buffer by Luchansky et al. [Supporting Information in M. S. Luchansky, *Biosens Bioelectron* 26, 1283-1291 (2010)]. However, this is in line with our observations that the wavelength shifts for LbL in NaCl solutions versus Tris buffers is in average 23% larger, see Fig. S4. Assuming an evanescent field decay of 65 nm, this implies that the construction of at least 10 bilayers is allowed without losing sensitivity.

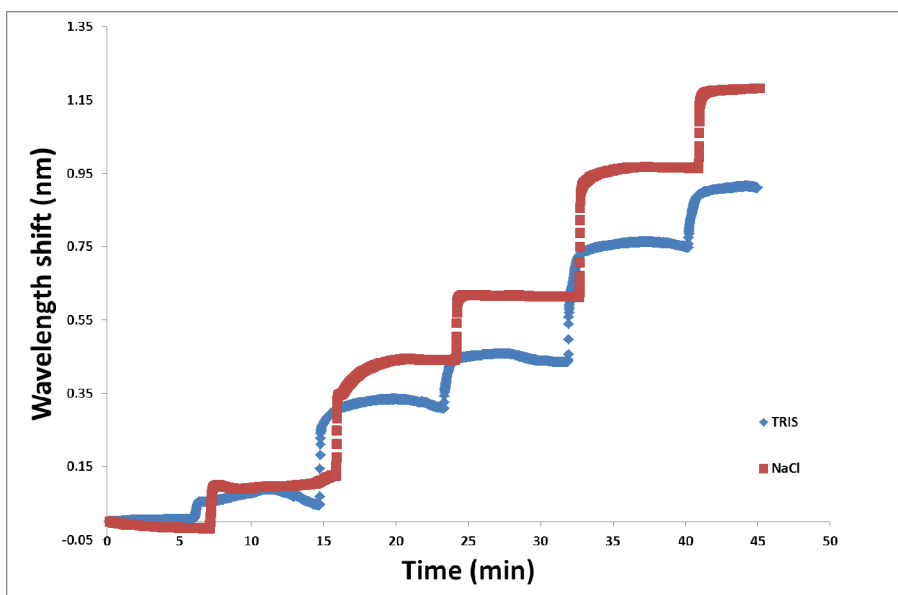


Figure B4. MRR wavelength shifts by addition of PE layers (PEI, PSS, PAH, PSS, PAH), using a 0.15 M NaCl solution (red) or a 0.15 M Tris buffer (blue).

Appendix C

Supporting Information to Chapter 6:

*Influenza A Detection by Free-space Coupled Optical
Microring Resonators*

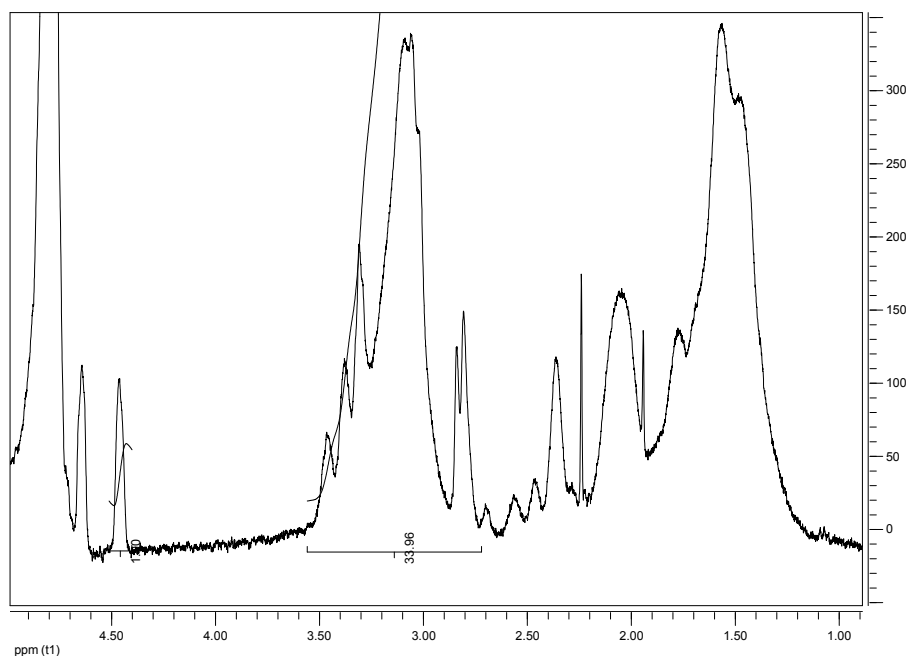


Figure C1. ^1H -NMR spectra of 6% biotinylated PAH.

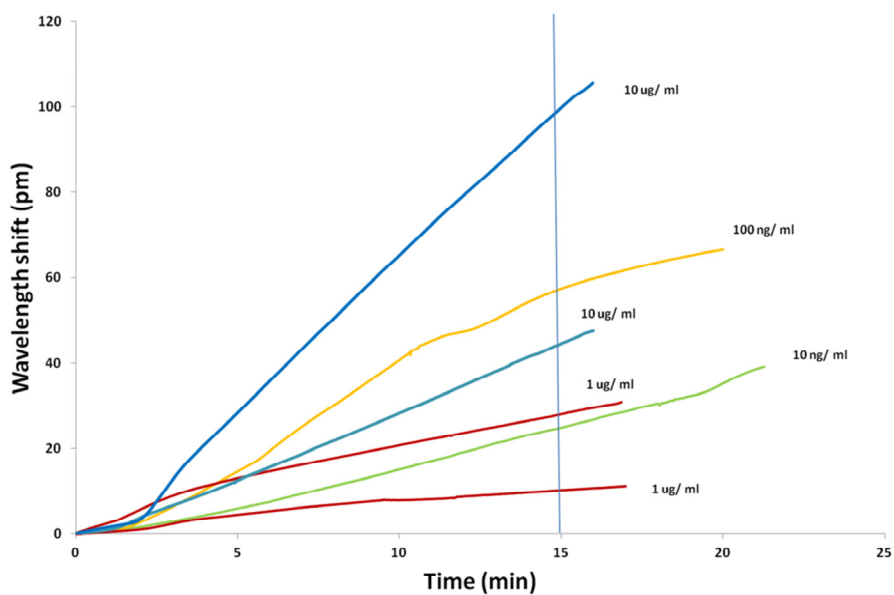


Figure C2. Real-time plots of influenza A analyte addition, which were used to obtain the values for Fig. 5b. The vertical line represents the point of data extraction.

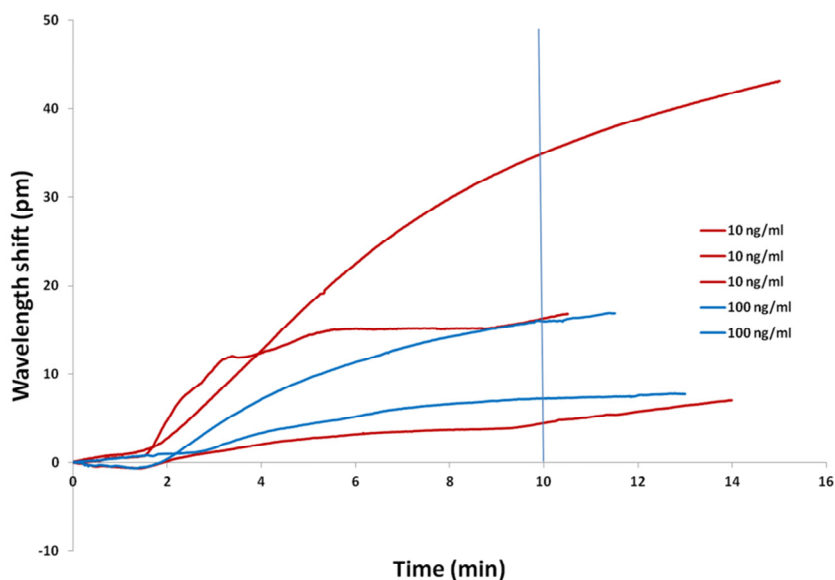


Figure C3. Real-time plots of influenza A analyte addition which were used to obtain the values for Fig. 6a (red). In this experiments 2nd BSA step was introduced. The values were extracted along the vertical line after 10 min of analyte exposure to MRR surface.

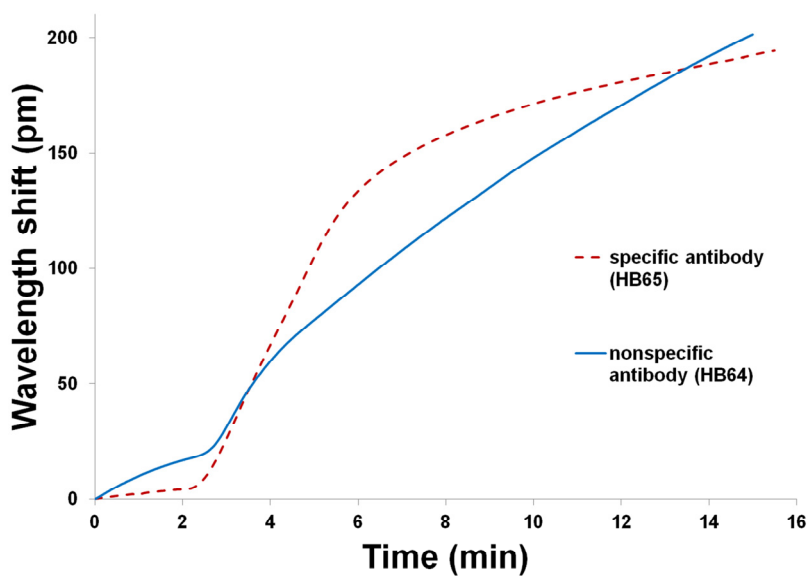


Figure C4. MRR responses to the addition of biotinylated specific and non-specific antibodies to MRR devices covered with PEs/streptavidin.

List of PhD Publications

- Influenza A Detection by a Free-space Coupled Optical Microring Resonator, **Ullien, D.**; Harmsma, P.J.; de Boer, B.M.; Bosma, D.; Sudhölter, E.J.R.; de Smet, L.C.P.M.; Jager, W.F. (manuscript in preparation)
- Controlled Amino-functionalization by Electrochemical Reduction of Bromo and Nitro Azobenzene Layers Bound to Si(111) Surfaces, **Ullien, D.**; Thüne, P.C.; Jager, W.F.; Sudhölter, E.J.R.; de Smet, L.C.P.M., *Phys. Chem. Chem. Phys.*, **2014**, *16*, 19258-19265.
- 'Click & Measure' Optical Interfacing to Silicon-On-Insulator Chips, Harmsma, P.J.; de Boer, B.M.; **Ullien, D.**; Sudhölter, E.J.R.; de Smet, L.C.P.M.; Jager, W.F.; Abdulla, S.M.C.; Abutan A.; Hagen, R.A.J., Proceedings of the 19th Annual Symposium of the IEEE Photonics Society Benelux Chapter, Enschede, November 3-4, **2014**, pp. 71-74.
- Protein Detection on Biotin-derivatized Polyallylamine by Optical Microring Resonators, **Ullien, D.**; Harmsma, P.J.; Abdulla, S.M.C.; de Boer, B.M.; Bosma, D.; Sudhölter, E.J.R.; de Smet, L.C.P.M.; Jager, W.F., *Opt. Express*, **2014**, *22*, 16585-16594 (Highlighted in the *Virtual Journal of Biomedical Optics*).
- Hydrogen Termination of CVD Diamond Films by High Temperature Annealing at Atmospheric Pressure, Seshan, V.; **Ullien, D.**; Castellanos-Gomez, A.; Sachdeva, S.; Murthy, D.H.K.; Savenije, T.J.; Ahmad, H.A.; Nunney, T.S.; Janssens, S.D.; Haenen, K.; Nesládek, M.; van der Zant, H.S.J.; Sudhölter, E.J.R.; de Smet, L.C.P.M., *J. Chem. Phys.*, **2013**, *138*, 234707.
- Organic Surface Modification of Silicon Nanowire-Based Sensor Devices, de Smet, L.C.P.M.; **Ullien, D.**; Mescher, M.; Sudhölter, E.J.R., *Nanowires - Implementations and Applications*, Abbass Hashim (Ed), InTech, Rijeka, Croatia, **2011**, pp. 267-288.

Acknowledgements

There are hardly any words to describe my gratitude to my promotor Prof. Dr. Ernst J. R. Sudhölter. Ernst, you were positive and believed in my abilities through the toughest times of my PhD experience. I am thankful for your encouragements throughout the whole process. Thank you for understanding and support.

I would like to express my gratitude to my co-promotor Dr. Louis C. P. M. de Smet and thank him for an immense supervision. Our weekly meetings kept me on my toes. Louis, you helped me to get more out of myself than I could do alone and you helped me to get even more focused on the projects. You taught me to look in detail on many things, not only scientifically. It was a pleasure to work under your supervision.

My sincere thanks to Dr. Wolter Jager, who supervised me on the optical part of the dissertation. Thank you for advices and insightful comments. My appreciation goes to the OMI technicians, especially Duco and Lars, who gave technical support for my experiments. Thank you for finding time for my research too. And many thanks to our secretaries Astrid, Marian and Karin. Thank you for the help in many various practical issues that I could not have done without you.

Special thanks to our various collaborators. Dr. Peter Harmsma, Shahina M. C. Abdulla and Bart de Boer from TNO were most helpful in providing optical sensors and the FRESCO set-up for our research. I am grateful to Thomas Moh and the Else Kooi Lab (formerly DIMES) team, Marleen Mescher and Philips Research for electrical sensors. I acknowledge Prof. Dr. Ron A. M. Fouchier from Erasmus MC as the source of influenza A. And I thank his team, Theo M. Bestebroer and Dr. William Garyfallou, for support. I thank the STW foundation for financial support and our project team, including Dr. Maarten A. Jongsma and Saurabh Srivastava. Thank you all for your guidance and fruitful discussions during my research.

My PhD experience was enriched by people who surrounded me these long years. Thanks to the people in the OMI, BOC and ASM groups. Especially I would like to mention Aldo Brinkman, my good friend. You took time to invest in our friendship and for that I am most grateful all the years to come. Marleen, Anping, Venkatesh and Sumit from OMI, thank you for all the coffee breaks and beer talks that we had. I thank William and Judith for good old times that we had in the beginning. Dainius and Iwona from ASM, thank you for the trips to the beach and it was great to arrange Christmas dinners together for our groups. I am grateful to Dr. Frank Hollmann from BOC for various interesting discussions in De Klomp. Thanks to Paul and Adeline from BOC for pancake/pannenkoek parties.

My sincere appreciation goes to the Russian community of Delft. Katya Churakova, Katya Ushakova, Gin and Natalie, Stas, Misha, Slava and many others, thank you for bringing excitement into my life. Katya Churakova, you have been a great pal throughout my PhD. Thank you for introducing me to the dancing community of the Netherlands. Katya Ushakova, thank you for becoming more than just a flatmate to me. It was a pleasure to be a witness to your wedding. Gin and Natalie, thank you for your hospitality and of course our Sunday coffee meetings in Mockamore. Stas, thank you for support in difficult times. Special thanks goes to Sveta and Gleb Vdovin. Thank you for your hospitality and invitations to various celebrations.

I would like to thank Kirsten de Brabander and Dr. Natalie Veen for their help in most difficult times.

I am thankful to the Genis family for providing a roof over my head, so I could finalize my dissertation in relative quietness.

Спасибо моей семье за поддержку. В особенности моему брату Денису и двоюродной сестре Анне. Спасибо, что вы готовы отозваться в любой момент.

Daniela Ullien
September 2015

Curriculum Vitae



Daniela Ullien was born on March 30th 1981 in Vladimir, USSR. She received her B.Sc. in Chemistry in 2004 from the Hebrew University of Jerusalem, Israel. Her M.Sc. was obtained in 2008 after completing a thesis on DNA-based nanoelectronics under the supervision of Prof. Danny Porath at the Hebrew University of Jerusalem, Israel.

In 2009 she started to pursue her Ph.D. studies in the Organic Materials and Interfaces group at the Department of Chemical Engineering at Delft University of Technology, the Netherlands, under the supervision of Dr. ir. Louis C. P. M. de Smet and Prof. dr. Ernst J. R. Sudhölter. The results of the research on optical and electrical biosensors for medical diagnosis is described in this dissertation.

